

November 2018

ENGINEERING HIGH PERFORMANCE EPOXY THERMOSETS USING NEXT-GENERATION IMPACT MODIFICATION

Madhura Pawar

Follow this and additional works at: https://scholarworks.umass.edu/dissertations_2



Part of the [Polymer and Organic Materials Commons](#)

Recommended Citation

Pawar, Madhura, "ENGINEERING HIGH PERFORMANCE EPOXY THERMOSETS USING NEXT-GENERATION IMPACT MODIFICATION" (2018). *Doctoral Dissertations*. 1459.
https://scholarworks.umass.edu/dissertations_2/1459

This Open Access Dissertation is brought to you for free and open access by the Dissertations and Theses at ScholarWorks@UMass Amherst. It has been accepted for inclusion in Doctoral Dissertations by an authorized administrator of ScholarWorks@UMass Amherst. For more information, please contact scholarworks@library.umass.edu.

**ENGINEERING HIGH PERFORMANCE EPOXY THERMOSETS USING
NEXT-GENERATION IMPACT MODIFICATION**

A Dissertation Presented

by

MADHURA PAWAR

Submitted to the Graduate School of the
University of Massachusetts Amherst in partial fulfillment
of the requirements for the degree of

DOCTOR OF PHILOSOPHY

September 2018

Polymer Science and engineering

© Copyright by Madhura Pawar 2018

All Rights Reserved

**ENGINEERING HIGH PERFORMANCE EPOXY THERMOSETS USING
NEXT-GENERATION IMPACT MODIFICATION**

A Dissertation Presented

by

MADHURA PAWAR

Approved as to style and content by:

Alan J. Lesser, Chair

Bryan Coughlin, Member

H. Henning Winter, Member

Bryan Coughlin, Department Chair, Polymer
Science and Engineering

DEDICATION

To my parents and my sister for their unconditional love and support

ACKNOWLEDGMENTS

First and foremost, I would like to thank Professor Lesser for being a wonderful advisor and a mentor. I have been able to develop as a scientist, a presenter and as a human being because of his guidance on my career and life decisions. I would also like to thank Professor Coughlin and Professor Winter for being on my committee and their insightful and valuable suggestions on my research. The faculty of PSE who have taught us our coursework in our first year have laid excellent foundation for my research.

I would like to sincerely thank the office staff: Lisa Groth, Maria Farrington, Linda Chatfield, Jessica Skrocki, Alyssa Kristek, Lisa McNamara, Trouble Mandeson and Jo-Ann Bourguignon made sure I did not have to worry about any administrative hassles in addition to our research work. All the facility co-ordinators have been excellent in giving advice and help on my experiments, especially Lou Raboin. It has always been a great pleasure to chat with Chris Coyle from EHS, Jim Leary and Dennis Glick and I really appreciate all these conversations which helped keep me motivated when spending long hours in the lab.

I have been fortunate to have worked alongside all the past and current members of the Lesser group and the visiting scholars. Chinmay, Liz, Nihal, Arif, Dan, Brendan, Connor, Brian, Matt, Amy, Ranadip, Silas, Koen, Marco, Christoph, Emily and Angela. I would like to thank Chinmay, in particular, for being an awesome sounding board and helping me out with experiments during the last part of my PhD.

I am grateful to BASF and BASF NORA for funding my dissertation work. My collaborator in Germany, Irene Gorman, has given me very valuable insights on my research, writing and career in all the three years we have worked together. She has also

helped me with details on starting a new life in Germany. I would also like to acknowledge the Center for UMass /Industry Research on Polymers (CUMIRP) Cluster M: Mechanics of Polymers and Composites for their support.

The PSE class of 2011 has been the best class to be a part of in this department. Daniel Acevedo, Nakul Bende, Jaewon Choi, Pırl Ertem, Alex Gerasimenko, Hongrui Guo, Pat Homyak, Mike Imburgia, Sveta Morozova, Connor Evans, Joel Sarapas, Zhiwei Sun, and Minchao Zhang made my transition into this new culture and new country extremely enjoyable. They have been excellent apartment mates, dance partners, lab partners, study mates but above all awesome friends. Mike and Nakul have helped me in research and making career decisions and Mike has been my partner in crime for all things melodramatic.

I have made amazing friends in the valley who have helped me in various aspects of life and graduate school and shared my love for travel. Srinivas, Konane, Sayantani, Swabarna, Liz, Chinmay, Dwaipayan, Poonam, Sohil, have all been solid pillars of support throughout this process. Outside of work, I will also cherish the dance performances with all the people in the events organized by the Indian student association and learning ballroom dancing at Amherst college. As I am about to embark on this new and unknown journey of moving to a new country, I surely will treasure all these moments spent with friends in the valley.

I would like to thank my undergraduate institution, Institute of Chemical technology for my foundation on Polymer Science and the wonderful friends I have made at that place. My teachers, Dr. Sabnis, Dr. Mhaske and Dr. Patwardhan, have been instrumental in me taking up this PhD in Polymer Science. I have made many beautiful

memories with Swapnali, Prerana, Reshma, Archit, Aditi Khadilkar and Madhura Joshi and Aditi Shankar. In the middle of me doing experiments and writing my thesis, Aditi Shankar has been my outlet for random thoughts/ most obscure Bollywood trivia and discussion topics which have kept me sane throughout this process.

I have lived with my sister and Sayantani as roommates for the past three years and have shared many-a-fun times together. I have also been fortunate to still be the best of friends with people I know since my school days. With Renuka and Harshada, it is always great to know that even with thousands of miles between us, I could still call them when I am stressed and no matter the situation, the phone call will cheer me up every single time.

Above all, I would like to thank my father Shrikar Pawar, my mother Surekha Pawar and my sister, Akshaya Pawar for all the sacrifices they have made for my education and their unquestioning and absolute faith in my abilities. My uncle, Rajendra Jadhav has also been very supportive of all my career decisions and I would like to thank him for his support. This PhD would absolutely have been possible without their love and support.

ABSTRACT

ENGINEERING HIGH PERFORMANCE EPOXY THERMOSETS USING NEXT-GENERATION IMPACT MODIFICATION

SEPTEMBER 2018

MADHURA PAWAR, B.TECH., INSTITUTE OF CHEMICAL TECHNOLOGY

M.S., UNIVERSITY OF MASSACHUSETTS AMHERST

Ph.D., UNIVERSITY OF MASSACHUSETTS AMHERST

Directed by: Professor Alan J. Lesser

Impact modification of high T_g epoxy thermosets has been conventionally performed using functional additives, preformed rubber particles and block copolymers as soft particles in the range of 5-20 vol%. Although there are numerous reviews studying the parameters for increasing the fracture toughness of epoxy thermosets, this study aims to systematically investigate different formulations and optimize the fracture toughness of high T_g thermosets using epoxy functional reactive impact modifiers. These modifiers initially formed a homogenous solution with the epoxy resin DGEBA (diglycidyl ether of Bisphenol A) and the curing agent, 4,4' Diaminodiphenylmethane (DDM) and phase separated out to form the second soft phase in the crosslinked epoxy thermosets. The epoxy functional modifiers were compatible with the DGEBA and the DDM used and were further evaluated for their glass transition temperature, morphology and fracture toughness. It has been established that modulus mismatch, particle size, interparticle distance are important parameters for optimizing the fracture toughness of epoxy thermosets. Curing kinetics of the epoxy resin was altered to vary these parameters to optimize fracture toughness. Also, different epoxy functional impact modifiers were pre-reacted with amines

of different functionality and chemical structure to form adducts. These adducts were then used as impact modifiers for the high T_g epoxy thermosets. Most of these adducts underwent reaction induced phase separation in the epoxy resins to form micron sized soft particle domains. The best performing impact modifiers showed an increase in fracture toughness of 70-80% while maintaining T_g s between 130 - 160°C with a trend showing the highest fracture toughness for larger particle sizes.

However, some of the impact modifiers used also showed a decrease in the glass transition indicating that the impact modifiers are staying miscible in the matrix and plasticizing or altering the network architecture. We investigated how the network structure of glassy thermosets is affected by impact modifiers and other functional additives by measuring the physical and mechanical properties of the network using different techniques like DSC, Dynamic mechanical analysis (DMA) and non-standard, non-linear compression testing. Different non-stoichiometric networks were made with DGEBA and DDM without impact modifiers by systematically going out of stoichiometry with excess mole ratio of amine and epoxy groups. The fracture toughness of the epoxy rich networks shows a decrease whereas that of the amine rich networks shows a slight increase as we go out of stoichiometry. Different techniques were used to correlate this engineering property to the structure of the epoxy networks. DSC showed a decrease in glass transition temperature for both epoxy and amine rich networks with increasing non-stoichiometry but the drop in the T_g was steeper in the case of epoxy rich networks. Non-linear compression testing was performed at true strain rates to probe the mechanical properties of the networks at low and high strains. The compressive modulus and strain hardening moduli showed behavior similar to the T_g of these networks. Yield stress increased for the epoxy rich networks and

decreased for the amine rich networks. Temperature sweeps were done using DMA on the non-stoichiometric networks to study the properties before and after the glass transition temperature. The storage moduli, and rubbery plateau moduli show behavior similar to that observed in the compression testing. These results indicate that properties in the low strain regions are indicative of the inter and intra chain interactions and in the high strain regions are related to the network connectivity.

The properties of the epoxy rich networks at low strain regions in compression testing and before the glass transition temperature in DMA, exhibit effects similar to physical ageing due to the unreacted monomers, low molecular weight constituents and dangling chain ends which have a greater degree of freedom and therefore can pack more efficiently. At high strain regions and above the glass transition temperature of these networks, the effects of crosslink density and network connectivity are evident from the sharp decrease in the rubbery plateau and strain hardening moduli of the epoxy rich networks as compared to the amine rich networks.

The fracture toughness showed a trend similar to that of the breadth of the α transition in these networks where the breadth increases for the more heterogenous epoxy rich networks and narrows for the amine rich networks as they decrease in cross-link density. This shows that the mechanical properties of the network can be probed using different techniques like DMA and non-linear compression testing and correlated to the behavior observed in an engineering property like fracture toughness.

Recently, block copolymers have been used to improve the fracture toughness of epoxy thermosets and it has been found that block copolymers resulting in a non-spherical wormlike micelle morphology have been more efficient in toughening these thermosets

than the spherical micelles. Expanding on this concept of using a single block copolymer, we blended two different block copolymers in different compositions in the DGEBA-DDM mixture to achieve phase separated non-spherical high surface area morphologies as crosslinking takes place. The different block copolymers were chosen such that they both have an epoxy compatible and an epoxy incompatible block and at least one of the blocks in the two different block copolymers is compatible with each other. The non-spherical morphologies will be thus kinetically trapped, as the block copolymers phase separate from each other and the matrix. The micromechanics of using this approach is discussed and techniques like optical and scanning electron microscopy were used to investigate the toughness mechanisms. Fracture toughness was measured for some impact modified systems with spherical and non-spherical modifiers. The effect of particle size and shape on the fracture was evaluated by putting forth a metric called shape factor. ImageJ analysis was performed on the SEM images of the morphology of these systems. The shape factor is defined as the non-sphericity of the impact modifier domains. Higher the shape factor, higher is the non-spherical nature of the domains. Fracture toughness was seen to correlate well with the morphology of the impact modifiers as the highest fracture toughness was obtained with the formulations having the highest shape factor.

TABLE OF CONTENTS

	Page
ACKNOWLEDGMENTS	v
ABSTRACT	viii
LIST OF TABLES	xv
LIST OF FIGURES	xvi
CHAPTER	
1. HISTORY OF IMPACT MODIFICATION IN POLYMERIC MATERIALS	1
1.1 Factors affecting fracture toughness of polymers.....	1
1.2 Classes of impact modifiers used.....	5
1.2.1 Soft particle impact modification.....	5
1.2.2 Thermoplastic impact modification	7
1.2.3 Rigid particle toughening.....	7
1.2.4 Hybrid systems with micron sized rubbers and nanosized silica particles.....	9
2. IMPACT MODIFIER OPTIMIZATION FOR HIGH T _g THERMOSETS	11
2.1 Introduction.....	11
2.2 Experimental	16
2.2.1 Sample preparation for morphology, thermal and mechanical property measurements	18
2.2.2 Scanning electron microscopy (SEM)	18
2.2.3 Glass transition temperature	18
2.2.4 Fracture toughness	18
2.2.5 Fracture energy release rate of impact modified carbon fiber composites.....	20
2.2.5.1 Sample preparation	20
2.2.5.2 Composite testing.....	20
2.3 Results and discussion	21
2.3.1 Strategies to control particle size	25
2.3.1.1. Altering curing kinetics.....	25

2.3.1.2 Synthesizing adducts.....	27
2.4 Conclusions.....	33
3. EVALUATING THE EFFECTS OF NETWORK DEFECTS ON THE PHYSICAL AND MECHANICAL BEHAVIOR OF GLASSY THERMOSETS	35
3.1 Introduction.....	35
3.2 Experimental.....	38
3.2.1 Materials	38
3.2.2 Sample preparation	39
3.2.3 Glass transition temperature	40
3.2.4 Fracture toughness	40
3.2.5 Compression Testing	40
3.2.6 Dynamic mechanical analysis (DMA).....	41
3.3 Results and discussions.....	42
3.3.1 Fracture toughness testing.....	42
3.3.2 Calculation of crosslink density based on stoichiometry.....	45
3.3.3 Differential scanning calorimetry	47
3.3.4 Non-linear compression testing	49
3.3.5 Fracture toughness testing on non-stoichiometric networks.....	58
3.3.6 Dynamic Mechanical Analysis	64
3.4 Conclusions.....	67
4. NEXT-GENERATION IMPACT MODIFICATION IN EPOXY THERMOSETS VIA NON-SPHERICAL HIGH-SURFACE AREA PARTICLES	69
4.1 Introduction.....	69
4.1.1 Theoretical approach for investigating the toughening using high surface area particles.....	70
4.1.1.1 Inter-particle Interaction	70
4.1.1.2 Effect of particle shape on cavitation stress.....	71
4.1.1.3 Secondary and other Hierarchical Morphologies	74
4.1.1.4 Potential Benefits of using hierarchical non- Spherical Impact Modification	75
4.1.2 Experimental approach achieving high surface area particles for improving fracture toughness.....	76

4.2 Experimental	80
4.2.1 Materials	80
4.2.2 Procedure for making plaques with block copolymer mixtures.....	81
4.2.3 Glass transition temperature	81
4.2.4 Fracture toughness	81
4.2.5 Scanning electron microscopy (SEM)	82
4.2.6 Optical Microscopy.....	82
4.2.7 Optical profilometry.....	82
4.3 Results and discussion	84
4.3.1 Fractographic analysis	88
4.3.2 Metric for relating the fracture toughness to the particle shape.....	95
4.4 Conclusions.....	101
4.5 Future work.....	102
4.5.1 Shape metric descriptors	102
4.5.2 Screening of different systems for further demonstrating proof of concept	103
4.5.3. Modeling and simulation studies	103
BIBLIOGRAPHY.....	104

LIST OF TABLES

Table	Page
2.1. List of all the impact modifiers used.....	16
2.2. Reactions for synthesizing adducts and their appearance after phase separation in epoxy resin	27
3.1. List of all chemicals used.....	39
4.1. General structures of the chemicals used.....	82
4.2. Solubility of the screened block copolymers in DGEBA	85
4.3. Solubility of the screened block copolymers in DGEBA	86
4.4. Appearance after curing with DDM and polyetheramine D-230 for different compositions of block copolymer blends	87

LIST OF FIGURES

Figure	Page
1.1. Fracture energy and T_g are in competition with each other	4
2.1. Schematic of a rubber particle before and after cavitation	12
2.2. Schematic of the process of fabrication of the carbon fiber composites.	20
2.3a. Glass transition as a function of concentration in non-phase separated networks	23
2.3b. Glass transition as a function of the crosslink density	23
2.4. Glass transition as a function of concentration in phase separated networks	23
2.5. Fracture toughness as a function of T_g of epoxy system with 15wt% epoxy functional modifiers	24
2.6. SEM images and particle size distributions of samples with ESO as impact modifier a) cured one-stage at 180 °C for 8 hours b) cured two-stage at 100 °C for 2 hours and 180 °C for 6 hours	25
2.7. SEM images and particle size distributions of samples with a 1:1 adduct of DMS E -09 + Aniline as impact modifier a) cured one-stage at 180 °C for 8 hours b) cured two-stage at 100 °C for 2 hours and 180 °C for 6 hours.....	26
2.8. SEM images of adduct compositions with 15 wt % adducts as impact modifiers	29
2.9. Morphology and particle size distribution of adduct composition with 15 weight% adducts as impact modifiers.....	30
2.10. Fracture toughness as a function of T_g of all the formulations tested.....	31
2.11. Fracture toughness vs particle size of formulations based on epoxy functional modifiers	32
2.12. Fracture toughness of the composites as a function of their glass transition temperature	33
3.1a. Fracture toughness in the neat resin of the impact modified formulations as a function of glass transition temperature. Inset: SEM image of the ESO modified formulation at 15 wt% b) Fracture toughness of the impact	

modified formulations as a function of glass transition temperature in carbon fiber reinforced composites.....	42
3.2. Curing exotherms of the reaction of DGEBA and DMSE-09 with DDM obtained by DSC	44
3.3. Main crosslinking reactions in the formation of DGEBA-DDM cross-linked network	45
3.4. Schematic of a) 1:1 Epoxy: Amine b) Amine excess c) Epoxy excess network	46
3.5. Plot of glass transition temperature vs crosslink density of the epoxy networks with different stoichiometries.....	47
3.6. Generic True stress vs Neo-Hookean strain curve for glassy polymers. The dashed lines indicate yield stress and rejuvenated stress in the polymer.....	49
3.7. True stress vs $-(\lambda^2 - 1/\lambda)$ curves for a) Epoxy excess and b) Amine excess epoxy networks	50
3.8. Yield stress against $1/M_c$ for both epoxy rich and amine rich epoxy networks. The modulus increases with decreasing crosslink density.....	51
3.9. Compressive modulus plotted against $1/M_c$ for both epoxy rich and amine rich epoxy networks. The modulus increases with decreasing crosslink density.....	52
3.10. Post yield stress drop increases in networks with amine excess and more steeply in networks with epoxy excess	54
3.11. The strain hardening modulus is dependent on the network connectivity when plotted against $1/M_c$ for networks.....	56
3.12. Fracture toughness of the out of stoichiometric networks as a function of the crosslink density.....	58
3.13a. Strain hardening modulus as a function of crosslink density for non-stoichiometric networks b) Load bearing fraction of the epoxy excess networks with increasing stoichiometric imbalance.	59
3.14. Strain localization parameter as a function of stoichiometric excess	62
3.15. Fracture toughness as a function of the strain localization parameter	63
3.16. a) Storage moduli b) Loss Moduli of non-stoichiometric networks as a function temperature	64

3.17. a) Linear fits of rubbery plateau region b) Slope of the Linear fits of the rubbery plateau region with respect to epoxy/amine mole ratio	65
3.18. a) Normalized Tan δ as a function of temperature b) FWHM of Tan δ transition as a function of the epoxy/amine mole ratio	66
4.1. Stress concentration at the surface of a particle with higher aspect ratio is much greater than that at the surface of a spherical particle.....	71
4.2. Cavitation stress is highly dependent on particle shape.....	72
4.3. Cavitation stress as a function of aspect ratio of the particle.....	73
4.4. Schematic of particles of different shapes a) before and b) after cavitation.....	74
4.5. Phase diagram of di-block copolymer self-assembly in solution	77
4.6. Mixing of two block copolymers with individual phase separated morphologies to obtain high surface area morphologies	79
4.7. Stresses in front of the crack.....	89
4.8. Optical micrographs of process zones of systems with different block copolymer blends	89
4.9. Morphology of 1) PE-PEO (Mn 2250) + PEO-PPO-PEO (15%) 2) Poly (vinylmethyl) ether (15%) 3) M51 + SBM (15%) 4) M51 + M53 (15%)	91
4.10. Optical micrographs of size of the process zones of 1) PE-PEO (Mn 2250) + PEO-PPO-PEO (15%) 2) Poly(vinylmethyl) ether (15%) 3) M51 + M53 (15%) 4) M51 + SBM (15%)	91
4.11. Fracture energy release rate vs size of the process zone.....	92
4.12. SEM images of the non-spherical domains 1) outside 2)inside the process zone	94
4.13. Fracture energy release rate vs roughness of the process zone.....	95
4.14. a) PEO-PPO-PEO (Mn = 5.8k) + PE-PEO (Mn = 2250) b) PVME c) M51+ SBM d) M51 + M53 e) M51 f) M53	98
4.15. Correlation between normalized fracture toughness and shape factor of spherical vs non-spherical impact modifiers.....	100
4.16. Reduction in stress required for cavitation	101

CHAPTER 1

HISTORY OF IMPACT MODIFICATION IN POLYMERIC MATERIALS

1.1 Factors affecting fracture toughness of polymers

Improving the energy dissipation of polymeric materials through the incorporation of soft or rubbery particles is a well-established technology that has been adapted to several polymeric materials over the past decades. Yet, fundamental questions still arise for particular polymeric materials with regard to what morphological characteristics provide optimum energy absorption during fracture while minimizing detrimental effects associated with other engineering properties including the elastic modulus, yield strength, and process viscosity. This dissertation focusses on epoxy-based thermosets that are an important class of polymers used in a wide range of products ranging from coating to high performance fiber reinforced composites. A key element that is important to keep in mind is that the micromechanics dictate the energy dissipation mechanisms in this technology. Therefore, the concepts applied to this class of materials also translate to other polymer systems from a microstructural point of view. The point where the physics and chemistry become important arises from achieving a particular morphological optimum with regard to soft particle size, interparticle distance, particle modulus and particle strength or particle matrix bond strength. In order to review how these factors play a role, it is first important to understand how energy dissipation occurs without the introduction of a second phase.

The theoretical strength of crosslinked glasses materials from a molecular perspective dictates that scission of covalent bonds would govern this property and it would be approximately one tenth the elastic modulus of the material. Yet these materials fail at

much lower stress levels and typically absorb more energy during their fracture that cannot be explained by this process alone. This arises from the flaws and defects present in the material that alter the local stress state and ultimately govern the overall strength of the material. Consequently, the strength in this class of materials, much like all materials, is governed by its fracture toughness which is a property that describes the energy absorbed or dissipated by the material when fractured in the presence of a flaw or defect.

In accordance with linear elastic fracture mechanics (LEFM), the local stress field in front of the crack tip can be described by the following equation:

$$\sigma_{ij}(r, \theta) = \frac{K_I}{\sqrt{2\pi r}} \tilde{\sigma}_{ij}(\theta) \quad (1.1)$$

$$K_I = \sigma_\infty \sqrt{\pi a} \quad (1.2)$$

where a is the crack length, r and θ are cylindrical coordinates, σ_∞ the far-field stress and $\tilde{\sigma}_{ij}$ is a θ -dependent function. K_I is the stress intensity factor related to the geometry and loading modes.

It is important to note that two key characteristics become important when reviewing the result of Equation 1.1. The first is that the stresses are singular and become infinite as the crack tip is approached. This means that some form of energy dissipation in the form of yielding, shear-banding or other forms of nonlinear deformation may occur in the vicinity of the crack tip at any arbitrary load or far-field stress. The second factor is that the state of stress is highly triaxial whereby for glassy thermosets, the hydrostatic component of stress is roughly twenty times that of the deviatoric stress. Given that the process of yielding and shear band formation are shear dominated phenomena (and highly

dissipative), many materials ultimately fail due to defects (see equation 1.2) with lower strengths and energy dissipation.

Argon and Cohen modeled different amorphous polymers and described all polymers as brittle based on the ratio of the maximum hydrostatic stress to the maximum deviatoric shear stress in front of the crack tip. This ratio was indicated as a measure of the cavitation resistance and the plastic shear resistance of the polymer. If the ratio was greater than 1.62, then the material failed by creation of new surface area before any plastic deformation could occur in front of the crack tip.¹

In actuality, when glassy thermosets fracture, energy is dissipated through a competition between two main processes; one is associated with nonlinear processes such as yielding in front of the crack tip and the other is associated with the creation of surface area. It is well established that the creation of a new surface area consumes little energy when compared to the energy intensive process of non-linear deformation. Also, since yielding in this class of polymers is a stress-induced thermally-activated phenomenon, the glass transition temperature of the polymer is related to the yield stress of the polymer.² Consequently high T_g materials result in materials that have a higher yield stress. This higher yield stress reduces the overall amount of energy dissipation resulting from yielding and more brittle fracture occurs. In contrast, in low T_g materials there is always a competition between the yielding mechanisms and creation of new surface area. Thus, a typical response is observed for these types of materials as shown in Figure 1.1

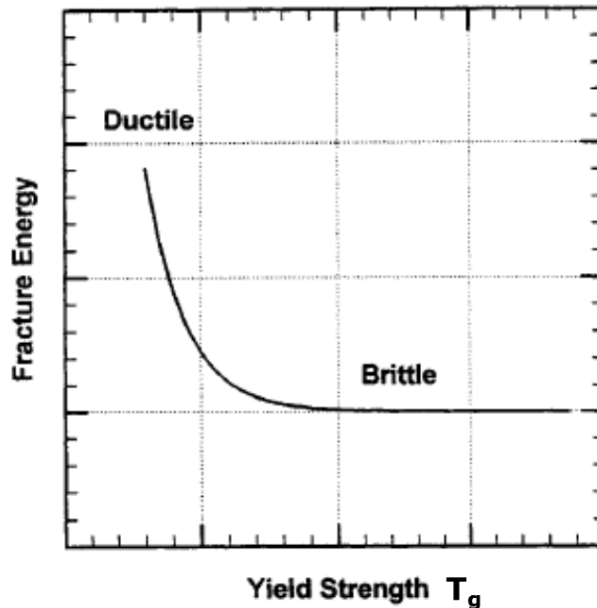


Figure 1.1: Fracture energy and T_g are in competition with each other ³

Many approaches have been used in literature to overcome this inherent competition between the properties. Generally, epoxy resins are made with a commercial aromatic difunctional epoxy resin diglycidyl ether of bisphenol A (DGEBA) cured with different curing agents such as amines or acid anhydrides.^{4,5,3} The choice of the curing agent is dictated by the application, glass transition temperature to be achieved and number of other properties like flexibility and toughness. Generally aliphatic amines are used as curing agents when tough epoxy resins are to be used at lower use temperatures. Aromatic amines or acid anhydrides are used to obtain high T_g epoxy systems which are stable at higher temperatures however, brittleness is a common issue with these high T_g systems due to the reasons mentioned above.

Molecular weights and backbone architectures of the epoxy resin and the curing agent used have been altered to enhance the toughness of the epoxy thermosets.⁶ Aromatic amines have been used in combination with aliphatic curing agents to form symmetric,

asymmetric and prestressed double networks to enhance the toughness of the epoxy resins.^{7,8,9}

The most common approach to obtain high T_g and high toughness systems is to introduce a second phase in a single-phase epoxy thermoset. There are different types of impact modifiers introduced as the second phase, some of which are listed as follows.

1.2 Classes of impact modifiers used

1.2.1 Soft particle impact modification

Extensive research has been done on epoxy impact modification using different soft particles. These include reactive liquid rubbers such as carboxy, amine, epoxy terminated butadiene acrylonitrile (CTBN/ATBN/ETBN) with different acrylonitrile contents, functional acrylates, functional polybutadienes, polysiloxanes, core-shell rubbers and block copolymers.

The reactive liquid rubbers form a homogenous solution with the epoxy resin and crosslinking agent mixture and then phase separate as the crosslinking reaction proceeds.¹⁰ CTBN rubbers have been found to be the most effective at toughening high T_g systems. Kim and Ma showed that for a DGEBA system cured with DDS, the fracture toughness doubled when 5 phr of CTBN rubber was used.¹¹ The functionality of the liquid rubbers affects the miscibility and adhesion of the particles to the matrix and therefore is an important parameter influencing the toughness.

Core shell rubber particles having hard shells and rubbery cores were pre-formed by emulsion polymerization and dispersed in the epoxy matrix. Different sizes of these particles were obtained by copolymerizing with different concentrations of monomers. The

fracture toughness of the epoxy systems modified using these particles show a dependence on the size, concentration as well as the chemical compatibility/interfacial bonding of the shell material with the matrix. Modest improvements were found in high T_g system of DGEBA cured with DDS when they were modified with CSR particles.

Recently, amphiphilic block copolymers (BCPs) have been investigated as toughening agents for epoxies.^{12,13,14,15} The BCPs are chosen such that one of the blocks is compatible with the epoxy amine mixture and the other is immiscible. Depending on the overall molecular weight of the block copolymer, the relative molecular weight of the individual blocks and the concentrations used, they self-assemble into different morphologies like spherical micelles, wormlike micelles. Different diblock and triblock copolymers such as styrene-methacrylate-butadiene, PMMA-PBA-PMMA, PEO-PPO-PEO, PEO-PEP have been used as efficient impact modifiers. It has been shown that adding just 5 wt% of BCP can double the fracture toughness of these nanostructured epoxy thermosets. Wormlike micelles were shown to be more efficient tougheners than the spherical micelles or vesicles especially in high T_g epoxy thermosets.¹³

There have been numerous reports investigating the effect of particle size, particle/matrix adhesion concentration and particle size distribution on the toughness of the epoxies.^{16,17,18,19,20,21} These include investigation of epoxy thermosets impact modified using reactive liquid rubbers as well as pre-formed particles. It was found that the cavitation stress is controlled by particle size²² and the shear yielding in the matrix is dictated by the interparticle distance and concentration. The reports investigating these effects are limited to a particular composition of impact modifier. Also, there have been very few reports on optimization of high T_g epoxy thermosets using metrics of particle size, concentration and

interparticle distance. In the next chapter, we will look at using a range of different impact modifiers to optimize a high T_g epoxy thermoset made from curing DGEBA with an aromatic tetra-functional amine, diaminodiphenylmethane (DDM)

1.2.2 Thermoplastic impact modification

Different thermoplastics like polyether sulfone, PMMA, polystyrene polyphenylene oxide, polyether esters and aromatic polyesters have been used as the second phase to improve the toughness of epoxy resins.^{23,24,25,26} The improvement in fracture toughness is related to the size and concentration of the thermoplastics, however it was found that for large concentration (>40%) of polyethersulfone is required even for improving the fracture toughness twice that of the control. Other thermoplastics too, performed poorly when compared to the soft particles used for toughening especially for high T_g thermosets.

1.2.3 Rigid particle toughening

There are different types of rigid particles that have been used historically to toughen epoxy thermosets. These include chopped carbon and glass fibers, glass beads, aluminum trihydrate, clays and silica particles. These are generally used to simultaneously increase the stiffness as well as toughness of the thermoset matrix. The size, shape and the concentration of filler used dictates the amount of toughening achieved in these systems.²⁷ Measurements were made on a range of particle sizes between 1- 20 μm and concentrations of 5- 40 wt%. In general, increasing the volume of the filler and the size of the particles has been found to have a positive effect on the modulus and the fracture toughness of the

epoxy thermosets for micron sized rigid particles. The fracture toughness usually, decreases after a certain concentration and particle size in these systems.²⁸

The adhesion between the matrix and the rigid particle can be tuned using surface treatments to influence the fracture toughness of the thermosets., however, it has been found that in case of rigid particles, good adhesion between the particle and the matrix is not a prerequisite for improved fracture toughness. Weaker adhesion can lead to debonding of the particles from the matrix which relieves the constraints imposed by the triaxial state of stress in front of the crack tip and therefore can activate similar mechanisms as that of cavitation in soft particle impact modification.

The toughening mechanisms of rigid particle filled thermosets usually crack wake mechanisms like crack bridging and crack pinning and have shown to lead to only modest improvements in fracture toughness as compared to soft particle impact modification ²⁹ Also, depending on the volume fraction of the modifier added, these may also decrease the fracture toughness of the epoxy systems.

Recently nanosized fillers have been investigated for their use in rigid particle toughening which include nanoclays, nanosilica, multiwalled and single walled carbon nanotubes and graphene nanoplatelets.³⁰ Nano-silica filled epoxies have been observed have shown better improvements in fracture toughness over micron-sized silica over the same range of concentrations. These improvements are much larger when the matrix is more ductile or when the crosslink density of the epoxy thermosets is reduced. These systems have shown improvements up to 150% in the epoxy systems.³⁰ However, as compared to the soft particle impact modification which can potentially give an increase in fracture toughness of orders of magnitude, the improvements in nano-particle filled epoxies

is also limited. Also, for effective toughening, there is a need for effective dispersion of these nano-fillers and this can be an energy and cost-intensive process. Even, with effective dispersion, the process viscosity of the system increases dramatically in these nano-filled thermosets especially at concentrations of 20-40 vol%. In addition, if the nano-particles are not dispersed well in the resin, the resulting agglomeration can lead to decrease in the fracture toughness due to the agglomerates acting as defects and leading to catastrophic failure in the thermosets.

1.2.4 Hybrid systems with micron sized rubbers and nanosized silica particles

In addition to rubber particles, hybrid systems of micron sized soft particles and nano-sized rigid fillers have been used in epoxies to improve the elastic modulus, hardness as well as fracture toughness of high T_g resins. The rubber particles can range from CSR The resulting fracture toughness obtained has been shown to be higher than the systems with just micron sized rubber particles or nano-sized fillers in the epoxy matrix.^{31,32} In high T_g systems, these hybrid systems can give modest to dramatic improvements in the toughness depending on the type, concentration and dispersion of rubber and the nanoparticle used.

The dominant mechanisms of toughening in the case of these hybrid systems have been identified to be particle debonding followed by inelastic void growth. In hybrid system containing silica nanoparticles along with spherical micron sized rubber particles, cavitation first occurs in the rubber particles and leads to shear yielding and plastic void growth of the matrix around the silica nanoparticles.³³ This interaction between the rubber and the silica nanoparticles then causes intensive shear banding between the rubber particles and cause a synergistic effect which further improves the toughness of the epoxy

systems.³² Thus, a lower concentration of rubber particles can be used to achieve the same improvements in fracture toughness. However, with any system comprising of nanoparticles effective dispersion and optimum concentration of fillers remains a challenge as agglomeration of nanofillers has been shown to have a negative effect on the fracture toughness of these systems causing them to fail catastrophically.

CHAPTER 2

IMPACT MODIFIER OPTIMIZATION FOR HIGH T_G THERMOSETS

2.1 Introduction

Epoxies are the largest class of materials used in continuous fiber applications like automotive and aerospace composites which need to have stability at high use temperatures as well as good fracture toughness. Conventionally, this has been difficult to obtain especially in high T_g epoxy thermosets because of the competing processes of non-linear deformation and creation of new fracture surface occurring during fracture as described in the previous chapter.^{3,29,34} Impact modification by introduction of soft particles is a well-established phenomenon for improving the fracture toughness of these particles. By introducing these particles, different mechanisms like cavitation, shear banding, yielding, are usually introduced in front of the crack tip to increase the size of the process zone, involve more material in the failure process and make tougher materials. In our study, we will be investigating the effects of adding a second soft phase to a brittle epoxy thermoset via reaction induced phase separation. In this system, the impact modifier initially forms a homogenous solution with the epoxy and amine used in the system and then phase separates out into rubbery domains as the crosslinking reaction proceeds and the molecular weight of the network grows.

For effective soft particle toughening, it has been experimentally observed that there needs to be a modulus mismatch of about an order of magnitude between the matrix and the particle for the particles to act as stress concentrators. The stress state in front of the crack tip is highly triaxial and therefore, cavitation of rubber particles takes place under certain applied stress to relieve this hydrostatic stress and introduce localized shear

deformation from the traction free surface of the cavitated particles.³⁵ The yielding process in epoxy systems is a deviatoric process that is inherently highly dissipative in nature. Consequently, the cavitation process prior to catastrophic failure is important to relieve the hydrostatic tension in the vicinity of the crack tip and allow for yielding via inter-particle interactions within the process zone in front of the crack tip. The nature of energy dissipation may vary from shear band formation between particles, to inelastic void growth of the cavitated domain, both of which consume a significant amount of energy during the fracture process. For high T_g systems, these processes become more limited resulting from the high yield stress and kinematic limitations from the network.

It has been experimentally observed that the particle size for effective toughening for most polymeric materials ranges somewhere between 0.1 and 10 μm with an optimum size different for each polymer. Above the particle size of 10 μm , the particles tend to act as defects and lead to premature failure of polymers. Below the size of 100 nm, the particles don't cavitate and therefore do not contribute to the toughening mechanisms.¹⁰ This scale effect for cavitation results from energy balance considerations as shown in Figure 2.1.

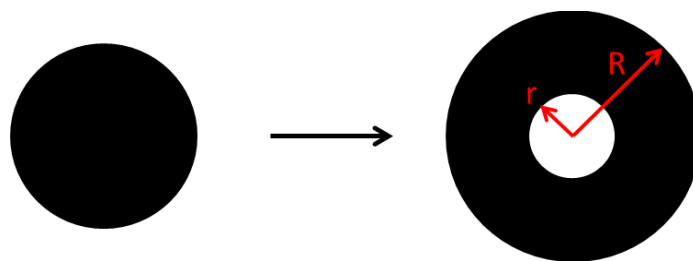


Figure 2.1: Schematic of a rubber particle before and after cavitation

For cavitation to occur, the strain energy stored in the particle must exceed the energy required to form the new surface area as seen in equation 2.1.

$$F \geq \gamma S \quad (2.1)$$

Where F is the strain energy stored inside the particle, S is the surface area created by cavitation, γ is the surface energy of the rubber particle.

Volumetric strain of the particle, ε_v is defined as the ratio of change in volume to the original volume.

$$\varepsilon_v = \frac{\Delta V}{V} \quad (2.2)$$

$$\frac{\Delta V}{V} = \frac{r^3}{R^3} \quad (2.3)$$

Where R is the radius of the particle and r is the radius of the cavity

The product of the strain energy density and the volume of the particle gives the strain energy stored inside the particle.

$$F = \left(\frac{1}{2} K_R \varepsilon_v^2\right) \left(\frac{4}{3} \pi R^3\right) \quad (2.4)$$

Where, K_R is the modulus of the rubber particle

$$S = 4\pi r^2 \quad (2.5)$$

Therefore, by substituting equations (2.2), (2.3), (2.4) and (2.5) in equation (2.1), we get

$$\left(\frac{1}{2} K_R \varepsilon_v^2\right) \left(\frac{4}{3} \pi R^3\right) \geq 4\pi r^2 \quad (2.6)$$

Now the strain in the matrix prior to cavitation is translated into the volumetric strain in the particle.

$$\varepsilon_v = \frac{r^3}{R^3} = \frac{\sigma_m}{K_m} \quad (2.7)$$

Where, K_m is the modulus of the matrix and σ_m is the mean stress applied to the matrix.

This gives rise to the critical particle size for cavitation which is given by the following equation.³⁶

$$R_c = \frac{6\gamma}{K_R (\sigma_m / K_m)^{4/3}} \quad (2.8)$$

Where R_c is the critical particle size required for cavitation.

Hence, larger particles cavitate at lower stresses followed by cavitation of smaller particles at higher stresses. For brittle polymers with high T_g , we need to engineer cavitation to occur at lower stresses so that the matrix surrounding the particles starts yielding before brittle failure occurs.

Once cavitation occurs, yielding starts at the rubber particle-matrix interface and propagates radially outward in the case of inelastic void growth or by forming shear bands between adjacent particles. In order to have effective toughening, it is necessary to have percolation of these processes between adjacent particles prior to catastrophic fracture in the system.

Once the particle size is fixed, the interparticle distance is dictated by the rubber volume concentration. For example, assuming a cubic array of particles, the relationship between the inter-particle distance, particle size and the concentration is given by Equation (2.9):³⁷

$$\text{Spacing} = D_p * \left[\left(\frac{\pi}{6C} \right)^{1/3} - 1 \right] \quad (2.9)$$

Where D_p is the diameter of the particle and C is concentration of the impact modifier domains in vol%.

It can be expected in high T_g systems that higher concentrations of rubber may be necessary reduce the interparticle distance and allow for percolation during the fracture process. There has been no consensus on the optimum concentration for epoxy-based

systems, but it has been shown to generally depend on the molecular weight, functionality and chemical structure of the impact modifier used. Different researchers have observed that the optimum rubber concentrations vary from 5-20 weight%.³⁸

There have been several reports studying the effects of particle size, concentration and distribution on epoxy systems, however, most of these involve the use of glassy particles or preformed rubber particles as it is easier to control the particle sizes of these impact modifiers.^{39,40,20,41} Recently, nanostructured and core-shell particles using block copolymers have also been investigated for their effect on cavitation and consequently on fracture toughness.^{42,12,14} All these studies have been done on epoxy systems cured with a wide variety of crosslinking agents and are not limited to high T_g systems cured with aromatic amines. Most of these studies also investigate only a few compositions with similar chemistries and therefore are not true indicators of the effect of particle size on the toughness of these systems. Therefore, a systematic investigation is needed for soft-particle impact modification achieved by functional impact modifiers and fracture toughness optimization using these systems.

In case of reaction induced phase separated particles, there is no comprehensive study which systematically varies the particle sizes and optimizes the fracture toughness of the system with respect to the particle size and interparticle distance. In this chapter we will systematically investigate and optimize a high T_g epoxy network of diglycidyl ether of bisphenol A (DGEBA) cured with diaminodiphenylmethane (DDM) using optimum concentration of soft particles as impact modifiers and understand the role of particle size and distribution to achieve high glass transition temperature as well as good fracture toughness.

2.2 Experimental

The diglycidylether of Bisphenol A (DGEBA) (Epoxy Eq. wt. = 175 g/mol) DER 332 was purchased from Dow chemicals. Aniline and diaminodiphenylmethane (DDM) (Amine eq. wt.= 49.565 g/mol) were obtained from Sigma Aldrich. The polyetheramine SD-231 was supplied by Huntsman corporation. The siloxane functional reagents were obtained from Gelest Inc., and the epoxidized soybean oil (ESO) obtained from Spectrum chemicals. All the chemicals were used without further purification unless otherwise specified.

Table 2.1: List of all the impact modifiers used (continued on the next page)

Structure	Name	Molecular weight
	SMS-092	7000
	SMS-042	7000
	SMS-142	4000
	DMS-B12	1000
	DMS-Z21	700

$\text{H}_3\text{C}-\text{Si}(\text{CH}_3)_2-\text{O}-\left(\text{Si}(\text{CH}_3)_2\right)_m-\left(\text{Si}(\text{CH}_3)_2-\text{CH}_2-\text{CH}_2-\text{NH}_2\right)_n-\text{Si}(\text{CH}_3)_2-\text{CH}_3$	AMS-191	2000
	SIB1092.0	382.69
	DMS-EC13	1000

$\text{H}_2\text{C}-\text{HC}(\text{O})-\text{H}_2\text{C}-\text{O}-\text{H}_2\text{C}-\text{H}_2\text{C}-\text{H}_2\text{C}-\text{Si}(\text{CH}_3)_2-\text{O}-\left(\text{Si}(\text{CH}_3)_2\right)_n-\text{Si}(\text{CH}_3)_2-\text{O}-\text{H}_2\text{C}-\text{H}_2\text{C}-\text{H}_2\text{C}-\text{O}-\text{CH}_2-\text{CH}(\text{O})-\text{CH}_2$	DMS E-09	363
	DMS E-11	500
	DMS E-12	1200
	DMS E-21	5000
$\text{H}_2\text{C}-\text{HC}(\text{O})-\text{H}_2\text{C}-\text{O}-\left(\text{H}_2\text{C}\right)_3-\text{Si}(\text{CH}_3)_3-\text{O}-\left(\text{Si}(\text{CH}_3)_2\right)_n-\text{Si}(\text{CH}_3)_2-\text{O}-\left(\text{H}_2\text{C}\right)_3-\text{O}-\text{C}-\text{CH}(\text{O})-\text{CH}_2$	PMSE-11	550
	PMSE-15	1400
$\text{H}_2\text{N}-\text{H}_2\text{C}-\text{H}_2\text{C}-\text{H}_2\text{C}-\text{Si}(\text{CH}_3)_2-\text{O}-\left(\text{Si}(\text{CH}_3)_2\right)_n-\text{Si}(\text{CH}_3)_2-\text{O}-\text{H}_2\text{C}-\text{H}_2\text{C}-\text{H}_2\text{C}-\text{NH}_2$	DMS-A11	800
	DMS-A12	1000
	DMS-A15	3000
	DMS-A21	5000
	ESO	1500

2.2.1 Sample preparation for morphology, thermal and mechanical property measurements

In all formulations, DDM and the impact modifier were dissolved in the DGEBA resin at 90°C until a clear solution was formed. The mixture was then quickly poured into rectangular glass molds with a thickness of 3 mm. Compositions with varying impact modifier concentrations of 5, 10, 15 and 20 weight % were added to stoichiometric quantities of DGEBA and DDM and cured at 100°C for 4 hours and 180°C for 4 hours, respectively. In the case of the functional modifiers, the stoichiometry of the samples was adjusted to account for the reaction between the epoxy functional groups and DDM.

2.2.2 Scanning electron microscopy (SEM)

A Magellan 400 scanning electron microscope equipped with a field emission gun and maximum operating voltages of 30kV was used to investigate the morphology of the cured samples. The plaques were first immersed in liquid nitrogen and cryofractured to make the SEM samples. A thin conducting layer of gold was coated on the fractured samples for SEM.

2.2.3 Glass transition temperature

T_g of the samples was measured using a TA instruments DSC Q200 at heating rate of 10 °C/min.

2.2.4 Fracture toughness

3 mm thick miniature compact tension (mini-CT) specimens were used to measure the fracture toughness of the samples following ASTM standard D5045-99. Lee and Jones⁴³ as well as Hinkley⁴⁴ have reported the use of mini compact tension specimens for

fracture toughness testing. In the case of our specimens, the plane strain condition was met as $B \geq 2.5 (K_q/\sigma_y)^2$ where K_q is the fracture toughness measured and σ_y is the yield stress of the samples. A diamond saw was used to introduce a notch in the sample. The samples were then immersed in liquid nitrogen and a sharp blade was inserted into the pre-notch to make a sharp pre-crack by lightly tapping the blade. An Instron 5500 fitted with 1kN load cell was used to record the Load-displacement curves of the samples at a crosshead speed of 0.5 mm/min at room temperature.

Fracture toughness was determined using the following equation:

$$K_q = \frac{P_c f(x)}{BW^{1/2}} \quad (2.10)$$

where P_c is the critical load in kilonewton (kN), B is the specimen thickness in centimeter (cm), W is specimen width in cm, and K_q is in $\text{MPa}\cdot\text{m}^{1/2}$. The use of K_q instead of K_{IC} depicts the use of a mini-CT specimen. The geometric factor $f(x)$ is a dimensionless power function in terms of x , which is equal to a/W , or the ratio of the pre-crack length to specimen width.

$$f(x) = \frac{(2+x)(0.886+4.64x-13.32x^2+14.72x^3-5.6x^4)}{(1-x)^{3/2}} \quad (2.11)$$

2.2.5 Fracture energy release rate of impact modified carbon fiber composites

2.2.5.1 Sample preparation

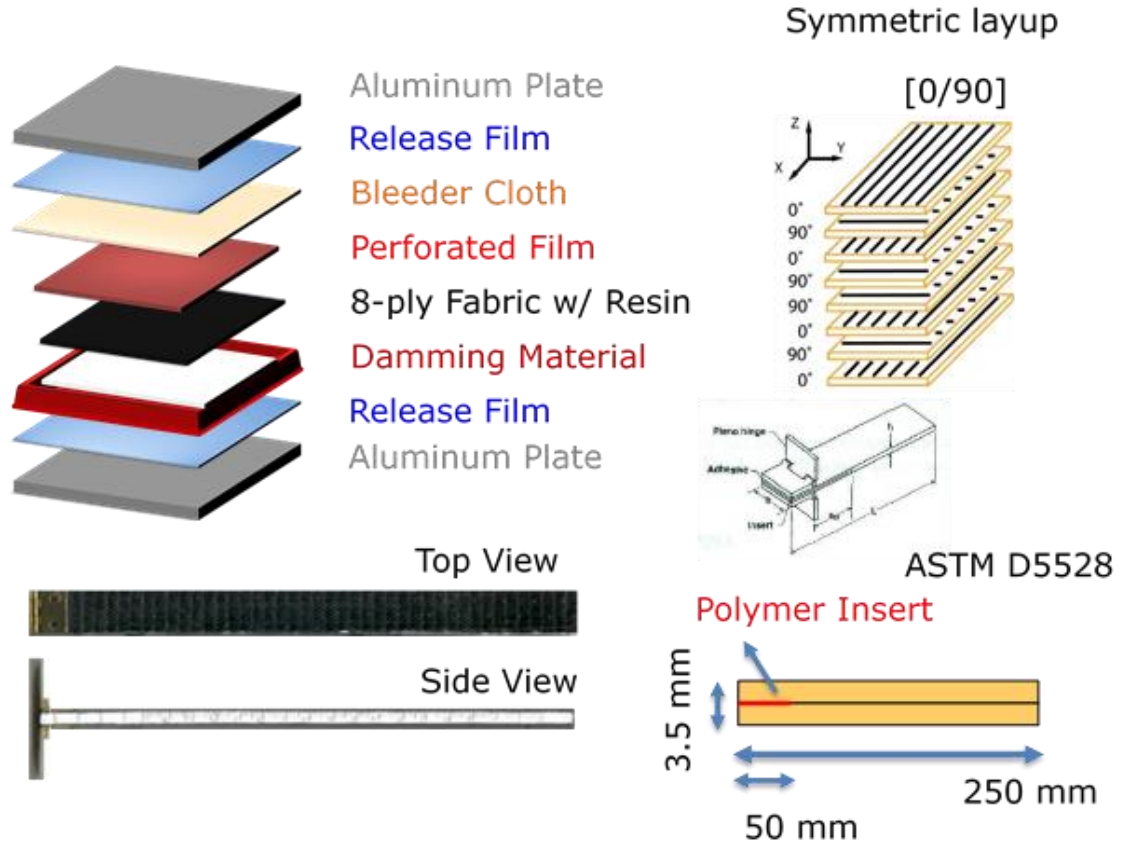


Figure 2.2: Schematic of the process of fabrication of the carbon fiber composites.

2.2.5.2 Composite testing

The biaxial carbon fabric used in the fabrication was supplied by BASF. The composites were fabricated with 8 plies in a symmetric 0-90 layup such that the fibers aligned in the 0-0 direction at the neutral axis. About half of the resin required for the composite was poured on the 4 plies, and for crack initiation, a non-adhesive PTFE film was inserted in the middle of the plies about 5 mm into the plies during fabrication. A perforated PET film, a bleeder cloth and a nylon film for mold release was used on both sides of the composite sample before placing it in a compression mold to remove all the

voids and excess resin to obtain around 30-40% carbon fiber volume for the composite sample. Samples of 25mm length and 20 mm width were then cut from these plaques and metal hinges were glued to the side of crack initiation as loading points. A double cantilever beam test in accordance with ASTM D5528 was performed for G_{1C} fracture toughness measurements. (Figure 2.2)

The test involves loading and unloading of the composite sample as a crack propagates. Incremental increases in strain were provided to observe the load response as the crack propagates. After the crack propagates, the sample is unloaded in a controlled manner manually using the Labview software, to get the compliance curve and then the test is started again till the crack propagates further. The test is performed on an Instron 4411 using a 5 kN load cell at a crosshead speed of 5mm/min. The crack length is measured visually during the test using a ruler. The crack length, maximum load and extension during crack propagation are then used to calculate the critical strain energy release rate according to the beam theory as described in the equation below.

$$G_{1C} = \frac{3 P \delta}{2b (a + |\Delta|)} \quad (2.12)$$

Where G_{1C} is the critical energy release rate, P is the load, δ is load point displacement, b is the sample width and a is the crack length. Δ is a correction factor which takes into account rotation of the beam at the crack front. Δ can be obtained experimentally as the x-intercept of the plot of the cube root of compliance, $C^{1/3}$ as a function of crack length.

2.3 Results and discussion

Over a hundred different formulations with different molecular weights, functionalities and backbone architecture were tested for their compatibility with the

DGEBA-DDM mixture. The modifiers with amine, carboxylic acid, anhydride and thiol functionalities were immiscible with the DGEBA and DDM resin mixture and led to gross phase separation even before the curing reaction started. The epoxy functional modifiers were compatible with both DGEBA and DDM and were thus investigated further to determine their effect on the mechanical and thermal properties of the crosslinked matrix. SIB1092 and DMS-EC13 were miscible only at very low concentrations less than 5 wt%. The ESO, SIB1092 and DMS-EC13 initially formed a homogenous solution with the DGEBA and DDM and then showed phase separation as the molecular weight of the network increased with crosslinking. The DMS-E09 and MCT-EP-13 initially stayed miscible in the DGEBA resin mixture but did not visually show phase separation after the cure schedule was completed.

In Figure 2.3a, the glass transitions of the systems with impact modifiers are plotted as a function of their concentrations and crosslink density. The solid symbols indicate visually opaque or phase separated systems. The hollow symbols represent the samples which are visually clear and did not phase separate. As expected, Figure 2.3b shows that the T_g of these systems decreased with increasing concentration and molecular weight between crosslinks. However, the T_g values of the uncross-linked DGEBA-DDM homopolymer obtained by fitting the Flory-Fox equation to the graphs of T_g as a function of crosslink density are negative and do not make physical sense, suggesting that the impact modifiers have not completely reacted with the surrounding crosslinked network and might be plasticizing the matrix.

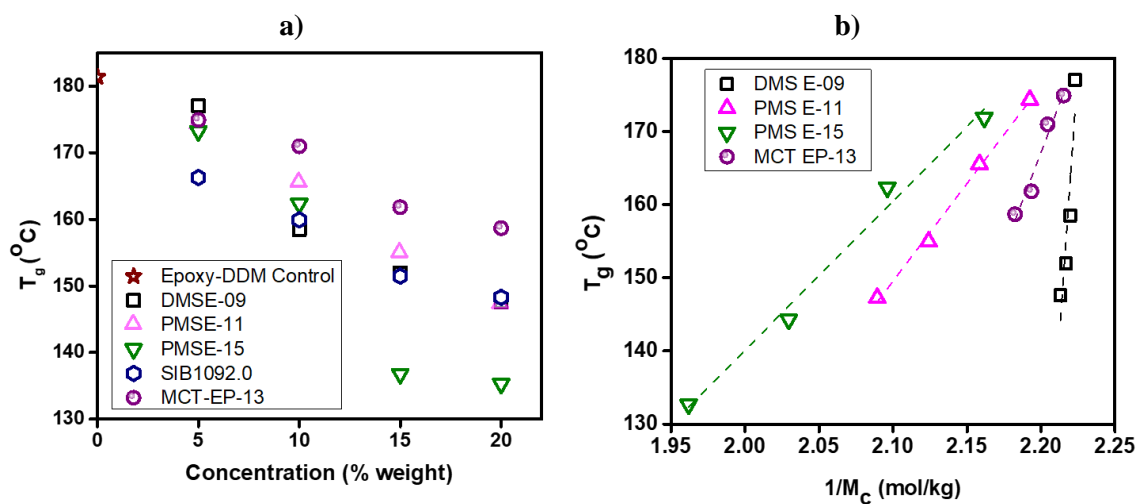


Figure 2.3 a: Glass transition as a function of concentration in non-phase separated networks 2.3 b: Glass transition as a function of the crosslink density.

In theory, in perfectly phase separated systems the T_g s of the surrounding crosslinked matrix should not change. However, reduction in T_g was observed, indicating incomplete phase separation with some fraction of the modifiers being soluble in the network, leading to plasticization of the matrix (Figure 2.4).

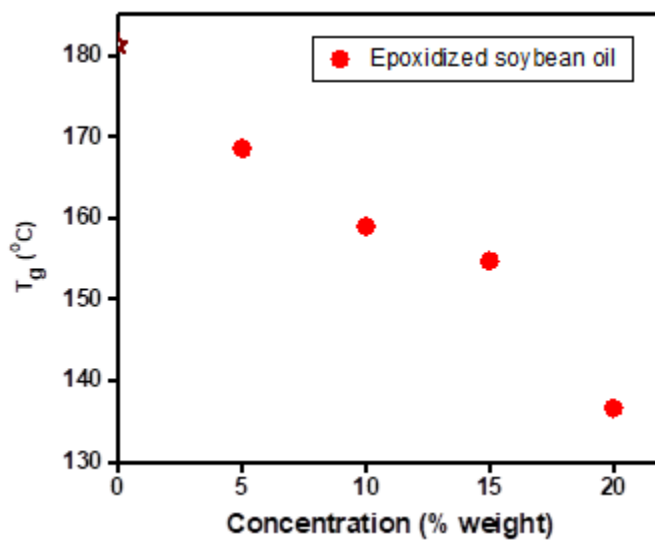


Figure 2.4: Glass transition as a function of concentration in phase separated networks

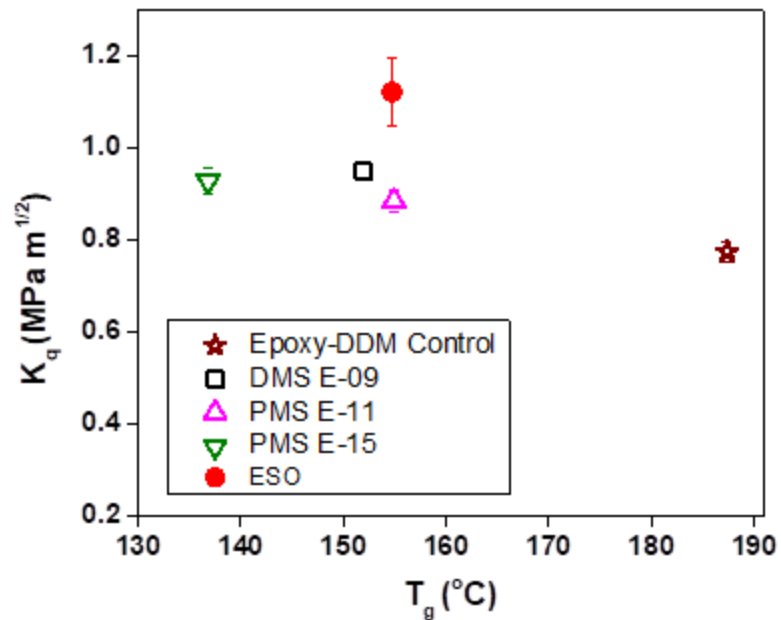


Figure 2.5: Fracture toughness as a function of T_g of epoxy system with 15wt% epoxy functional modifiers

Since, the interparticle distance is dependent on the concentration and particle size, we decided to formulate systems with 15wt% impact modifiers to study the effect of particle size on these systems. The concentration chosen was based on different studies with rubber modified epoxy systems and basic principles of impact modification using soft particles which showed that for engineering tough high T_g systems, generally a concentration between 10-15wt% proved to be the most effective. The fracture toughness of some of the impact modifiers is plotted as a function of their glass transition temperature in Figure 2.5. The fracture toughness of the non-phase separated formulations showed an increase of about 20 - 30% while the sample which phase separated demonstrated a 60% increase in fracture toughness. The glass transition temperatures of all these formulations indicated that the impact modifiers led to some amount of plasticization in the epoxy matrix. Also, the principles of impact modification suggest that fracture toughness could

be improved much further with samples that achieve complete phase separation over that of the samples where the siloxane modifiers just act as plasticizers. Hence, we decided to systematically alter process conditions to achieve complete phase separation and control the size and interparticle distance in these high T_g systems.

2.3.1 Strategies to control particle size

2.3.1.1. Altering curing kinetics

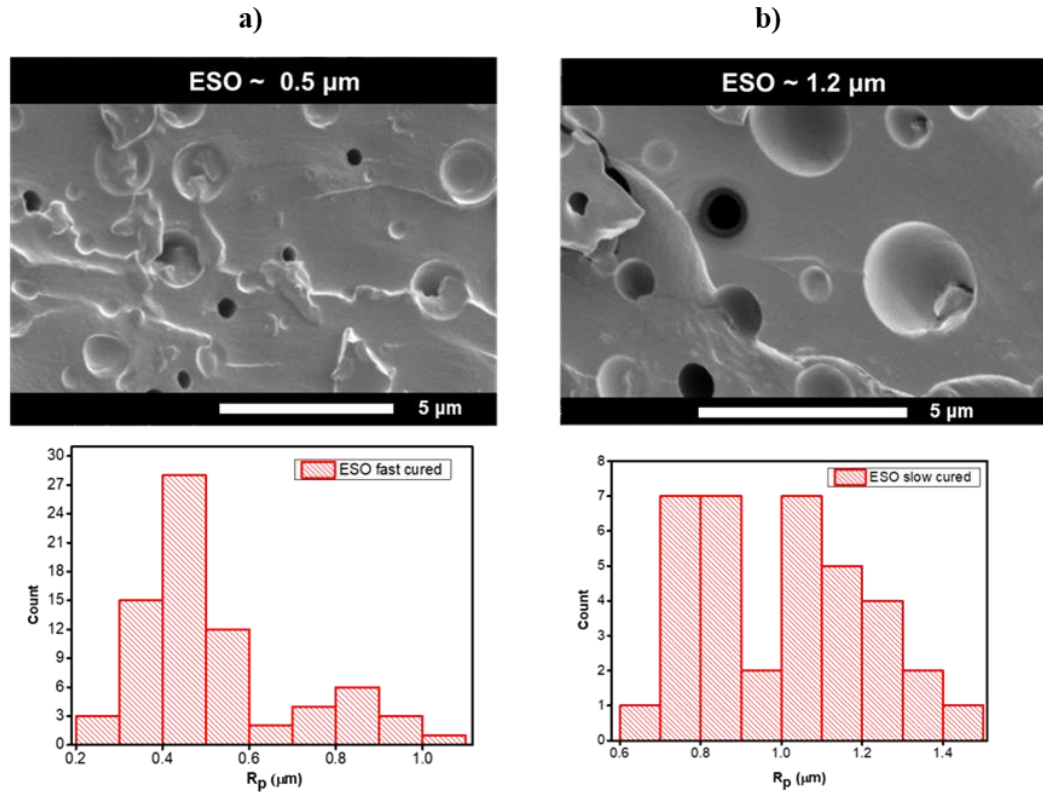


Figure 2.6: SEM images and particle size distributions of samples with ESO as impact modifier a) cured one-stage at 180 °C for 8 hours b) cured two-stage at 100 °C for 2 hours and 180 °C for 6 hours

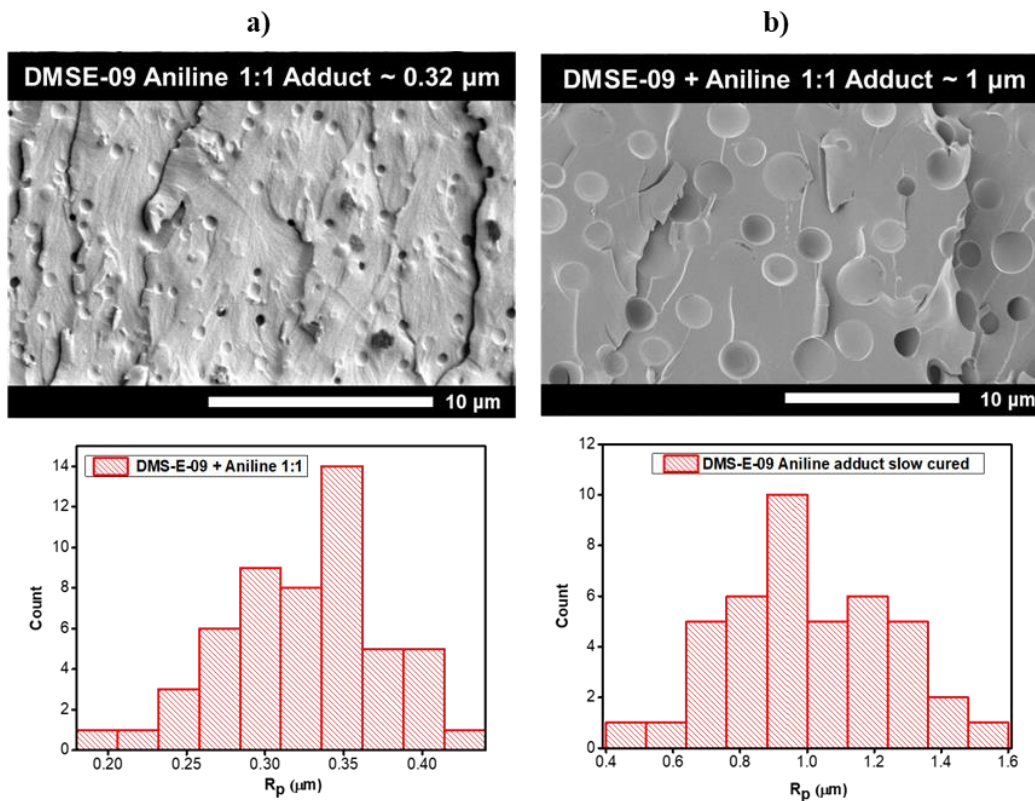


Figure 2.7: SEM images and particle size distributions of samples with a 1:1 adduct of DMS E-09 + Aniline as impact modifier a) cured one-stage at 180 °C for 8 hours b) cured two-stage at 100 °C for 2 hours and 180 °C for 6 hours

Since the phase separation of particles takes place by spinodal decomposition or nucleation and growth, the curing kinetics can be altered to alter the particle sizes.⁴⁵ In Figures 2.6 and 2.7, the SEM micrograph on the left shows the morphology of the sample cured in a single step at 180 °C for 8 hours whereas the image on the right shows a sample cured at 80 °C for 4 hours and 150 °C for 8 hours. The system cured in two stages displayed larger particle sizes. At 80 °C the polymerization of the network proceeds slowly, therefore the viscosity of the mixture is lower, and this allows time for the nucleation and growth of the phase separated particles before gelation of the network takes place. In the system with a one stage cure, the gelation of the epoxy network occurs rapidly and therefore the phase separated particles cannot evolve into larger particles by coalescence. Also, the samples

which are cured faster have a narrower size distribution with a larger number of smaller particles whereas, the particle size distribution in the slower cured samples is wider. Thus, to obtain particles of different sizes and distributions, the system can be cured at a range of temperatures to allow for this competition between the kinetics of crosslinking and phase separation.

2.3.1.2 Synthesizing adducts

Table 2.2: Reactions for synthesizing adducts and their appearance after phase separation in epoxy resin

Composition	Mole ratio	Adduct	Samples phase separation
PMS E-11 + DDM	2:1	Overnight at 100 ° C (Gel/rubber formed)	Not applicable
PMS E-11 + DDM	4:1	Overnight at 100 ° C	No
DMS E-09 +DDM	2:1	Overnight at 120 ° C (Gel/rubber formed)	Not applicable
DMS E-09 +DDM	4:1	Overnight at 120 ° C	No
PMS E-15 + DDM	1:1	Overnight at 80 ° C	Yes
PMS E-15 + DDM	2:1	Overnight at 80 ° C	Yes
PMS E-11 + SD-231	1:1	Overnight at 120 ° C	Yes
PMS E-11 + Aniline	1:1	Overnight at 120 ° C	Yes
DMS E-09 + SD-231	1:1	Overnight at 120 ° C	Yes
DMS E-09 + Aniline	1:1	Overnight at 120 ° C	Yes
PMS E-15 + SD-231	1:1	Overnight at 120 ° C	Yes

The epoxy functional modifiers were pre-reacted with different amines as described in the table 2.2 above. Adducts were made with three different amines: DDM, SD-231 and Aniline. These modifiers were then introduced in the DGEBA-DDM mixture as non-reactive functional modifiers. The DDM is a tetra-functional amine whereas the SD-231 and aniline are both di-functional amines. As DDM is compatible with DGEBA, it can potentially enhance the miscibility of the adducts made with DDM in the DGEBA resin. Aniline is an aromatic amine whereas the SD-231 is an aliphatic amine. Therefore, the molecular weights and backbone architectures of the adducts synthesized from these different amines would vary giving rise to different compatibilities of these adducts with the DGEBA-DDM resin mixture. Hence, introducing these adducts can change the onset of reaction induced phase separation and also the modulus of the rubbery domains obtained after phase separation. While making adducts with DDM, the low molecular weight epoxy functional modifiers, DMS-E-09 and PMS E-11, gelation occurred at 2:1 ratio. Therefore, they could not be used as impact modifiers.

The other synthesized adducts were screened based on their relative compatibility with the DGEBA/DDM mixture and investigated for their morphologies after phase separation. With the PMSE-15 adduct made with DDM, a shallow sphere morphology was observed as seen in Figure 2.8. This indicated a reduced modulus mismatch between the matrix and the phase separated rubbery domains. Due to the tetra functionality of DDM and the resulting increase in crosslink density of the rubbers, the modulus of the rubber increased. Aniline was then used as a chain extender as it was similar in chemical structure to the DDM ensuring compatibility, but its di-functionality would allow for more flexible

adducts. The linear aliphatic difunctional SD-231 was also used as a chain extender to obtain flexible adducts with a greater modulus mismatch (Figure 2.8).

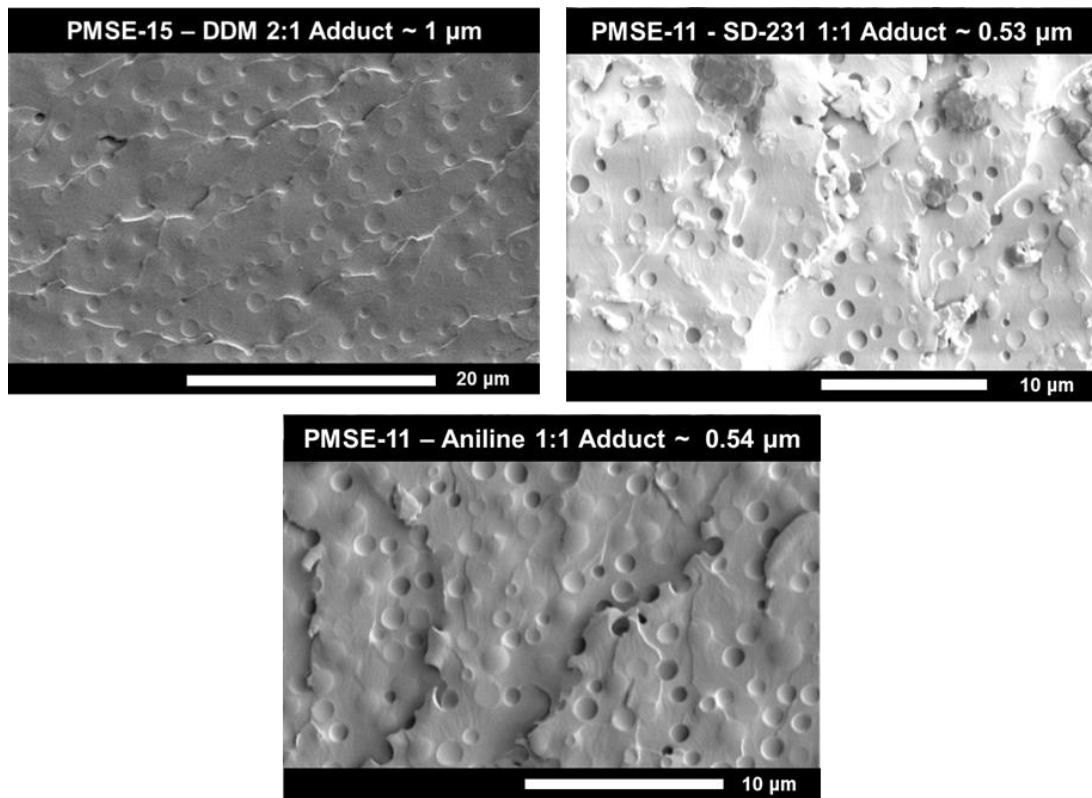


Figure 2.8: SEM images of adduct compositions with 15 weight % adducts as impact modifiers

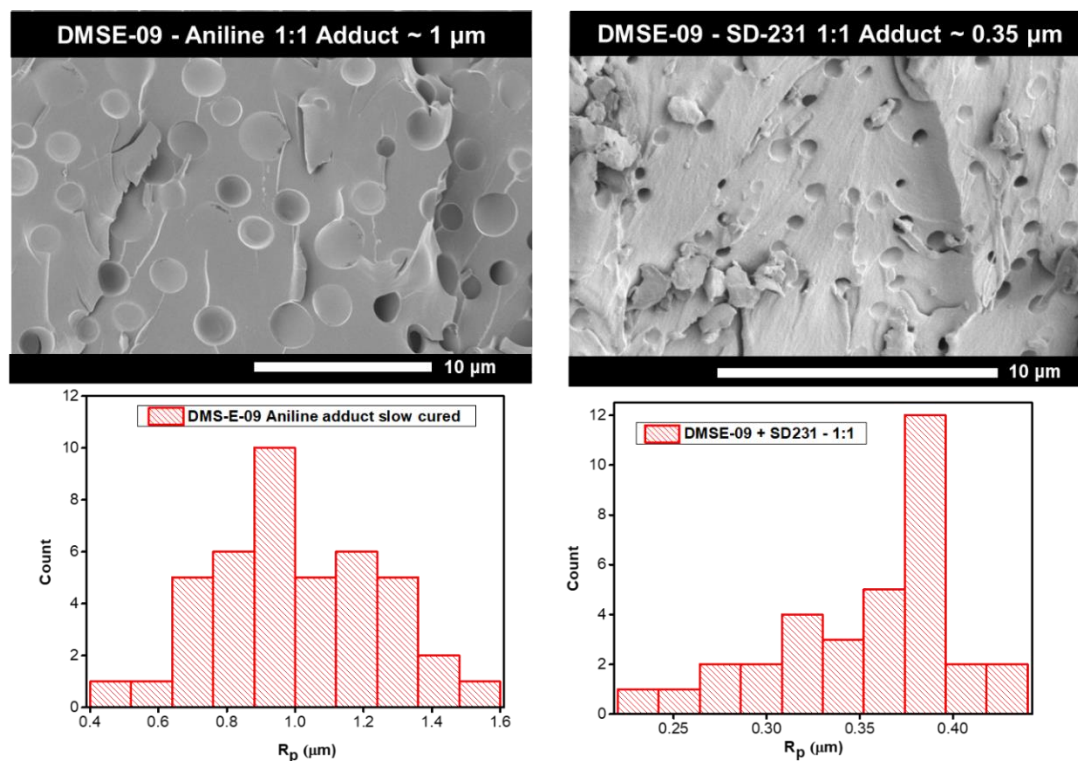


Figure 2.9: Morphology and particle size distribution of adduct composition with 15 weight% adducts as impact modifiers

All samples employing adducts as impact modifiers were made assuming complete reaction between the amines and epoxy groups during synthesis of the adduct modifiers, e.g. the functionality of the impact modifiers was not considered initially. Stoichiometric quantities of DGEBA and DDM were used and various weight percentages of adducts were added as impact modifiers. The mixtures were then cured in a one stage cure at 180 °C for 10 hours. Figure 2.9 shows the difference in particle sizes and particle size distributions that can be achieved when an epoxy functional modifier DMS-E09 is pre-reacted with aniline and SD-231 and used as an impact modifier. The particle size achieved in the case of the adduct with aniline is more than double than that obtained from the adduct with SD-231. Since aniline is an aromatic amine, the adduct with aniline might be more compatible with the DGEBA-DDM mixture thus leading to change in the onset of reaction induced

phase separation and therefore giving rise to different particle sizes. Thus, a wide range of particle sizes ranging from about 0.4 μm to 2 μm were obtained by just pre-reacting the epoxy functional reagents with different amines.

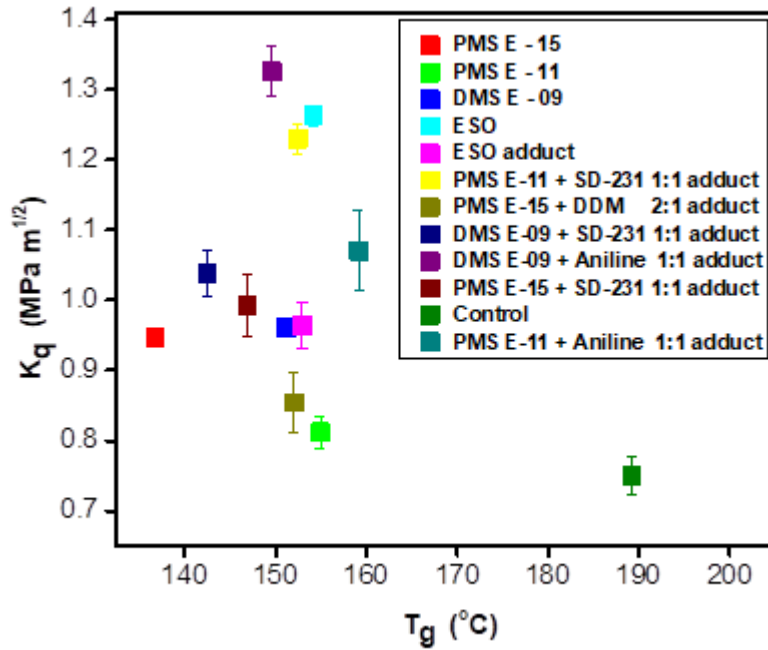


Figure 2.10: Fracture toughness as a function of T_g of all the formulations tested

When we look at the fracture toughness of these systems with respect to the glass transition temperatures of these systems we see that the samples which did not phase separate (PMS E-11, PMSE-15, DMS E-09) show moderate increases in fracture toughness but also show a large decrease in the glass transition temperatures (Figure 2.10). Lowering of the T_g is related to the lowering of yield stress and therefore we can expect to see a higher fracture toughness with respect to the control for these systems, however, larger improvement in fracture toughness is observed from the phase separated samples. Hence, we decided to look at the effect of another parameter: particle size, on the fracture toughness of these systems. To decouple the effects of lowering of T_g on the fracture toughness of the phase separated systems, it was normalized by the T_g of the control. This

trend in the fracture toughness with respect to the particle size of a variety of formulations in Figure 2.11 showed that the formulations with the largest particle size gave better fracture toughness, which is consistent with what we have learned for rubber particle toughening of brittle polymers.

There is some scatter in the data arising from irregularities in the network architecture and imbalance in stoichiometry, but the trend shows improved fracture performance with larger particle sizes. Therefore, for the DGEBA resin cured with DDM we could achieve an increase of around 100% while maintaining a T_g of 150 °C using epoxy functional modifiers which underwent reaction induced phase separation. The optimum particle size in this system was observed to be around $R_p = 1.3 \mu\text{m}$ which corresponded to an interparticle distance of 0.4 μm at a concentration of around 15wt%.

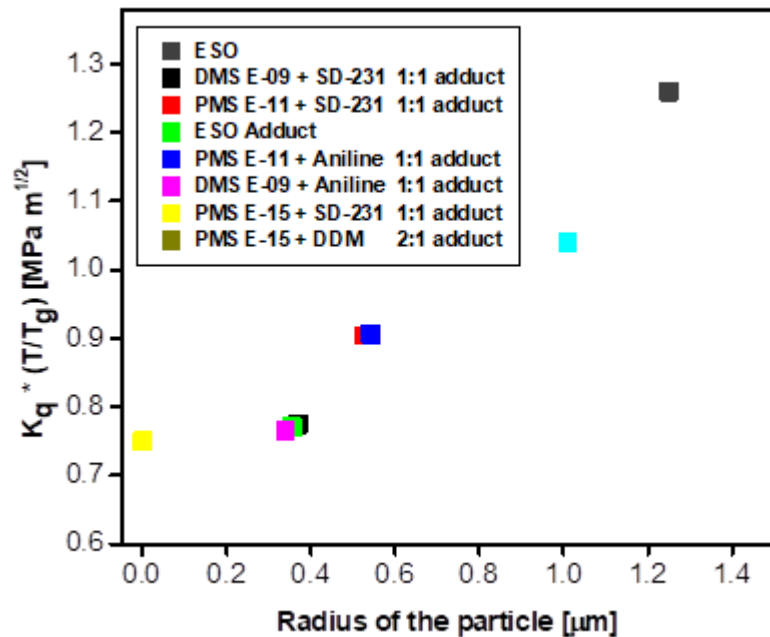


Figure 2.11: Fracture toughness vs particle size of formulations based on epoxy functional modifiers

Another major challenge is translating the improved fracture toughness performance in neat resins to composites. The incorporation of fibers reduces the amount of matrix polymer available for yielding and energy dissipation, and the confinements imposed by the stiff carbon fibers further restricts the growth of the process zone.

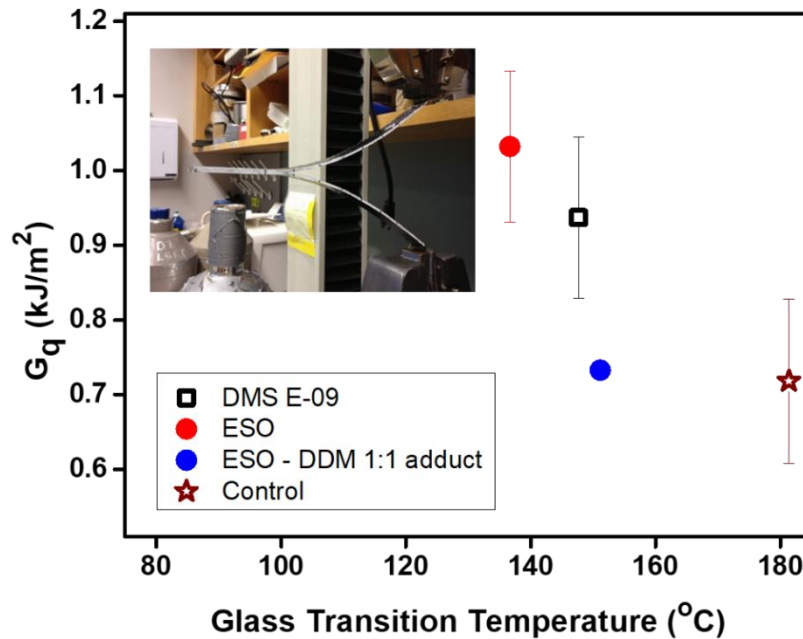


Figure 2.12: Fracture toughness of the composites as a function of their glass transition temperature

As seen in Figure 2.12, the fracture toughness of the composites displayed an increase to about 50%, for the one clear as well as one phase separated system, relative to the control. The increase in fracture toughness achieved in the neat resins however couldn't be translated to the composites due to the constraints in mentioned above in improving the fracture toughness of fiber-reinforced composites.

2.4 Conclusions

A range of functional modifiers were investigated as additives for impact modification of a crosslinked DGEBA/DDM network. Of all the modifiers screened, epoxy

functional modifiers afforded the best compatibility with the DGEBA/DDM mixture. The mechanical and thermal properties of a DGEBA/DDM system incorporating these epoxy functional modifiers were extensively evaluated. Some of these modifiers, such as ESO and adducts made from epoxy functional siloxane modifiers, underwent reaction induced phase separation, whereas other modifiers did not phase separate. Strategies were also adopted for controlling the particle size and distribution of these phase-separated systems with impact modifiers. Different cure conditions were used to achieve different particle sizes and to study the relationship between particle size, inter-particle distance and fracture toughness. In addition, adducts were made by pre-reacting the epoxy functional modifiers with amines of different functionalities and backbone structures to obtain particle sizes ranging from around 0.2 to 1.5 μm . For this particular system of DGEBA cured with DDM having a high T_g , the trend of largest particle sizes giving the highest fracture toughness was found. The optimum fracture toughness in the neat resin was with particle size of around 1.3 μm which corresponded to an interparticle distance of 0.4 μm at a concentration of 15 vol% of modifier. The fracture toughness in the carbon fiber reinforced composites was also evaluated using some epoxy functional impact modifiers and was found to be limited as compared to that obtained in neat resins.

CHAPTER 3

EVALUATING THE EFFECTS OF NETWORK DEFECTS ON THE PHYSICAL AND MECHANICAL BEHAVIOR OF GLASSY THERMOSETS

3.1 Introduction

Epoxy-based thermosets cured with different amines have been used in a variety of applications like coatings, adhesives, automotive and aerospace composites. Many of these applications involve the use of functional different fillers and additives such as adhesion promoters, impact modifiers, pigments. In chapter 2 we also showed how rubber toughening can be used to improve the inherent brittleness of single phase epoxy resins. However, there are concerns regarding the assessment of accurate functionality of these commercially available impact modifiers. Furthermore, their relative reactivity with respect to DGEBA with different crosslinking agents (hardeners) can lead to stoichiometric imbalance in the network by not completely reacting into the network. In addition, due to their different solubility in different resins and hardeners, the modifiers can act as a plasticizer instead of phase separating and producing the necessary rubbery domains. Moreover, adding fibers and nanoparticles which have undergone surface treatment for effective wetting and dispersion can also lead to imbalance in stoichiometry at local level due to their interactions with the matrix.

So, the key challenge in complex systems containing additives such as impact modifiers is characterizing their network formation and structure and what effects this has on the physical and mechanical properties of the matrix. Much research has been done on the epoxy amine reaction mechanism to inspect the development of network formation. Differential scanning calorimetry (DSC) has been used in some studies to determine the T_g

of the network with non-stoichiometric quantities of epoxy and amine, which is indicative of the homogeneity of the network.^{46,47} Theories have also been developed to predict the glass transition temperature in these networks.⁴⁸ Dynamic mechanical analysis (DMA) has been done on different non-stoichiometric ratios of epoxy and amines as well as networks with nanosilica and CNT to ascertain the impact of stoichiometry on yield stress, bending moduli and fracture toughness of these networks.^{49,50}

However, decrease in T_g can be due to plasticization, chain extension or network disruption and therefore DSC is not a selective technique to examine network structure. Also, mechanical testing at lower strains is an indicator of the processing history of the glasses and cannot be used to gauge network response. To date, no studies have been reported that use mechanical testing to correlate physical and mechanical properties of networks to the network formation and structure in epoxy thermosets and in turn relate it to an engineering property like fracture toughness.

This study addresses these concerns in a more fundamental way by purposefully altering components in non-stoichiometric amounts to impose changes in the network structure and probe how these changes alter key physical and mechanical properties. The methods employed herein will include DSC, DMA, and non-linear compression testing to distinguish between the effects of chain extension, connectivity, or plasticization, in glassy thermosets. The study then aims to correlate these fundamental physical and mechanical properties measured from these techniques to a complex engineering property like fracture toughness which is sensitive to network structure.

In contrast to tensile testing, compression testing is much more informative because it allows for larger strains to be imposed in the material since flaws are not activated and,

if done properly, suppresses geometric instabilities such as necking, crazing, or shear banding, thereby allowing for affine deformation in the non-linear regime. Previous studies where this method was employed include work on fully cured aromatic and aliphatic networks of different crosslink densities. These studies have demonstrated that the strain hardening moduli of epoxy networks were highly dependent on their crosslink densities while being independent of backbone stiffness⁵¹. Similarly, Detwiler and Lesser⁵² have also analyzed network formation in glasses during the process of curing. By investigating the network formation of partially cured epoxies cured at different temperatures, they established that the large strain response of the networks was strongly correlated with the connectivity of the network.

Zhang, Detwiler *et al* performed DMA and compression testing on symmetric double networks cured with aromatic and aliphatic amines.⁸ More recently Ganguly and Lesser also measured the non-linear properties of asymmetric double networks using non-linear compression techniques and DMA.⁹ The symmetric double networks were synthesized using varying fractions of aliphatic and aromatic amine and systematic three-stage curing of DGEBA resin with aliphatic and aromatic amines was done to synthesize the asymmetric networks. When these networks were tested above their glass transition temperature, the strain hardening regime showed significant differences from single networks of the same cross-link density. Fracture toughness of the double networks also was higher than their single network counterparts with similar molecular weight between the crosslinks. Thus, a non-linear engineering property like fracture toughness could be correlated to the properties of the network and the details of network formation could be captured using compression testing at higher strains.

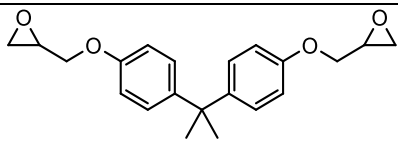
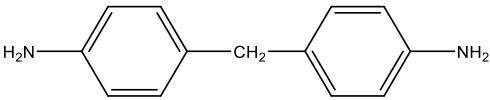
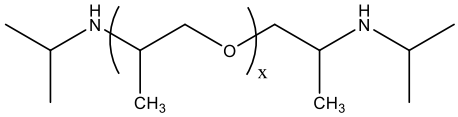
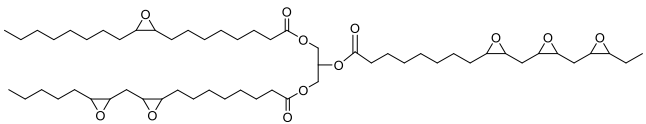
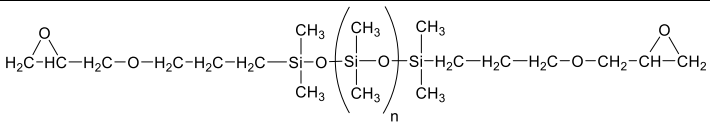
By employing DMA and compression testing, we can observe not just the thermal response of the networks and their α transitions but also the mechanical post-yield stress response. This can enable us to calculate network connectivity as well as give information on segmental mobility and chain packing thus making it excellent probes to estimate the network defects. Thus, the effect of functional additives on stoichiometry in the epoxy networks can be understood and ultimately aid in formulating epoxy networks with good fracture toughness by calculating the amount of epoxy or amine needed for perfect stoichiometry.

3.2 Experimental

3.2.1 Materials

DGEBA (Epoxide Equivalent weight ~ 175 g/mol) DOW ER 332 was purchased from Olin chemicals and Diaminodiphenylmethane DDM, (Amine equivalent weight = 49.565 g/mol) was obtained from Sigma Aldrich. The mold release agent Surfasil was purchased from Pierce chemicals. The siloxane functional reagents obtained from Gelest Inc. and the epoxidized soybean oil (ESO) obtained from Spectrum chemicals were used as the impact modifiers for the epoxy resins. SD-231 (Amine equivalent weight ~ 158 g/mol) supplied by Huntsman corporation was reacted with a siloxane functional modifier, DMS E-09 (Epoxide equivalent weight ~ 181.5 g/mol) in a 1:1 stoichiometric ratio to obtain an adduct for use as impact modifier. All the chemicals were used without further purification unless otherwise specified.

Table 3.1: List of all chemicals used

Chemical name	Chemical structure
Diglycidylether of Bisphenol - A	
Diaminodiphenylmethane (DDM)	
SD-231	
Epoxidized soybean oil (ESO)	
DMS-E-09	

3.2.2 Sample preparation

A range of epoxy networks with non-stoichiometric ratios 1.1:1, 1.2:1, 1.3:1, 1.4:1 and 1.5:1 (10%, 20%, 30%, 40%) of excess epoxy resin and excess amine were prepared with DGEBA and DDM and used as model systems to investigate the effect of network formation on yield behavior of glasses. The amount of DDM required to make an epoxy or amine rich network was dissolved in the DGEBA resin at 80 °C until a clear solution was formed and then quickly poured into rectangular glass plates which were treated with the mold release agent Surfasil and separated by a 3mm Teflon spacer. All the plaques were cured in a nitrogen purged oven in a two-stage cure schedule: 120 °C for 4 hours and 180 °C for another 4 hours.

For compression testing samples, the clear solution was poured in test tubes treated with Surfasil and cured in a nitrogen purged oven at 120 °C for 4 hours and 180 °C for 4 hours.

For DMA, the specimens were made by pouring the different non-stoichiometric epoxy formulations in rectangular glass plates which were treated with the mold release agent Surfasil and separated by a 1 mm Teflon spacer.

3.2.3 Glass transition temperature

The glass transition temperature was measured using TA instruments DSC Q200 as described in Chapter 2 Section 2.2.3.

3.2.4 Fracture toughness

Fracture toughness measurements were made following ASTM standard D5045-99 as described in Chapter 2 Section 2.2.4.

3.2.5 Compression Testing

Cylindrical bullets with 1:1 height-to-diameter ratio were machined from samples cured in test-tubes (Diameter ~ 15.4 mm). Both the edges of the bullets were polished to make them parallel to each other and perpendicular to the sides of the sample. According to ASTM D695, the samples should have a height to diameter ratio of 2:1 but machining them to 1:1 decreases the possibility of samples buckling during the experiment. In addition, just prior to the experiment each end of the bullet was coated with silicone oil and covered with PTFE tape. A drop of silicone oil was also placed on each platen between the PTFE tape and the sample. This helps in creating a nearly frictionless surface and ensures

gross yielding throughout the height of the sample and affine deformation over a large range of strains.

Uniaxial compression test was conducted on an Instron 5800 universal tester fitted with a 50kN load cell at 20 °C at a constant true strain rate of 0.1 mm/mm/min controlled using Bluehill software. In the plot of true stress vs. $\lambda^2 - 1/\lambda$, the strain hardening modulus (G_R) was calculated using the equation 3.1 below at 90% true strain of the sample.

$$G_R = \frac{\partial \sigma_t}{\partial (\lambda^2 - 1/\lambda)} \quad (3.1)$$

Where, σ_t is the true stress, $\lambda^2 - 1/\lambda$ is the Neo-Hookean strain, and λ is the compression ratio. Different research groups have similarly used non-linear compression testing on glassy thermoplastics to measure the post-yield response and calculate the strain hardening modulus and correlate it to the entanglement density of the thermoplastics.^{53,54,55}

3.2.6 Dynamic mechanical analysis (DMA)

The specimens were machined to the dimensions of 2 cm x 1 mm x 1.5 mm from the epoxy plaques. TA instruments DMA Q800 was used to measure the storage modulus, loss modulus and $\tan \delta$ as a function of temperature. The samples were subjected to a temperature sweep of 3 °C/min from 40 °C to 240 °C at a frequency of 1 Hz. The rubbery plateau moduli were recorded at temperature $T_g + 40$ °C. The full width at half maximum was obtained from the $\tan \delta$ peak of the α transition by fitting the peak to a Gaussian curve.

3.3 Results and discussions

3.3.1 Fracture toughness testing

The toughening of epoxy resins and carbon fiber reinforced composites by different functional modifiers was investigated in this study. The reactive functional modifiers were so chosen that they react either with the oxirane ring of the DGEBA or the amine functional group of the DDM. Out of all the modifiers used, the epoxy functional modifiers were compatible with both the DGEBA and the DDM which means that they formed a homogenous solution with the DGEBA and the DDM used. The stoichiometry of the DGEBA and the DDM required was adjusted to adapt for this reaction of the impact modifiers with the DDM. When the ESO was formulated into the system, it was initially completely miscible in the DGEBA-DDM mixture and then phase separated out to form spherical rubbery domains of the size of about 3-4 μm as the molecular weight of the network structure grew. (Fig. 3.1 a) The plaque made from DMS-E-09, however, stayed clear and did not turn opaque unlike the plaque made with ESO.

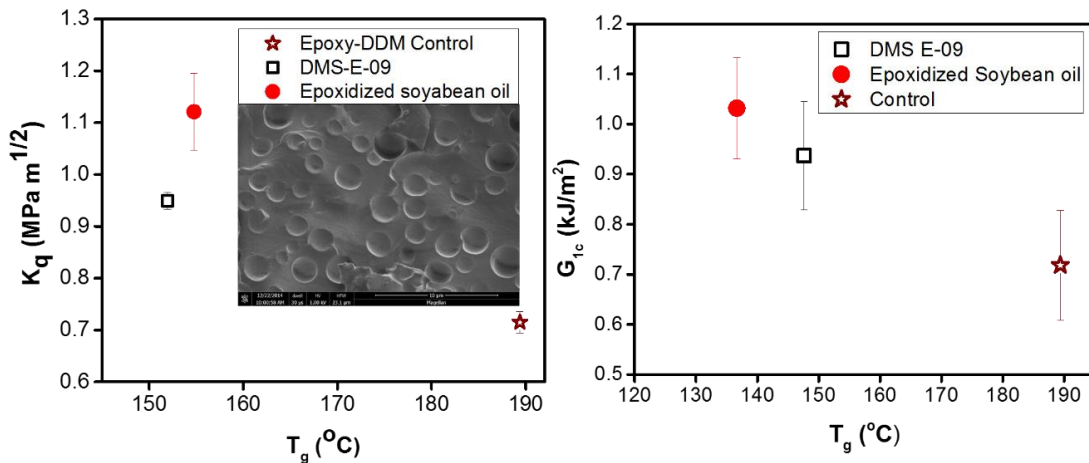


Figure 3.1 a: Fracture toughness in the neat resin of the impact modified formulations as a function of glass transition temperature. Inset: SEM image of the ESO modified formulation at 15 wt% b) Fracture toughness of the impact modified formulations as a function of glass transition temperature in carbon fiber reinforced composites.

The fracture toughness of the systems with impact modifiers improved by 50% over the control in the neat resin. However, there was a marked drop in the T_g associated with this improvement. A similar trend is observed when the fracture energy of the carbon fiber reinforced composites is evaluated. (Figure 3.1 b) This leads to the question whether the improvement in fracture toughness was because of plasticization of the matrix or yielding at lower stresses due to decrease in T_g or conventional rubber toughening mechanisms due to phase separation.

Furthermore, The DSC curing exotherms of the reaction of DMS-E-09 used with DDM show that the DGEBA starts reacting with the DDM at 90 °C with a maximum curing exotherm at 120 °C which is much lower than the maximum curing temperature of DMS-E-09 (~200°C) (Figure 3.2). This difference in the relative reactivity indicates that by the time the modifiers start reacting with the DDM, the DGEBA resin has almost completely reacted. At this point, the network would be vitrified, and the reactivity of the modifier would be then limited to diffusion within the glassy matrix, thus also possibly disrupting the network structure. Hence, some amount of impact modifier can react into the network while the other fraction just remains soluble and plasticizes the matrix.

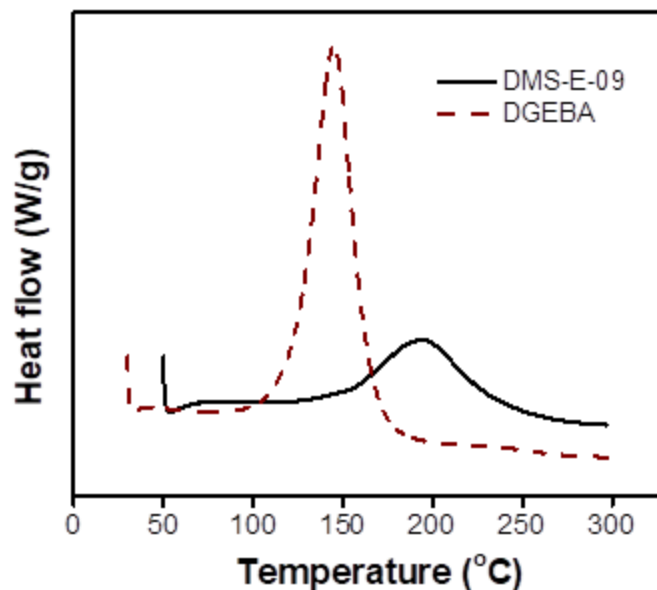


Figure 3.2: Curing exotherms of the reaction of DGEBA and DMSE-09 with DDM obtained by DSC

This can lead to an excess of either epoxy or amine groups in the crosslinked network. Thus, it is difficult to predict the functionality as well as the reactivity of these functional modifiers and to correlate its effects on the formation of these epoxy networks. So, the key challenge faced when additives are introduced in the system is finding a technique to determine any disruption in network formation.

In order to investigate the effects of impact modification on the network architecture and properties, we systematically disrupted our network of DGEBA and DDM by going out of stoichiometry in the amine rich and the epoxy rich direction. The thermal and mechanical properties of the non-stoichiometric formulations were probed to investigate their effects on network structure.

3.3.2 Calculation of crosslink density based on stoichiometry

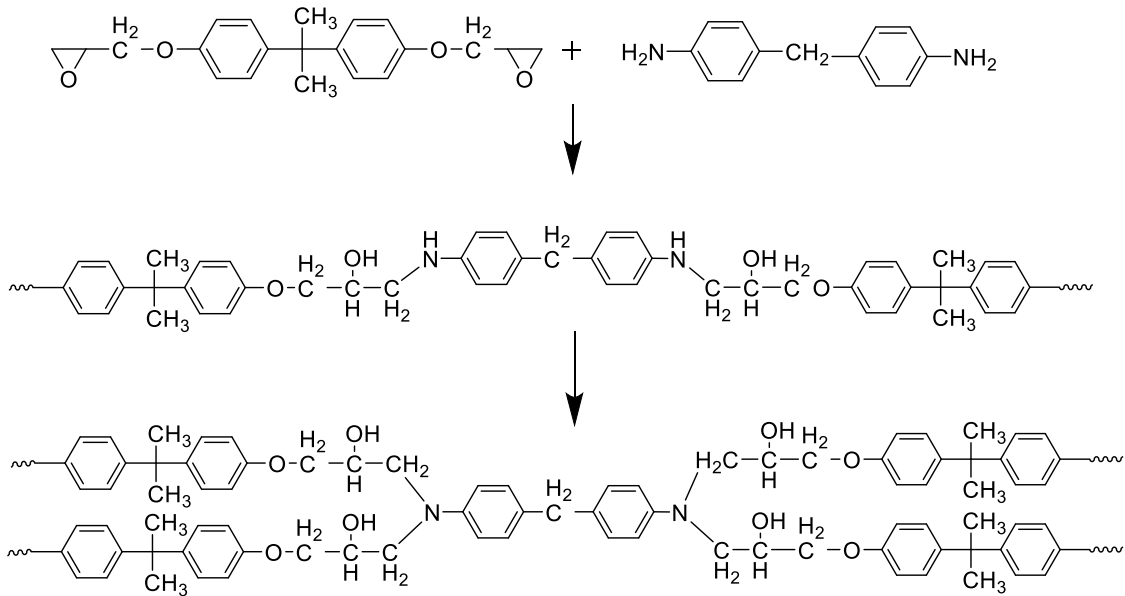


Figure 3.3: Main crosslinking reactions in the formation of DGEBA-DDM crosslinked network

M_c in epoxy rich networks is calculated by the following equation:

$$M_c = 2 * (M_{ep} * x + M_a) \quad (3.2)$$

Where M_{ep} is the epoxide equivalent weight of the DGEBA resin (~175 g/mol), x is the percent mole excess and M_a is the amine equivalent weight of the cross-linker, DDM (49.565 g/mol) For a perfectly stoichiometric network, M_c is 450g/mol.

For amine rich networks, the average molecular weight between crosslinks of the out of stoichiometry networks is calculated by assuming that the primary amine groups of the tetra functional DDM react with the epoxy group first thus making it a di-functional amine and then it crosslinks the remaining epoxy groups as a tetra functional cross linker.

$$M_c = \frac{1}{2} * \left(\frac{100 * Mol. wt_{ep} + x * Mol. wt_a}{(100 - x)} \right) \quad (3.3)$$

Where $Mol. wt_{ep}$ is the molecular weight of the epoxide monomer and $Mol. wt_a$ is the molecular weight of the amine and x is the molecules of amine reacted per 100 epoxy groups.

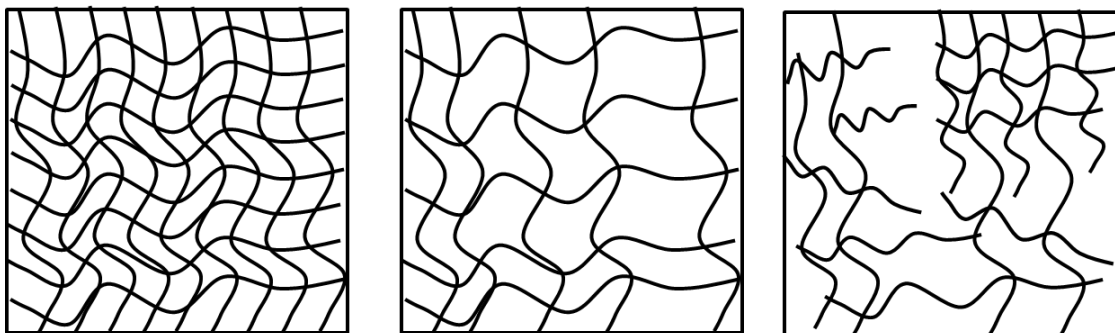


Figure 3.4: Schematic of a) 1:1 Epoxy: Amine b) Amine excess c) Epoxy excess network.

Figure 3.3 shows the reaction scheme for the general curing reaction of the epoxy resin with an amine. If we have perfect stoichiometry of epoxy and amine groups in the network, the network should be fully crosslinked like the one in Figure 3.4 (a). In the case of amine rich networks, the epoxide groups on the DGEBA react first with the primary amine groups leading to chain extension and the secondary amine groups thus formed, crosslink with the remaining epoxide functionality. This leads to a fully intact but more lightly crosslinked network architecture as seen in Figure 3.4 (b). In the epoxy rich networks however, there isn't enough amine functionality for chain extension and crosslinking and hence there are regions in the network where the crosslink density is similar to that of the perfect network but there are also regions with dangling chain ends, low molecular weight oligomers and even unreacted monomers which leads to a fragile, fragmented network similar to the one in Figure 3.4 (c).

3.3.3 Differential scanning calorimetry

One of the traditionally used techniques to probe network defects is using the reduction in glass transition temperature to demonstrate network disruption.

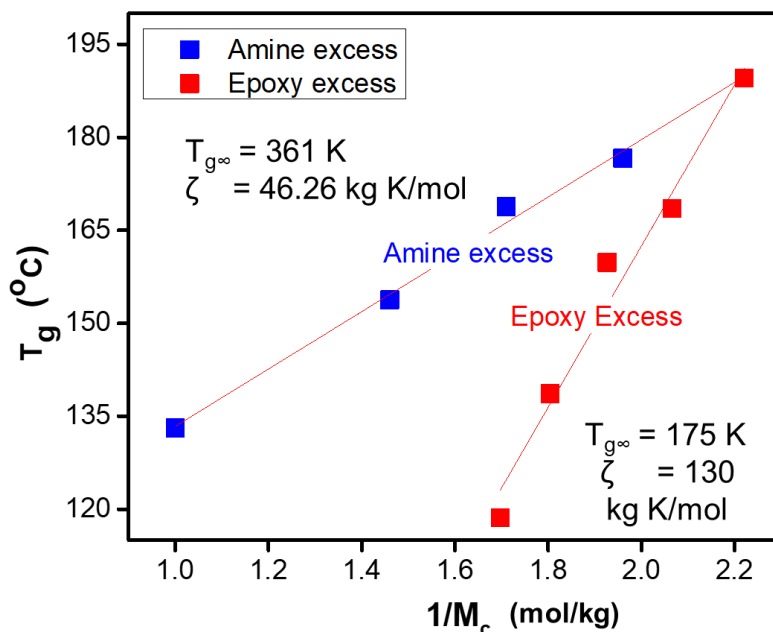


Figure 3.5: Plot of glass transition temperature vs crosslink density of the epoxy networks with different stoichiometries.

As we plot the T_g of the networks with respect to the crosslink density of these networks, we can see that the T_g decreased in the non-stoichiometric networks as the amount of excess epoxy or amine is increased. This reduction in T_g , however, is not symmetric for excess epoxy and amine in the system. The networks with excess epoxy show a more detrimental effect on the T_g of the network as compared to the excess amine formulations. (Figure 3.5)

Changes in network rigidity, plasticization or network structure and connectivity can affect the T_g of a network. Previous work in the group has shown that changing the chemical backbone (aromatic vs aliphatic), adding fortifiers (anti-plasticization) and changing the network architecture (varying crosslink density) can alter the T_g of the

crosslinked epoxy network.^{56,57,58,52} In the case of amine rich networks, as we increase the excess of amine, more of the amine groups act as chain extenders and less of them act as cross linkers, thus decreasing the T_g of the network. With the epoxy rich networks, the dangling epoxy chain ends increase the free volume in the network and also disrupt the network connectivity leading to a decrease in the T_g of the network as the amount of excess epoxy groups is increased.⁴⁸ The molecular mobility is also associated with the number of crosslinks and crosslink density and thus networks with lower crosslinks and crosslink density (out of stoichiometry networks) progressively decrease in T_g as the networks go out of stoichiometry. The epoxy networks have a much steeper decrease in the T_g because, unlike the amine rich networks, the network is fragmented and the T_g is a response of a completely connected network. Also, the chain ends due to uncrosslinked epoxy groups have higher segmental mobility and have a more pronounced effect on the T_g .

However, T_g is not a selective technique as the decrease in glass transition temperature can be due plasticization, chain extension or a fragmented network. The Flory-fox equation (Equation 3.4) predicts the T_g of the crosslinked epoxy polymer as a function of the number of crosslinks.

$$T_{gx} = T_{g\infty} + \frac{\zeta}{M_c} \quad (3.4)$$

Where T_{gx} is the T_g value of the crosslinked polymer having molecular weight between crosslinks M_c , $T_{g\infty}$ is the value of the polymer of unlimited molecular weight or the uncrosslinked homopolymer of the monomers used for crosslinking. ζ is a constant that relates to the free volume of a given polymer.

The T_g value for the un-crosslinked polymer obtained from the fits of Flory-Fox equation⁵⁹ seen above for amine rich networks agrees fairly well with the T_g value expected

of a linear DGEBA: functionalized DDM homopolymer ($T_g = 354$ K) whereas the value obtained for the epoxy rich networks is much lower than the literature value; indicating that T_g alone is not a very good indicator of network architecture. Since T_g alone cannot clearly indicate the mechanism of network disruption, in this study we have used non-linear compression testing as another technique to characterize network structure.

3.3.4 Non-linear compression testing

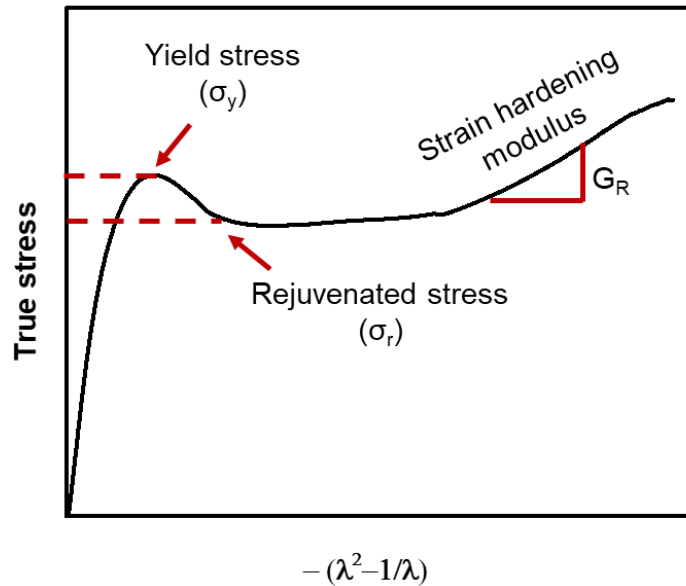


Figure 3.6: Generic True stress vs Neo-Hookean strain curve for glassy polymers. The dashed lines indicate yield stress and rejuvenated stress in the polymer.

Figure 3.6 shows a typical compression curve for glassy polymers. The low strain region of the curve provides information about the chain packing and processing history of the glass, and at large strains, information about network formation and connectivity can be garnered.⁵⁴ The compressive modulus is calculated as the slope of the initial linear elastic region of the true stress vs true strain curve at less than 1% strain. The yield stress of the network is the maximum stress at which the slope of the true stress vs true strain goes to zero. The material overcomes the energy barriers required for segmental mobility

and starts deforming in a plastic manner after the yield stress is reached.⁶⁰ For a glass that has been quenched and aged, once you deform it enough to disrupt the Van der Waals forces between the chains, the glass reaches the rejuvenated state and its only at high strains that we can measure the response due to entanglement if it is an amorphous glass or crosslink density if it is a crosslinked network. This stress minimum that occurs on the compression curve after the large-scale plastic deformation occurs in a material is referred to as the rejuvenated stress σ_T . At large strains post the stress drop after yielding, the stress increases further as the stress is now being applied to the covalent bonds if it is a crosslinked network or physical entanglements if it's a glassy thermoplastic. The response of the networks now can be more accurately characterized using a neo-Hookean strain instead of using true strain. The slope of the true stress vs the Neo-Hookean strain is the strain hardening modulus, G_R . Hence, it is the intra and intermolecular interactions between the chains that dictate the properties of the networks at low strains and only after deforming the polymer at large strains we can kinematically erase the thermo-mechanical history to gather the response due to connectivity of the network.

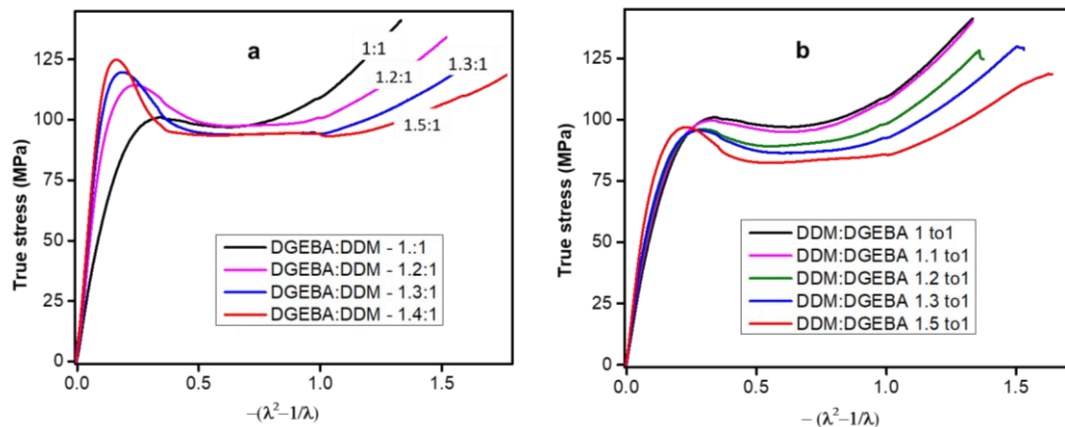


Figure 3.7: True stress vs $-(\lambda^2 - 1/\lambda)$ curves for a) Epoxy excess and b) Amine excess epoxy networks.

Since we wanted to study the non-linear properties of the network, compression testing was a better test method than a tension test as it prevents premature failure of the polymer due to flaws and defects in the network and geometric instabilities like necking and crazing.

When compression testing was performed on these networks, the compression curves in Figure 3.7 showed that there was no significant effect on the yield stress and modulus of the amine rich networks, but the strain hardening modulus increased systematically as the networks went further out of stoichiometry. In contrast, the epoxy rich networks showed a marked increase in their yield stress and modulus with increase in stoichiometric imbalance. Their strain hardening modulus also showed a sharp decrease as compared to that of the amine rich networks. Qualitatively too, the epoxy rich networks were more brittle and failed at lower strains than the amine rich networks due to stiffening and densification.

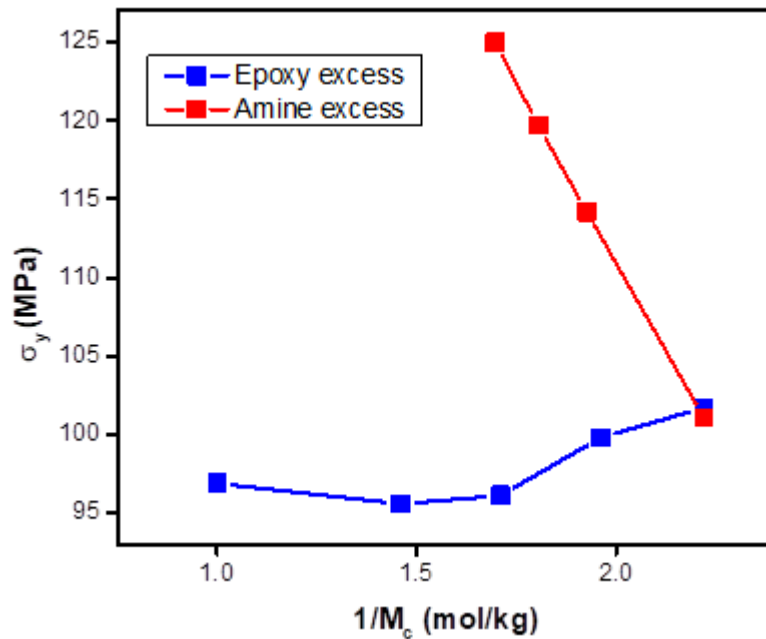


Figure 3.8: Yield stress against $1/M_c$ for both epoxy rich and amine rich epoxy networks. The modulus increases with decreasing crosslink density.

When the chains in the glassy polymers can no longer relax and realign when subject to deformation, yielding occurs in glassy networks. The yield stress of the epoxy networks increased as the networks became more epoxy rich in nature. This is akin to the effects of physical ageing in glassy networks (Figure 3.8). As glassy networks age physically, the free volume of these thermodynamically non-equilibrated amorphous structures decreases by molecular rearrangements and chain realignments taking place as they come closer to being in equilibrium. This leads to physical densification and stiffening of the networks.⁶¹ Now, for epoxy networks which are out of stoichiometry, there are fewer crosslinks and more dangling chain ends and low molecular weight oligomers. These increase as the networks go further out of stoichiometry. It is known that the chain-ends or the dangling epoxy groups have more conformational entropy and therefore can easily realign and orient as stress is being applied to the network.

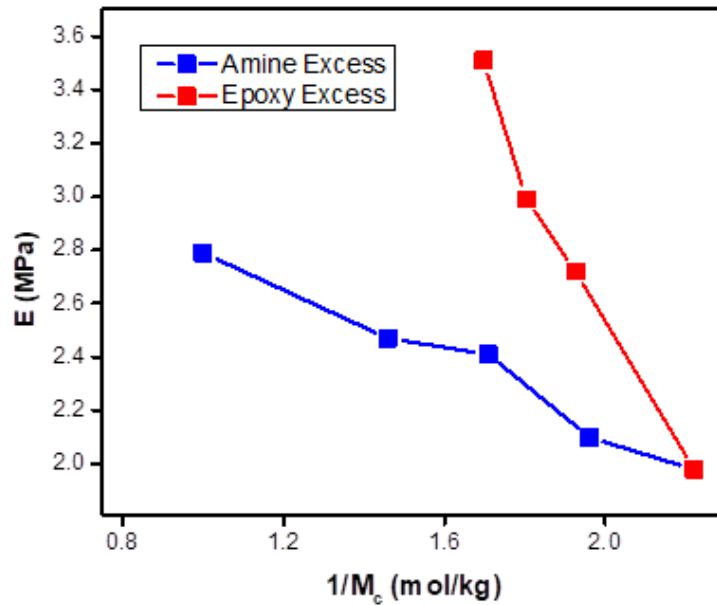


Figure 3.9: Compressive modulus plotted against 1/M_c for both epoxy rich and amine rich epoxy networks. The modulus increases with decreasing crosslink density.

The steric topological restrictions imposed due to crosslinked chains is higher than free chain ends and therefore the free ends pack better and increase the yield stress of the networks.^{62,63}

The modulus of both the excess epoxy and amine rich networks increased with increasing molecular weight between crosslinks as illustrated in Figure 3.9. While this is counter intuitive, it is related to the amount of unreacted epoxy and amine groups in the networks. For glassy networks much below their T_g , the crosslinks are immobile at test temperatures. The polymer chains between the crosslinks is what is being deformed and hence the stiffness is not governed by the crosslink junctions but by the bonds between them. Since the small unreacted groups can pack more effectively than the chains between the crosslinks in the networks, they reduce the free volume available for segmental mobility of the chains in the network. The modulus thus increases with increased amount of excess epoxy or amine groups. In case of the epoxy excess, the modulus increases more than the amine excess because of the dangling ends and low molecular weight oligomers that have more conformational freedom than the secondary amine groups inside the network thus leading to the densification of the network caused by filling of the free volume of the network by the unreacted epoxy groups. This has also been proven previously by Bellenger *et al* using dynamic mechanical analysis measurements where the loss modulus decreases when the system is cured with non-stoichiometric quantities of amine as compared to those cured at stoichiometry.^{64,65} This increase in both the modulus and yield stress of epoxy rich networks is similar to the effects observed due to physical ageing as demonstrated by McKenna *et al*.⁶¹ Previous work by Detwiler and Lesser has shown that partially cured epoxy networks showed increase in both yield stress and modulus due to densification as

the unreacted epoxy monomers, low molecular weight constituents and dangling epoxy groups can rearrange and pack more efficiently.⁵²

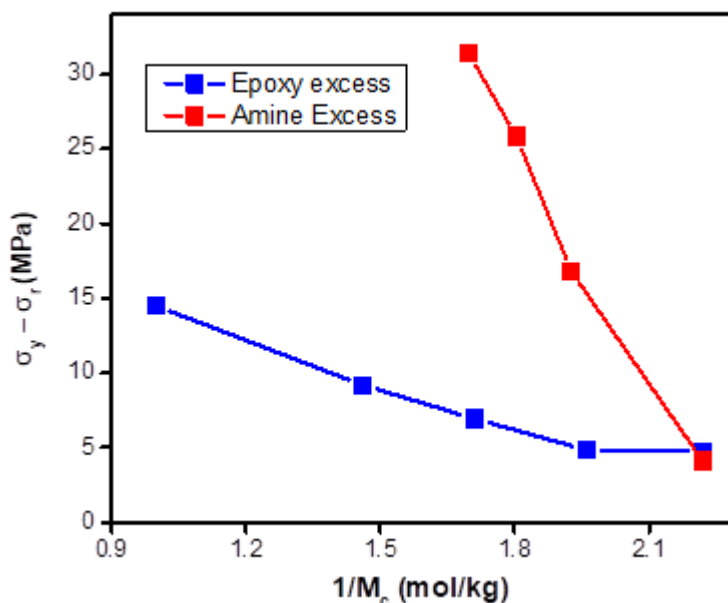


Figure 3.10: Post yield stress drop increases in networks with amine excess and more steeply in networks with epoxy excess.

The rejuvenated stress is the point on the true stress - strain curve where the stress is minimum after localized plastic deformation. As shear bands are forming in the material, the measured stress drops. The stress continues to decrease after yielding as more shear bands form in the material and reaches a minimum when shear bands incorporate more and more material in the compression bullet. The post yield stress drop is the difference between the yield stress and rejuvenated stress of the polymer. Figure 3.10 showed that the post yield stress drop is proportional to the crosslink density of the networks and increases with increased molecular weight between crosslinks.⁶⁶

The amine rich networks showed a smaller drop in the stress after yielding compared to that of the epoxy networks. Previous work by Detwiler et al has demonstrated that while yield stress is dependent on the thermomechanical history of the polymer, the

rejuvenated stress is dominated by the network connectivity than thermomechanical history. Therefore, as the molecular weight between crosslinks increases, the rejuvenated stress should decrease. This is exactly what we see in the Figure 3.10. In both the networks with excess epoxy and amines, rejuvenated stress is smaller than the yield stress of the networks. The yield stress is indicative of how efficiently the chains pack between the crosslink junctions. The rejuvenated stress is a measure of the stress required for plastic flow to continue after the yield point of the polymer. If a network is perfectly crosslinked with stoichiometric quantities of epoxy and amine, we see a minimal drop in the stress after yielding. The network chains are well connected and therefore resist any further plastic deformation in the polymer. In case of fully intact but loosely crosslinked amine rich networks, the stress drop, while not very significant, still exists because of the imperfect network architecture. The stress drop increases due to increasing imbalance of stoichiometry. In epoxy rich networks, the higher post yield stress drop is due to the fact that the yield stress increased with increasing stoichiometric imbalance due to efficient chain packing of the unreacted epoxy groups⁶³ whereas the rejuvenated stress decreased because of the disruption in network connectivity due to the formation of dangling chain ends due to unreacted epoxy groups in the network.

Considerable research has been done to study the post yield behavior of thermoplastic glasses. Yielding in polymers is a thermally activated phenomenon and the polymer can be described as behaving more like a rubber with crosslinks than like a glassy polymer at its yield stress.

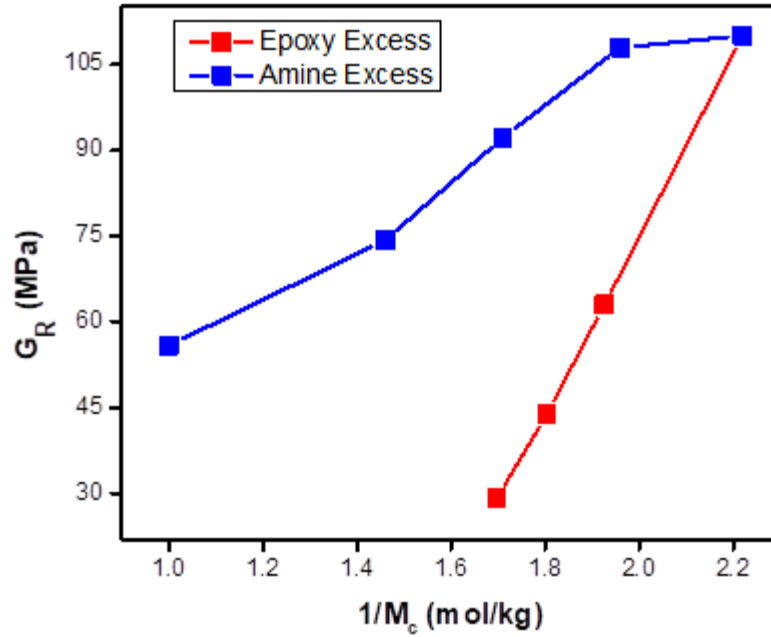


Figure 3.11: The strain hardening modulus is dependent on the network connectivity when plotted against $1/M_c$ for networks

Various groups have used rubber elasticity models to predict the behavior of thermoplastics with physical entanglements at large strains. An important concept based on these models is the association of stress to the changes in entropy of the entangled network at high strains leading to strain hardening. Constitutive equations have been developed by various groups to describe the strain hardening response.^{67,68,69,70,71} These equations use Neo-Hookean type of behavior to explain the strain hardening response of polymers at high strains. In this type of response, the strain hardening modulus which is the slope of the linear region of the neo-Hookean strain vs true stress is calculated using the following equation:

$$\sigma_T = G_R \left(\lambda^2 - \frac{1}{\lambda} \right) \quad (3.5)$$

where σ_T is the true stress of the material, G_R is the strain hardening modulus, λ is the extension ratio.

For thermoplastics with molecular entanglement networks, the strain hardening modulus is related to the molecular weight between entanglements by the following equation:

$$M_e = \frac{\varphi \rho R T}{G_R} \quad (3.6)$$

Where T is the test temperature, ρ is the mass density of the polymer and R is the gas constant. φ is the constant related to mobility of the crosslinks which for immobile crosslinks can be assumed to be equal to 1. For glassy thermosets like epoxies, the entanglements are covalently bound crosslinks instead of being physical and therefore M_e is equivalent to M_c , the molecular weight between crosslinks.

From Equation (3.6), it is clear that the strain hardening modulus is inversely proportional to the molecular weight between crosslinks and therefore should increase as the crosslink density increases. Figure 3.11 shows that the correlation is true for our networks as it increased with increasing crosslink density for both the epoxy and amine rich network. The strain hardening modulus decreased markedly in epoxy excess networks than the amine excess networks. This is because it is a measure of the connectivity of the network and therefore a more fragmented network has a greater effect on the strain hardening modulus than a fully intact one.

We can see that in both epoxy and amine rich networks, slope of the true stress vs the neo Hookean strain increases does not increase linearly but has a steeper increase. This is because, the constitutive equation relating the strain hardening modulus to the molecular weight between crosslinks is assuming Gaussian coil deformation behavior without finite extensibility. For tightly covalently crosslinked epoxy networks with high crosslink densities, finite extensibility of the network and steric hindrances can come into

consideration. These networks instead of following a purely neo-Hookean behavior are expected to follow a more inverse Langevin type of response. Further research needs to be done to model these networks by including inverse Langevin and other functions but for the scope of this work, the trends in the strain hardening moduli are quite evident using the current methods.

Thus, the linear region and the non-linear region of the compression curves along with the T_g can capture details of network formation.

3.3.5 Fracture toughness testing on non-stoichiometric networks:

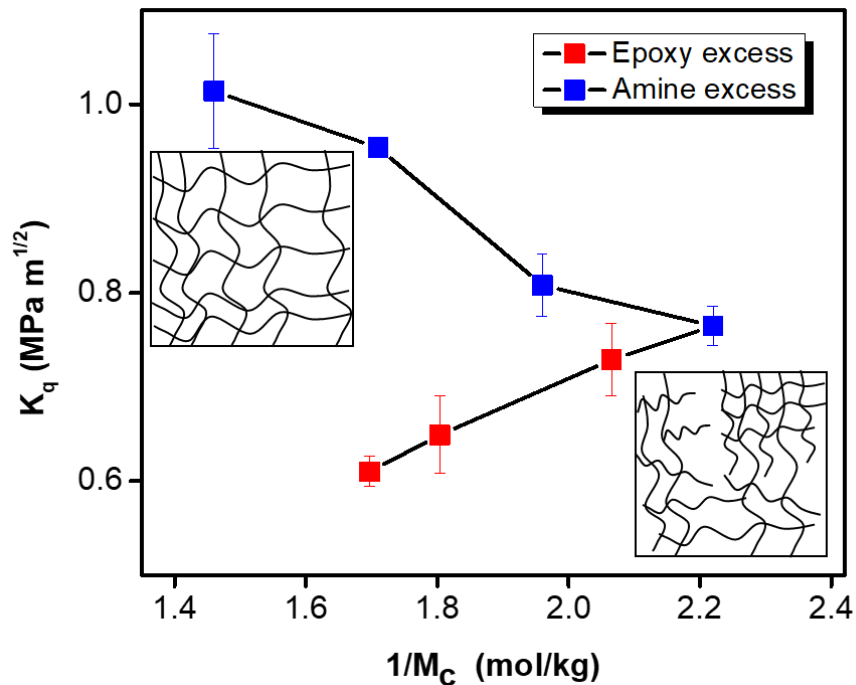


Figure 3.12: Fracture toughness of the out of stoichiometric networks as a function of the crosslink density

When we looked at the compact tension fracture toughness of the epoxy rich and amine rich networks, we saw that the epoxy rich formulations have a lower fracture toughness than the control. This is expected from a heterogenous fragmented network

whereas the amine rich networks with a fully intact but lightly crosslinked network show increase in the fracture toughness as stoichiometric imbalance increases.

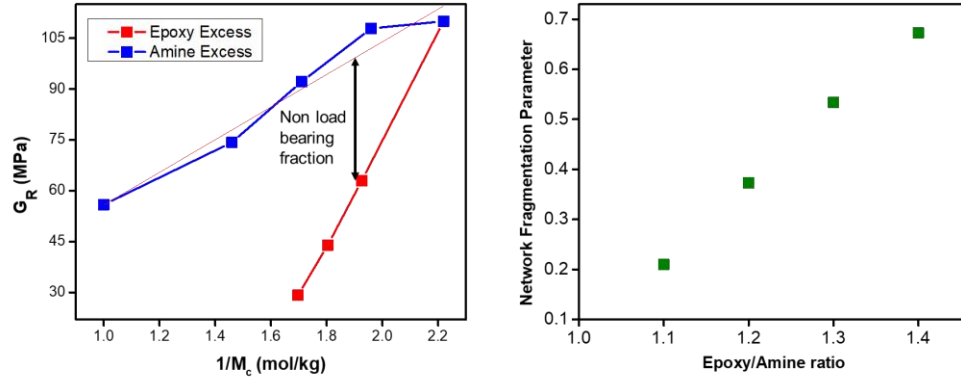


Figure 3.13 a) Strain hardening modulus as a function of crosslink density for non-stoichiometric networks b) Load bearing fraction of the epoxy excess networks with increasing stoichiometric imbalance.

This trend in the fracture toughness can be explained in terms of fraction of the epoxy rich networks which is not completely crosslinked into the network and therefore, does not contribute to the toughness. Since the excess amine groups act as chain extenders, it leads to a fully crosslinked network with lower crosslink densities as we increase the percentage mole excess of amine in the network. Because it is a fully crosslinked network, the entire network contributes to the load bearing properties and the strain hardening modulus is indicative of the network connectivity of a fully crosslinked network at that cross-link density. The epoxy rich network has a fraction which contributes to the load bearing property of the network and the other which is fragmented. If the network with epoxy excess was a fully crosslinked network, it should have the same strain hardening modulus as that of the amine rich networks at a given cross-link density, however, the strain-hardening modulus is much lower as and the difference between the strain hardening modulus as seen in Figure 3.13 a) is the non-load bearing fraction of the fragmented

network which does not contribute to the strain hardening modulus. Now, the fraction of network which is fully crosslinked into the network can be given by:

$$\frac{X_{CL} - X_{CF}}{X_{CL}} \quad (3.7)$$

Where, X_{CL} is the crosslink- density of the load bearing fraction, and X_{CF} is the crosslink density of the non-load bearing fraction.

As seen from Equation 3.6, the strain hardening modulus is proportional to the crosslink density X_C

$$M_c \sim \frac{1}{G_R}; G_R \sim X_C$$

Therefore, the percentage of the network which is completely crosslinked can be defined by the strain hardening modulus:

$$\frac{G_R^a - G_R^e}{G_R^a} \quad (3.8)$$

Where G_R^a is strain hardening modulus of the load bearing amine excess network and the G_R^e is the strain hardening modulus of the non-load bearing fragmented epoxy excess network

Figure 3.13 b) shows the load bearing fraction of the epoxy excess networks with increasing stoichiometric imbalance. It is evident that even with 20% excess of epoxy groups in the network, only 65% of the network is non-load bearing and this fraction decreases rapidly as more epoxy groups are added to the network.

In order to interpret the relationship between the information gathered from compression testing regarding chain packing and connectivity of the network and relate it to a non-linear engineering property such as fracture toughness, a parameter was proposed which quantifies the strain localization in the material.

Haward *et al* put forth a strain localization criterion which related yield stress and strain hardening modulus of the network to λ , the draw ratio or the extension ratio in the necked material. If the ratio was less than 3 then the material underwent an affine deformation and if it was greater than 3, the strain was localized in the form of a neck. This criterion was further modified by van Melick and van Govaert to the ratio between yield and the rejuvenated stress, K_y . This ratio is a measure of the stress necessary to disrupt the chain packing in the polymer and cause plastic deformation compared to the stress required for deformation after yielding. (Equation 3.9)

$$\frac{\sigma_y}{G_R} = \frac{\left(\lambda - \frac{1}{\lambda}\right)}{\left(K_y \lambda - 1\right)} \quad (3.9)$$

For different stoichiometric ratios of epoxy and amine, we can calculate the draw ratio in the necked material. The higher the extension ratio needed to stabilize the neck, the more is the strain localization in the material. Physical aging which increases the K_y , thus increases λ . As λ increases the material becomes more brittle. Therefore, λ can be interpreted as a strain localization parameter or is a measure of ductility in the system.

For highly crosslinked glassy epoxy networks, plastic deformation predominantly occurs via shear banding as compressive loading suppresses the geometric instability which leads to necking. In previous work Lesser *et al* extended the concept by Haward and Goveart to put forth a shear band stability criterion, which relates the octahedral shear stress and K_y to the extension ratio, λ required to stabilize a shear band. (Equation 3.10)

$$\frac{\sqrt{2}}{3} \frac{\sigma_y}{G_R} = \frac{\left(\lambda - \frac{1}{\lambda}\right)}{\left(K_y - 1\right)} \quad (3.10)$$

The predicted values of λ required to stabilize the shear band for different stoichiometric ratios of epoxy resins, were calculated from yield stress and strain hardening

values determined from compression tests. Figure 3.14 shows the strain localization parameter, λ , as a function of the stoichiometric excess ratio of the epoxy networks.

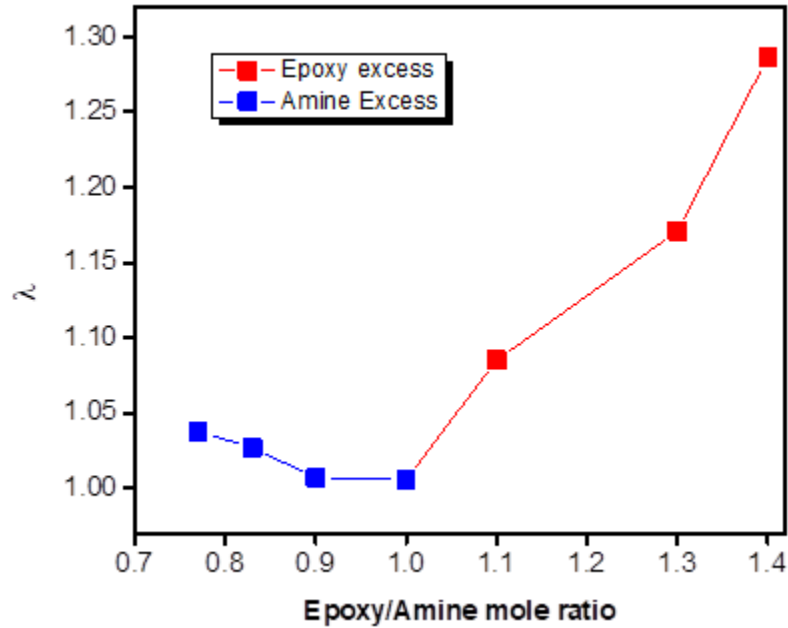


Figure 3.14: Strain localization parameter as a function of stoichiometric excess

Due to effects akin to physical aging, the yield stress is higher as we go out of stoichiometry and the post yield stress drop is also significant in the epoxy rich networks. Therefore, epoxy rich networks with higher K_y should be more brittle than the amine rich networks which we see in the fracture toughness of these networks. For epoxy networks, as the K_y increases, the strain localization parameter increases rapidly with increasing stoichiometric imbalance. The increase in the λ is not as significant for amine rich networks. This corresponds to the trends in T_g and strain hardening modulus obtained by DSC and non-linear compression testing.

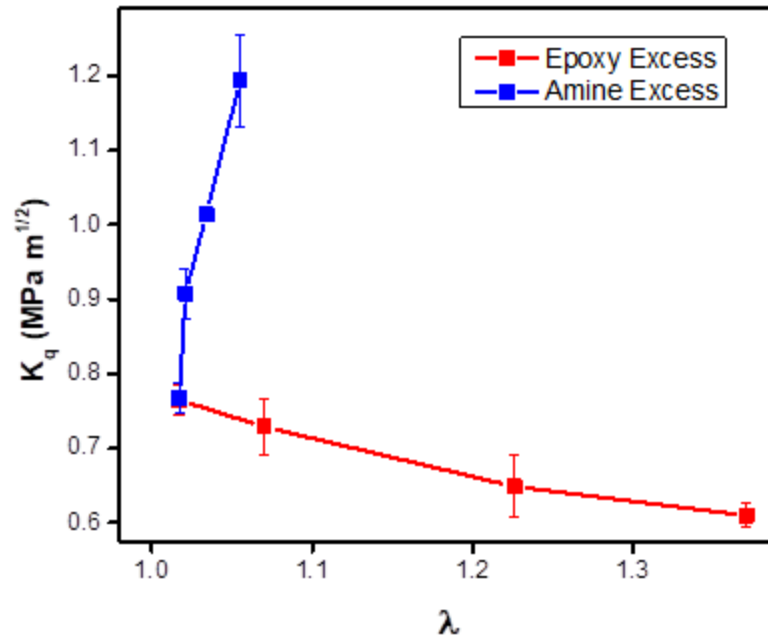


Figure 3.15: Fracture toughness as a function of the strain localization parameter

Figure 3.15 shows that the fracture toughness decreases with the strain localization parameter in epoxy rich networks due to the fragmented network being more brittle and increases in amine rich networks. Higher λ in epoxy rich networks suggests that the epoxy rich networks require a higher extension ratio to stabilize the shear bands and therefore have increased strain localization than the amine rich networks, however, further analysis is required to come up with a parameter to fully parametrize the ductility of these networks using non-linear compression testing.

3.3.6 Dynamic Mechanical Analysis:

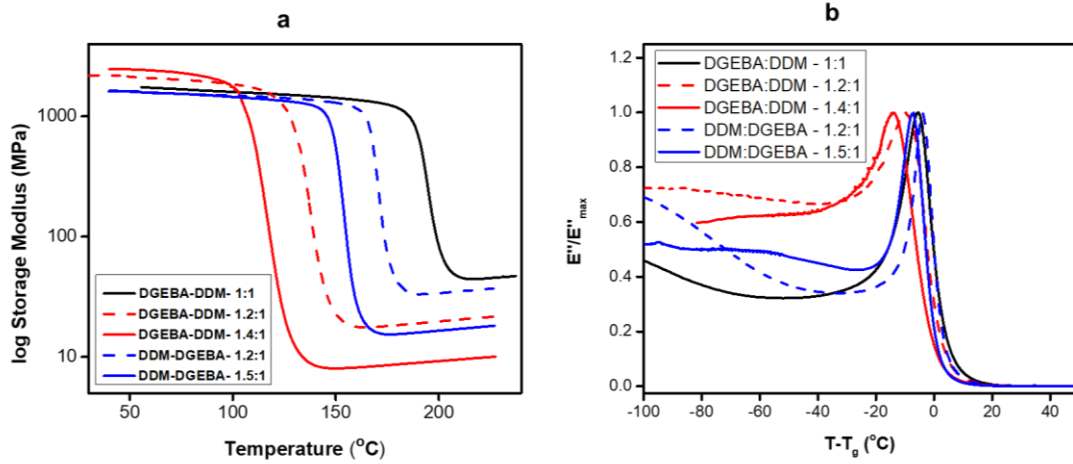


Figure 3.16 a) Storage moduli b) Loss Moduli of non-stoichiometric networks as a function temperature

DMA was also used as another tool to investigate the physical and mechanical behavior of networks. Figure 3.16 a) shows the storage moduli of non-stoichiometric epoxy networks as a function of temperature with increasing stoichiometric imbalance. The storage moduli obtained from DMA show a similar trend as the results obtained from the elastic modulus in compression testing. The networks with epoxy excess have higher storage modulus and it increases with increasing non-stoichiometry due to anti-plasticization of the unreacted components and oligomers in the fragmented networks. In case of amine rich networks, the storage modulus is lower than that of the fully crosslinked 1:1 network. Figure 3.16 b) shows the normalized loss moduli as a function of temperature. The epoxy rich networks have broader α transitions as compared to fully crosslinked stoichiometric network, whereas the amine rich networks have a narrower transition. The rubbery plateau moduli also show a steep drop in case of the epoxy rich networks and systematic decrease in amine rich networks. This decrease is proportional to the crosslink density and agrees well with the results obtained from non-linear compression testing.

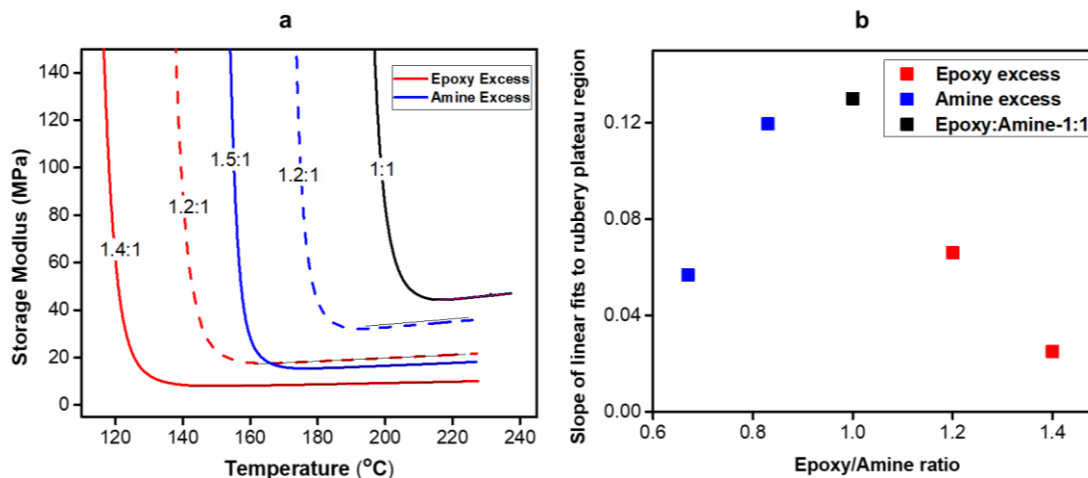


Figure 3.17 a) Linear fits of rubbery plateau region b) Slope of the Linear fits of the rubbery plateau region with respect to epoxy/amine mole ratio

Figure 3.17 shows the slope of the linear fits to the rubbery plateau region as a function of the epoxy amine ratio. The rubbery plateau region of the DMA curve as a function of temperature was fit linearly from T_g+20 °C to the end of the test temperature and the slope obtained thereof. The slope scales with the crosslink density in accordance with theories of rubbery elasticity and according to equation 3.6.

For non-stoichiometric networks, the cross-link density should decrease with increasing non-stoichiometry and hence both the amine rich networks and epoxy rich networks show a decrease in the slope with increasing non-stoichiometry. The rubbery modulus is a measure of the network connectivity so the epoxy rich networks which are more heterogenous and fragmented show a much steeper decrease in the slopes as we go out of stoichiometry. This result also follows the trends obtained from the strain hardening modulus measured from non-linear compression testing.

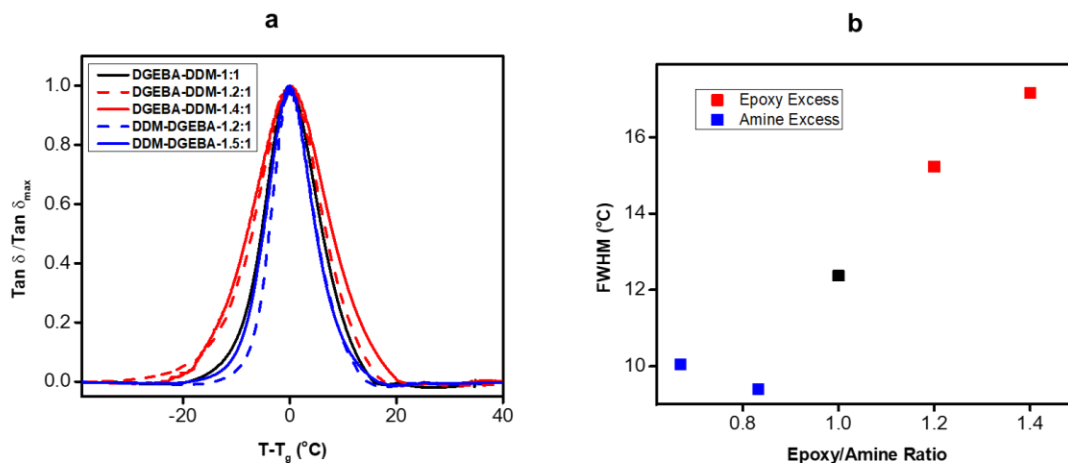


Figure 3.18 a) Normalized $\tan \delta$ as a function of temperature b) FWHM of $\tan \delta$ transition as a function of the epoxy/amine mole ratio

The full width at half maximum of the $\tan \delta$ peak is a measure of the breadth of the α transitions of the networks. The epoxy excess networks have broader transitions than the fully stoichiometric network as seen in Figure 3.18 a) and b). This breadth is related to the heterogeneity in the network.⁷² It has been shown that miscible blends of different polymers also show a broadening in the $\tan \delta$ transition as seen in the epoxy networks. The increase in the breadth is a result of heterogeneity due to the mobility of the individual polymers. In epoxy rich networks, too, there is topological heterogeneity due to regions of high and low crosslink density along with mobility of the unreacted monomers and oligomers and increased degree of freedom of the dangling chain ends. Lesser and Detwiler also observed a similar trend in their double networks which were cured with two different amines with different backbone flexibility.⁸ The topological heterogeneity of the amine segments as well as the difference in the crosslink density afforded due to these two amines contribute to the broadening of these transitions. The amine rich networks however, show a decrease in the breadth of these transitions. It has been shown that the breadth of the transition scales linearly with the crosslink density.⁷³ Thus, the amine rich network with its

lower crosslink density than the fully cured perfectly stoichiometric network shows a smaller breadth of these transitions. In case of the epoxy networks, the effect of the mobility and heterogeneity of the oligomers and low molecular weight constituents dominates over that of the crosslink density on the $\tan \delta$ transitions.

Therefore, the DMA is a more sensitive tool to correlate the mechanical properties of the network to the fracture toughness as the amine rich networks show a decrease in the FWHM corresponding to the increase in the fracture toughness of these networks and vice versa. However, more work is needed to fully investigate the amplitude and breadth of these transitions to accurately describe a parameter for correlating the network structure and defects to the physical and mechanical behavior of these networks.

3.4 Conclusions

The commercially available impact modifiers may not be fully functional or reactive with the cross linker used. The decrease in the T_g of the formulations with impact modifiers suggests some disruption in the network architecture but needs further investigation to understand details of the mechanism of disruption. To examine the effects of this irregularities in the network on the properties of the network, DSC, DMA and non-linear compression tests were done on DGEBA-DDM formulations with varying stoichiometric ratios of excess amine or epoxy groups in the network. For the amine rich networks, the crosslink density is reduced which leads to systematic decrease in the T_g , yield stress, strain hardening modulus as the networks go out of stoichiometry. In contrast, the results of the epoxy rich networks show complex trends with increasing yield stress and modulus as we go further out of stoichiometry. This is due to efficient packing of the chains in epoxy rich networks because of more conformational freedom from dangling

chain ends and low molecular weight oligomers causing network densification by reduction of free volume. The strain hardening moduli of epoxy rich networks also shows sharp decreases owing to poor network connectivity. A strain localization parameter was introduced based on the results obtained from compression testing to characterize the strain localization and therefore the fracture toughness of these non-stoichiometric networks. The storage moduli, rubbery moduli also followed similar trends due to stoichiometric imbalance when DMA was performed on these networks. The DMA also showed that the breadth of the tan delta transition depends on both the crosslink density and the degree of freedom of the constituents of the network and thus can be used as an effective probe to correlate the physical properties of the non-stoichiometric networks to their fracture toughness. Thus, non-linear compression testing and DMA can be powerful tools to determine stoichiometry and network connectivity in epoxy networks with additives in combination with other techniques like DSC, to obtain tough networks with improved fracture toughness.

CHAPTER 4

NEXT-GENERATION IMPACT MODIFICATION IN GLASSY EPOXY THERMOSETS VIA NON-SPHERICAL HIGH-SURFACE AREA PARTICLES

4.1 Introduction

Extensive research has been conducted on impact modification using spherical soft particles and the parameters required to optimize the fracture toughness in epoxy systems.^{35,4,37} In Chapter 1, the fracture toughness of high T_g epoxy composites was optimized using reactive liquid rubbers which phase separated into spherical domains after reaction induced phase separation. Mechanistic arguments demonstrated that interparticle distance, concentration and particle size are important parameters when toughening epoxies with spherical domains.

However, conventional reactive liquid rubbers can also disrupt the epoxy-network structure causing a decrease in fracture toughness when not employed appropriately. Additionally, the improvement in fracture toughness is limited with soft spherical domains as there are only two parameters (interparticle distance and particle size) available to tune it. Furthermore, the soft rubber particles can negatively impact parameters such as stiffness and optical properties. Therefore, there is a growing need to identify next-generation toughening mechanisms which can further increase the fracture toughness of these systems without significant detrimental effects on other physical properties.

Recently, hybrid systems with synergistic combinations of micron sized rubber particles and nano-sized rigid particles have been used to improve the fracture toughness while maintaining the stiffness of the systems.^{32,30,74} However, effective dispersion of the nano-sized modifiers is a significant challenge. Additionally, even with effective

dispersion, the system viscosity is increased drastically when nano-sized modifiers were employed, making the use of these hybrid systems difficult, especially in fiber-reinforced composites. In this chapter, we investigated the feasibility of improving fracture toughness of the epoxy thermosets by making high surface area, non-spherical particles using concepts of micromechanics and block copolymer physics.

4.1.1 Theoretical approach for investigating the toughening using high surface area particles

Reducing cavitation stress and increasing the inter-particle interactions have been proven to be very important for activating toughening mechanisms in the matrix by delocalizing the failure process and involving more volume of material in the failure process. Compared to spherical particles, both of these mechanisms can be enhanced by altering the shape of the toughening domains.

Consider the simple case of a primary non-spherical structure where the sphere has been transformed into an axisymmetric ellipsoidal structure like a prolate or an oblate spheroid.

4.1.1.1 Inter-particle Interaction

Williams et al⁷⁵ described the stress field in front of a “blunt crack” (prolate spheroid or cylinder) by:

$$\sigma_c = \sigma_\infty \left[1 + 2 \sqrt{a/r} \right] \quad (4.1)$$

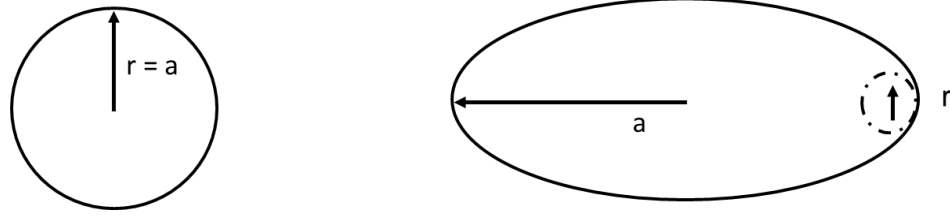


Figure 4.1: Stress concentration at the surface of a particle with higher aspect ratio is much greater than that at the surface of a spherical particle

Where, $2a$ is the length of the cylinder (semi-major axis of the ellipse), r is the local curvature at the tip of the cylinder, σ_∞ is the stress in the absence of the particle, and σ_c is the stress increase at the tip of the cylinder after cavitation occurs. Note that Equation 4.1 reduces to the stress concentration for that of a sphere (i.e. 3) when the semi-major axis equals the radius ($a = r$). (Figure 4.1)

Increasing the aspect ratio results in increasing the local stress near the tips of the ellipsoids (cylinders). Therefore, local yielding can also occur at lower stresses compared to that of spherical particles. However, a locally anisotropic response will be observed due to the higher stresses being localized only in the regions of the tips of the cylinders. Hence, the interparticle interactions which depend upon features like particle size, particle shape, and relative configuration (distance and orientation are expected to be more complex in these ellipsoidal particles.

4.1.1.2 Effect of particle shape on cavitation stress

As described in Chapter 2, for spherical impact modification, the stress at which particle cavitation occurs is size dependent. When the particles become too small, there is insufficient energy required to cavitate the particle and relieve the hydrostatic stress.

For non-spherical particles, the cavitation stress is both size and shape dependent. The critical particle size a_c of an ellipsoidal particle of length $2a_c$ and tip radius r is

proportional to properties of the rubber particle and matrix and applied stress by the following equation:

$$a_c \left(\frac{a_c}{r} \right)^\alpha \sim \left(\frac{\gamma}{K_R} \right) \left(\frac{K_m}{\sigma_\infty} \right)^{4/3} \quad (4.2)$$

Where γ and K_R are the surface energy and bulk modulus of the rubber particle, respectively. Additionally, K_m is the bulk modulus of the polymer matrix, σ_∞ is the far-field stress (stress in the absence of the particle), and α is the shape factor intensity.

Asymptotic analyses indicate that the shape factor intensity is bounded between $2/3 \leq \alpha \leq 2$. For a spherical particle, the result is independent of the shape factor intensity since $a_c = r = R_c$. More importantly, Equation 4.2 shows that both size and shape are important for cavitation.

$$\sigma_\infty \sim \left(\frac{\gamma}{K_R} \right)^{3/4} K_m \left(\frac{a_c}{r} \right)^{-(3/4)\alpha} \left(\frac{1}{a_c} \right)^{3/4} \quad (4.3)$$

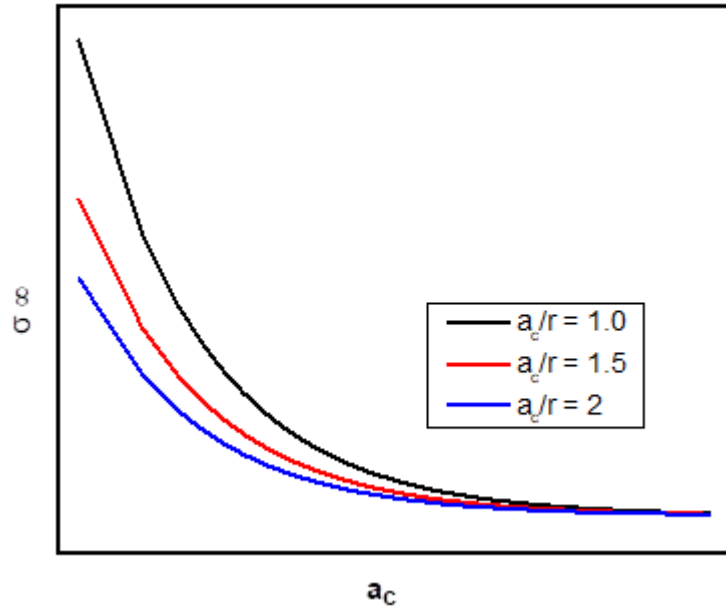


Figure 4.2: Cavitation stress is highly dependent on particle shape

In Figure 4.2, the cavitation stress, σ_∞ of a non-spherical particle is plotted as a function of particle size, a_c . When the aspect ratio of the particle (a_c/r) is varied, we see that for the same particle size, the cavitation stress can be reduced drastically especially for smaller particle sizes. Therefore, the lower bound of particle size that governs cavitation in from spherical modification does not apply for non-spherical geometries. Cavitation can now occur at much lower stresses as the particles become more and more non-spherical in nature. Thus, energy dissipation can occur at much lower stresses before brittle failure of the polymer can occur.

Normalizing the cavitation stress for a non-spherical particle with respect to the cavitation stress for spherical particle, we get:

$$\frac{\sigma_\infty^{NS}}{\sigma_\infty^S} = \left(\frac{a_c}{r}\right)^{-(3/4)\alpha} \quad (4.4)$$

σ_∞^{NS} is the far-field stress for non-spherical particle

σ_∞^S is the far-field stress for spherical particle

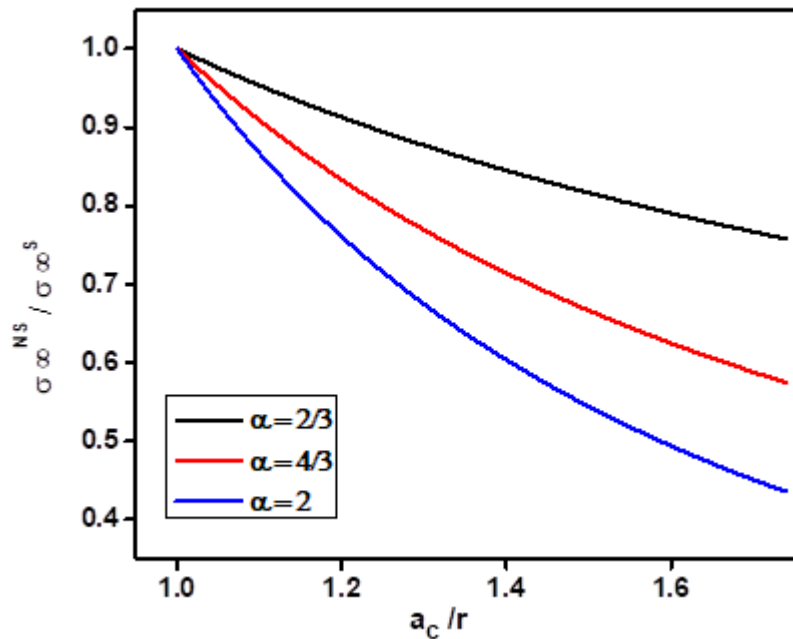


Figure 4.3: Cavitation stress as a function of aspect ratio of the particle

From equation 4.4 and Figure 4.3 we see that as compared to a spherical particle, the stress required for cavitation for a particle decreases when we change the aspect ratio. For the same aspect ratio, when we change the shape factor intensity, we can decrease the stress required for cavitation even further. Therefore, particles which are highly non-spherical in nature, can cavitate at much lower stresses and therefore lead to local yielding as well as increases interparticle interactions as discussed in the earlier section.

With the graph of cavitation vs shape intensity factor in Figure 4.3, we can see that higher the dependence of the cavitation stress on the particle shape, lower is the cavitation stress.

4.1.1.3 Secondary and other Hierarchical Morphologies

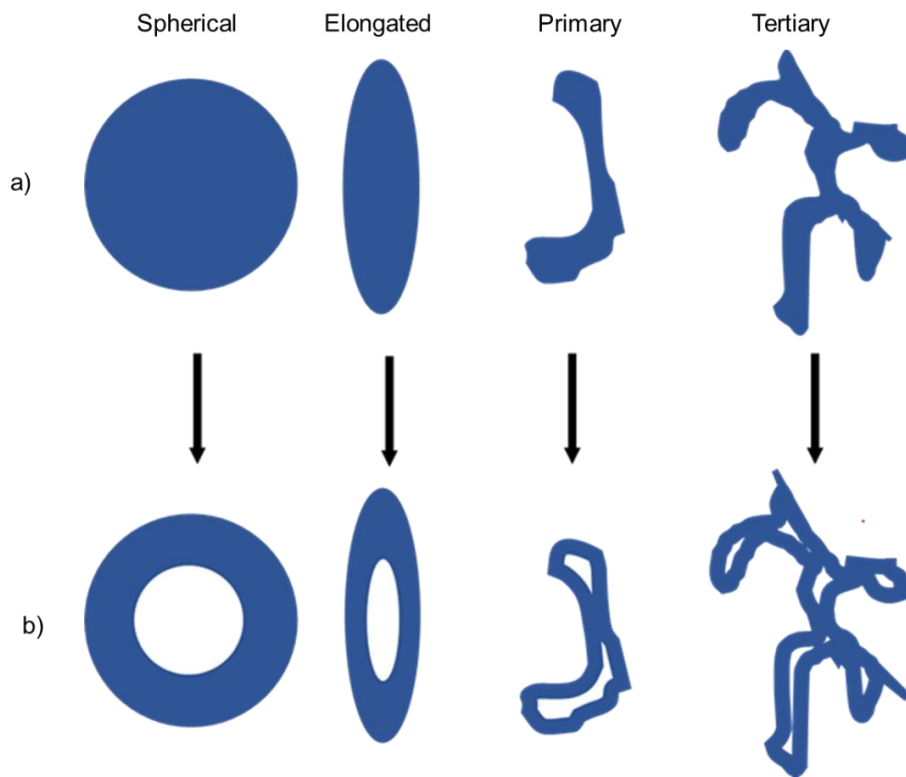


Figure 4.4: Schematic of particles of different shapes a) before and b) after cavitation.

While these ellipsoidal structures have many benefits as compared to traditional spherical impact modification, they also have limitations in terms of their anisotropic local yielding effects due to their local orientations. For a fully isotropic hydrostatic stress relief and for interparticle interactions to take place effectively, a distribution of randomly oriented elongated structures is imperative. For this reason, we can look at hierarchical high surface area structures like the secondary and tertiary structures shown in the Figure 4.4.

4.1.1.4 Potential Benefits of using hierarchical non-Spherical Impact Modification

If the matrix has more of the hierarchical, high-surface area structures, then there is a possibility of isotropic interactions between the particles as well as an increase in the energy dissipation and volume involved in the damage by having both inter and intra particle interactions.

We can see from the discussion in the earlier section that both the particle size and shape can be altered to tune the cavitation stress such that cavitation occurs at stresses lower than the stress at which brittle failure can occur. Since the local stresses at the points in the particles are increased and the stress field between the particles is also altered, interparticle interactions can be promoted.

Not just interparticle interactions, but intraparticle interactions can be promoted as the different arms of the tertiary particles can now interact with each other as well as other particles (Figure 4.4). Therefore, as compared to a spherical particle of similar volume, a non-spherical high surface area particle can significantly increase the damage density as well as energy dissipation. Due to the percolation of the stress field, a larger volume of material is involved in the fracture process. As a consequence of this, less amount of impact

modifier can be used which can lead to several practical benefits in the formulations employing these impact modifiers. Smaller volumes of soft particles can lead to less detrimental effects on the modulus, coefficient of thermal expansion and heat distortion temperature of the system. Depending on the size and shape of the hierarchical particles, the optical properties may be improved as the different arms/tips can scatter light differently as compared to the spherical particles.

4.1.2 Experimental approach achieving high surface area particles for improving fracture toughness

Block copolymers have been widely used for obtaining non-spherical morphologies for impact modification. These block copolymers are characterized in terms of their degree of polymerization (N_A and N_B) which is proportional to the molecular weight of each block (A and B), the relative fraction of each block and a temperature dependent Flory Huggins interaction parameter (χ) which represents the thermodynamic interaction between the two blocks.

Owing to the inherent incompatibility and immiscibility, individual block experiences energetic repulsion driving the system for phase separation. Although covalent linking between the blocks prevent the macrophase separation, block copolymers can self-assemble via microphase separation. Temperature dependent χ parameter governs the free energy cost associated with the microphase separation, whereas, the molecular weight of each block and relative weight fraction dictates the domain size and morphology (lamellar, cylindrical, spherical, etc.) of phase-separated domains respectively. (Figure 4.5)

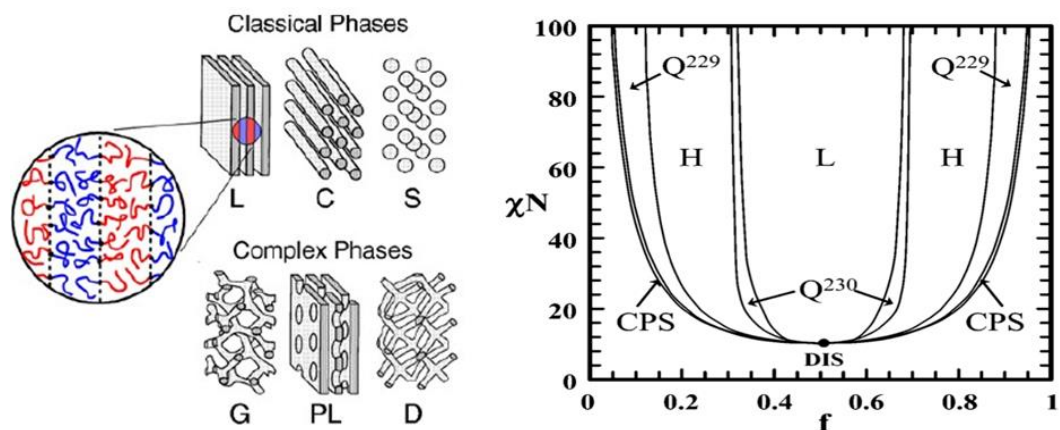


Figure 4.5: Phase diagram of di-block copolymer self-assembly in solution.^{76,77}

A block copolymer melt is in disordered homogeneous phase above Order-Disorder temperature (ODT). As the temperature of the melt decreases, block copolymers self-assemble in an ordered morphology. Similarly, in solutions, block copolymer can self-assemble based on energetic repulsion, length of the individual block segments, relative fraction and importantly, the interaction parameter between the block and the solvent controls the resultant morphology of self-assembled structure. Solvent annealing, as well as thermal annealing, are most common techniques to promote the self-assembly of block copolymers. Self-assembly of block copolymers in solution can be utilized to obtain well-defined nanostructure and microstructure geometries by precisely synthesized block copolymers and tuning the block copolymer solvent interaction. Some recent studies have successfully incorporated block-copolymer rubber systems into thermoset matrices to obtain interesting non-spherical morphologies which were found to demonstrate superior toughening compared to their spherical counterparts.^{78,13,79} These studies demonstrated that by choosing block copolymer systems with inherent curvatures (eg, spherical, cylindrical, lamella etc.), particles with high surface area may be attainable.^{80,81,82,83}

However, precise control over the relative molecular weight and polydispersity of the blocks is needed to access a specific morphology, and this requires tedious and complex polymerization techniques. One strategy which has been proven useful in obtaining complex morphology in solution is blending of block copolymers.^{84,85,86} It has been observed that when two block copolymers with identical chemical backbone structure but different molecular weight are blended in solution, it yields unconventional morphologies, such as cylinder end capped with a sphere or vesicles with branches. These geometries are a result of local trapping and segregation of similar blocks in the solution. Consequently, mixing two block copolymers with different chemical identity leads to more complex shapes. It has also been shown that by choosing a block copolymer which phase separates into a domain with inherent curvatures (eg, spherical) and blending it with other block copolymer which phase separates into a domain of different curvature can lead to morphologies with an intermediate curvature. Thus, blending two block copolymers in different ratios you can swell one block and change its curvature as opposed to synthesizing a new block copolymer with precise molecular weight of the individual blocks to obtain that specific morphology. In this way, morphologies of the phase separated regions can be changed and/or more easily match the toughening system to the matrix. The toughening mixture can be fine-tuned by simply blending vs complex synthesis.

In this research we are investigating the feasibility of blending two block copolymers to achieve complex high surface area morphologies in the epoxy systems. (Figure 4.5) So, expanding on this concept of using single block copolymers to achieve non-spherical, high-surface area particles, we blended together two different block copolymers or a block copolymer and a homopolymer of varying molecular weights and

architectures to further disrupt local curvatures in the phase-separated particles. Entropy dictates the self-assembly of block copolymer blend in DGEBA-DDM solution. Microphase separation of the block copolymer blend from the epoxy matrix is driven by enthalpy. The chains of the two block copolymers which are epoxy-philic will attempt to diffuse in the DGEBA-DDM solution, change the radius of curvature and self-assemble to minimize entropy. At the same time, as the DGEBA-DDM solution cures, the block copolymers will also want to phase separate out of the matrix. Theoretically, given infinite time for curing of the matrix, the epoxy-philic and the epoxy-phobic chains of the block copolymer chains will diffuse towards each other and self-assemble into equilibrium structures with the least surface energy. However, we could take advantage of the inherent competition between the kinetics of phase separation among the blocks of the two block copolymers, and the phase separation of block copolymers from the epoxy matrix to kinetically trap these non-equilibrium high surface area morphologies. Depending on the rate and temperature at which the epoxy is cured we can achieve different shapes and sizes of these non-equilibrium morphologies.

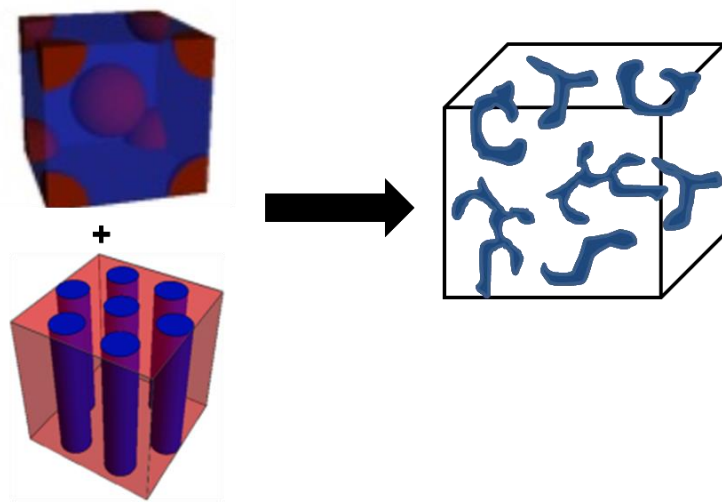


Figure 4.6: Mixing of two block copolymers with individual phase separated morphologies to obtain high surface area morphologies

The use of block copolymers as impact modifiers, and their resulting non-spherical morphologies allow for significantly more energy dissipation, as compared to that which is achievable with classical spherical particles. It follows, that a lesser amount of non-spherical impact modification is required to achieve the same performance attainable with spherical impact modification. Reduced loading levels of non-spherical modifiers also reduces the negative impact modifiers sometimes have on modulus, processability, and optical properties.

In the following chapter, we explored in more detail, the feasibility of the approach of using blends of block copolymers to readily achieve non-spherical domains, and aimed to understand the underlying toughening mechanisms of non-spherical domains in comparison to state-of-the art approaches.

4.2 Experimental

4.2.1 Materials

Diglycidylether of Bisphenol-A (DGEBA) (Epoxy Eq. wt. = 175 g/mol) DER 332 was purchased from Dow Chemicals and diaminodiphenylmethane (DDM) was purchased from Sigma Aldrich. Epoxidized soybean oil (ESO) was obtained from Spectrum chemicals. Triblock copolymers M51, M53 (polymethylmethacrylate-b-polybutylacrylate-b-polymethylmethacrylate) family. SBM (Styrene-b-butadiene-b-methacrylate) were purchased from Arkema Inc. Styrene-butadiene-styrene block copolymers (SBS) were supplied by KRATON. The series of PEO-PPO-PEO (Polyethyleneoxide-b-polypropyleneoxide-b-polyethyleneoxide) triblock PE-PEO (Polyethylene-b-polyethyleneoxide) diblock copolymers were purchased from Sigma-Aldrich. The series

of PEO-PDMS (Polyethyleneoxide-polydimethylsiloxane) diblock copolymers were obtained from Gelest. Polyvinylmethylether (PVME) was purchased from Polymer Products Inc. The mold release agent Surfasil was purchased from Pierce chemicals. All the chemicals were used without further purification unless otherwise specified. Table 4.1 describes the structures of the chemicals used.

4.2.2 Procedure for making plaques with block copolymer mixtures

An appropriate amount of each block copolymer was introduced into the DGEBA resin at 130 °C and stirred for 6 hours. Care must be taken to ensure that the block copolymers are dissolved and not just swollen in the epoxy resin. After the two block copolymers were completely dissolved, the solution was cooled to 90 °C and DDM was added to the solution. Once the DDM was completely dissolved (ca. 10 minutes), the solution was immediately degassed for 2-3 minutes and poured into 3 mm thick glass molds which were pretreated with Surfasil.

4.2.3 Glass transition temperature

TA instruments DSC Q200 was used to measure the glass transition temperature according to the procedure described in Chapter 2 Section 2.2.3.

4.2.4 Fracture toughness

Fracture toughness measurements were conducted using the procedure described in Chapter 2 Section 2.2.4.

4.2.5 Scanning electron microscopy (SEM)

SEM images were taken in accordance to the procedure in Chapter 2, Section 2.2.2.

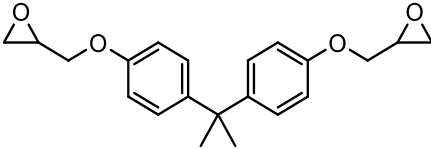
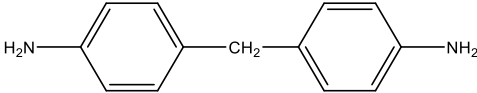
4.2.6 Optical Microscopy

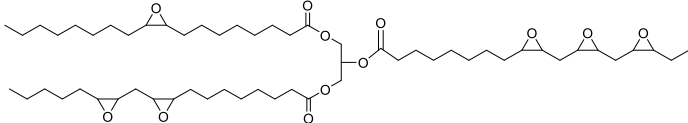
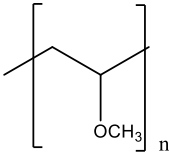
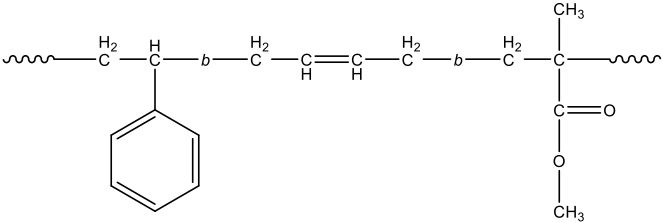
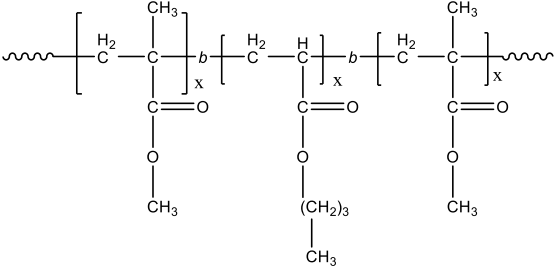
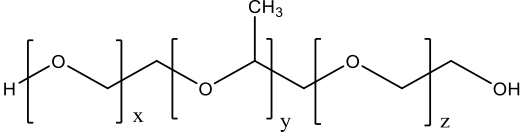
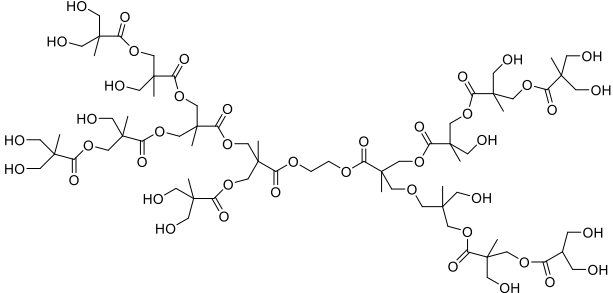
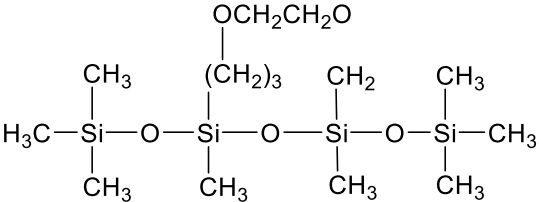
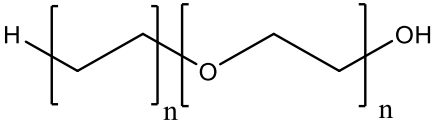
The process zone of the fractured surfaces was observed using a Zeiss Discovery V12 microscope. Compact tension samples fractured in accordance to ASTM 5045-99 were used for this purpose. The two sections of the fractured compact tension sample were placed under the microscope and process zone was observed under the reflected light using Axiom 105 color camera of the Zeiss microscope at various magnifications. To enhance the contrast, brightness of the light was adjusted accordingly. For further investigation of the surface properties of the process zone, optical profilometry was done.

4.2.7 Optical profilometry

A Zygo New View 7300 (Zygo Corp.) optical profilometer was used to quantify the topography of the process zone in the fractured surfaces of the compact tension samples with a 10 X optical zoom. The average roughness of the sample was reported as the root mean square value.

Table 4.1: General structures of the chemicals used (continued on the next page)

Chemical name	Chemical structure
Diglycidylether of Bisphenol – A (DGEBA)	
Diaminodiphenylmethane (DDM)	

<p>Epoxidized soybean oil (ESO)</p>	
<p>Poly (vinyl methyl) ether (PVME)</p>	
<p>Polystyrene -b- polybutadiene-b- poly(methyl methacrylate) (SBM)</p>	
<p>Poly(methylmethacrylate) - b- poly (butyl acrylate) – b poly(methylmethacrylate) (M51/M53)</p>	
<p>Poly (ethylene glycol) - block-poly (propylene glycol) - block-poly (ethylene glycol) (PEO-PPO-PEO)</p>	
<p>Hyperbranched G3- PEG20k-OH (Dendrimer)</p>	
<p>Polyethylene-<i>block</i>-poly (dimethylsiloxane) (PEO-PDMS)</p>	
<p>Polyethylene-<i>block</i>-poly (ethylene glycol) (PE-PEO)</p>	

4.3 Results and discussion

The block copolymers used in this study were chosen as they can easily be dissolved in the (DGEBA) resin at moderate temperatures and do not require high shear mixing. Also, one block of the block copolymer used for the blend should be compatible with the epoxy resin while the other block should be incompatible so that they can self-assemble into micellar structures. A portion of the miscible block was compatible in at least one of the two blocks of the block copolymer.

For this particular approach, the block copolymer and the miscible polymer can comprise copolymers having the same block structure except that a weight average molecular weight of the block copolymer is different than the weight of the other block copolymer. The two block copolymers can comprise different copolymers having different block structures having same weight average molecular weight. The two block copolymers can have different block structures having different weight average molecular weights. They can also comprise copolymers having same structure and overall molecular weight but different weights of the individual blocks. Some commonly occurring blocks which are incompatible with the DGEBA resin are siloxane, olefinic, vinyl monomer, different acrylates (depending on the molecular weights), polybutadiene-based blocks. The blocks usually compatible with the DGEBA are polyethylene glycol, polystyrene, methyl acrylate, polycaprolactone, polyTHF based blocks. So we decided to use commercial block copolymers having these blocks in this study.

The ratio of the epoxy-philic block dictates the curvature of the self-assembled block copolymer domains in the epoxy. The interfacial curvature decreases with increasing epoxy-philic block length.^{87,88} These block copolymers self-assemble in the epoxy resins

in a manner similar to the self-assembly of amphiphilic block copolymers in water due to the selective compatibility of one block in the DGEBA resin. When curing occurs, the chains which are compatible with each other will try to diffuse towards each other but at the same time will try to phase separate out from the epoxy matrix and it is this competition between the enthalpically driven phase separation and entropically driven self-assembly that leads to kinetically trapped non-equilibrium morphologies of phase separated domains.

Based on these criteria, a range of block copolymers with different chemical structures, individual block copolymer content and molecular weights were screened for their solubility in the DGEBA resin.

Table 4.2: Solubility of the screened block copolymers in DGEBA

Weight %	Polymer	Molecular weight	Composition	Solubility
5	G6 Dendrimer	20K-16 OH groups		Insoluble
10	PCL-PTHF-PCL	2000		Soluble
5	poly(D,L-lactide-co-glycolide)-block-poly(ethylene glycol)-block-poly(D,L-lactide-co-glycolide) based poly(ether ester urethane)	6000-15000	13:70:17 PEG:Plactide-PLGA	Insoluble
5	poly(D,L-lactide-Acrylic Acid)	21k	PDLLA: PAA = 5000:18000	Insoluble
5	DBE-U12 PEO-PDMS-PEO	1500-1600		Insoluble
5	Hyperbranched bis-MPA polyester-16-OH, generation 2	1749.17		Insoluble
5	G5 Dendrimer	20K-16 OH groups		Insoluble
5	poly(ethylene glycol) methyl ether-block-poly(ϵ -caprolactone)	M _n 30,000	PEG M _n 5,000, PCL M _n 25,000	Insoluble
5	Poly(lauryllactam) -block-poly(tetrahydrofuran)	Melt index- 7-11 gm/10 min		Soluble

In general, from Table 4.2 and Table 4.3 it was seen that the block copolymers with relatively higher content of epoxy philic blocks were completely compatible with the DGEBA resin while the others were incompatible. In the M51 and M53, the PMMA blocks are compatible with the epoxy resin, while the polybutylacrylate blocks which are epoxy phobic can self-assemble to form soft rubbery domains for impact modification. The two block copolymers have the same chemical structure but different overall molecular weights and different molecular weights of the individual blocks. In PEO-PPO-PEO based block copolymers, the PEO block is epoxy-philic and the PPO block is epoxy-phobic. The PE block in the PE-PEO based polymers is epoxy-phobic and the PEO block and PMMA blocks are compatible with each other. In the styrene-butadiene-methacrylate triblock copolymer, the styrene and the methacrylate are compatible with each other and the epoxy-resin whereas the butadiene is incompatible with the DGEBA.

Table 4.3: Solubility of the screened block copolymers in DGEBA

Block copolymer	M _n	PEG wt %	Solubility
PEO-PPO-PEO	1900	50	Soluble
	2800	10	Soluble
	5800	30	Soluble
	14600	82.5	Soluble
PE-PEO	575	20	Soluble only upto 3 wt%
	920	50	Soluble only upto 8 wt%
	2250	80	Soluble
PEO-PDMS	5000	90	Soluble
	20000	65	Soluble
	4400	85	Soluble

The block copolymers were then blended with each other with a total weight percentage of 15 wt% in a 50:50 weight ratio in the DGEBA. An aliphatic polyether amine D-230, aromatic amine DDM and a cycloaliphatic amine IPDA were used to cure these compositions. From the different block copolymers screened, following compositions were studied in more detail for their morphology and fracture toughness mechanisms as the first composition showed a spherical core shell like morphology and the next two showed a non-spherical morphology.

- 1) PEO-PPO-PEO with a PEO content of 30% and Mn-5800 gm/mol, (henceforth referred to as PEO-PPO-PEO- 5.8k) + PE-PEO with PEO content of 80% and Mn 2250 gm/mol (henceforth referred to as PE-PEO-2250)
- 2) M51+ M53
- 3) M51+ SBM

Along with these blends, a composition with PVME in the DGEBA amine system was also studied for comparison of these blends to a system with conventional impact modifier which phase separated into spherical domains.

Table 4.4: Appearance after curing with DDM and polyetheramine D-230 for different compositions of block copolymer blends

	PEO-PPO-PEO (PEO 30%) [Mn-5800]	M51	SBM	PE-PEO [Mn-2250] (PEO-80%)
PEO-PPO-PEO [Mn-5800] (PEO-30%)	N/A	Opaque	Opaque	Opaque
M51	Opaque	N/A	Opaque	Opaque
SBM	Opaque	Opaque	N/A	Opaque

Table 4.4 describes the solubility of the blends with each other in the DGEBA resin and its appearance after curing with two different amines.

4.3.1 Fractographic analysis

The stress field in front of a crack tip is described by the following equation, where all the stresses are concentrated in front of the crack tip:

$$\sigma_{ij}(r, \theta) = \frac{K_I}{\sqrt{2\pi r}} \tilde{\sigma}_{ij}(\theta) \quad (4.5)$$

r and θ are the cylindrical coordinates, σ_{ij} the distant applied tensile stress and $\tilde{\sigma}_{ij}$ is a θ dependent function. From this equation it can be seen that the stresses become infinite as the distance from the crack tip decreases. Non-linear deformations, crazing, shear bands, cavitation, inelastic void growth, and gross yielding can occur in this region to relieve the infinitely high stresses in front of the crack tip. According to the Dougdale and Barenblatt model, scaling laws indicate that:

$$r_p \sim \left(\frac{K_q}{\sigma_y} \right)^2 \quad (4.6)$$

where r_p is the radius of the process zone and K_{IC} is the stress intensity factor and σ_y is the yield stress of the material. (Figure 4.7)

As the fracture energy release rate, J_q scales with the stress intensity factor as follows:

$$J_q \sim \left(\frac{K_q}{E} \right)^2 \quad (4.7)$$

For ductile materials which exhibit non-linear deformations, the radius of the process zone is given by:

$$r_p \sim \frac{J_q E}{(\sigma_y)^2} \quad (4.8)$$

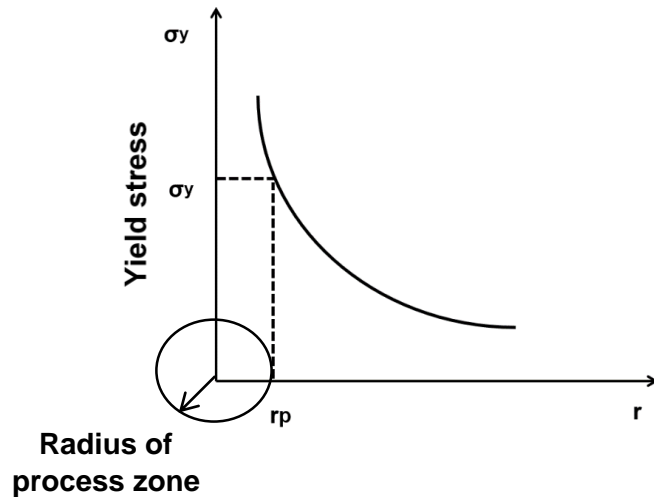


Figure 4.7: Stresses in front of the crack

Therefore, size of the process zone can correlate to fracture toughness, as described by Equation 4.6. In other words, as the area of the process zone increases, so does the fracture toughness. Both, the spherical and non-spherical samples, were imaged by optical microscopy to determine the size of the process zones. The process zone on a compact tension sample is the whitened region due to the damage occurring in front of the crack tip. The size of the active process zone was measured as the distance from the start of the crack tip to the furthest visible damage of the stress whitened region.

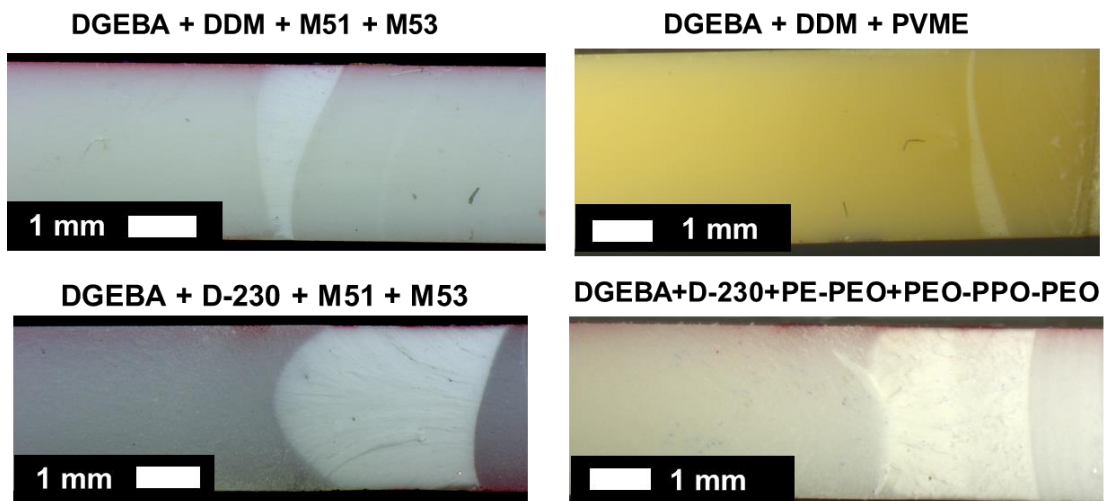


Figure 4.8: Optical micrographs of process zones of systems with different block copolymer blends

Figure 4.8 shows the optical micrographs of the process zones obtained from compact tension samples after they have been fractured according to ASTM D5045. All the samples cured with DDM showed brittle failure and therefore fracture toughness was calculated as K_{Ic} according to linear elastic fracture mechanics. The systems cured with the aromatic amine DDM have a higher yield stress and cross-link density compared to the ones cured with the longer chain aliphatic polyetheramine D-230. Therefore, they show a smaller process zone, with the majority of the energy contributing to the formation of new surface area, e.g. crack propagation. In the more ductile system cured with D-230 a larger process zone is visible, indicating a larger proportion of inelastic deformation mechanisms.

As seen in Figure 4.9, the systems 1 and 2 show spherical morphologies whereas systems 3 and 4 show non-spherical morphology. Comparing non-spherical and spherical domains, the non-spherical impact modifiers also led to an increase in process zone size (Figure 4.10). This could be due to the ability of non-spherical particles to initiate not only inter- but also intra-particle interactions, effectively decreasing the yield stress of the material and involving more volume in the failure process.

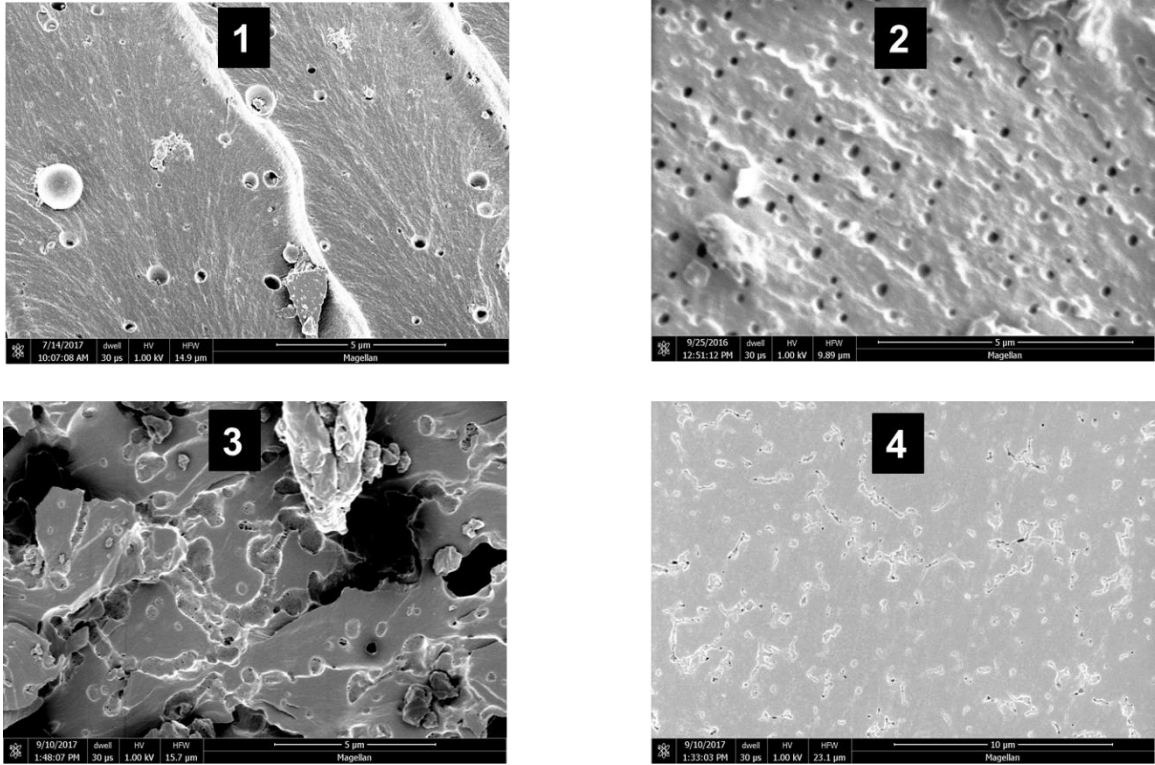


Figure 4.9: Morphology of 1) PE-PEO (M_n 2250) + PEO-PPO-PEO (15%) 2) Poly (vinylmethyl) ether (15%) 3) M51 + SBM (15%) 4) M51 + M53 (15%)

The systems cured with D-230 show ductile behavior in their compact tension tests. So, the non-linear fracture energy was calculated as a combination of the linear elastic contribution and the plastic contribution. The graph in Figure 4.11 shows the fracture energy release rate J_q as a function of size of the process zone.

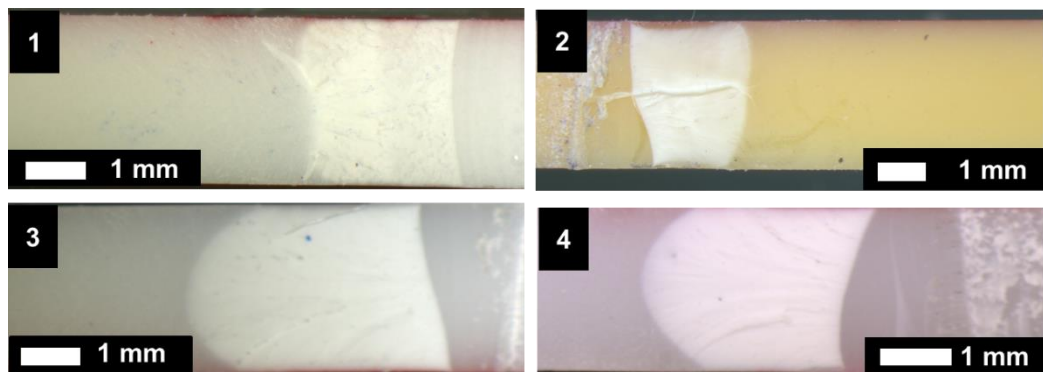


Figure 4.10: Optical micrographs of size of the process zones of 1) PE-PEO (M_n 2250) + PEO-PPO-PEO (15%) 2) Poly(vinylmethyl) ether (15%) 3) M51 + M53 (15%) 4) M51 + SBM (15%)

It shows that the systems with the largest process zones gave the highest fracture toughness.

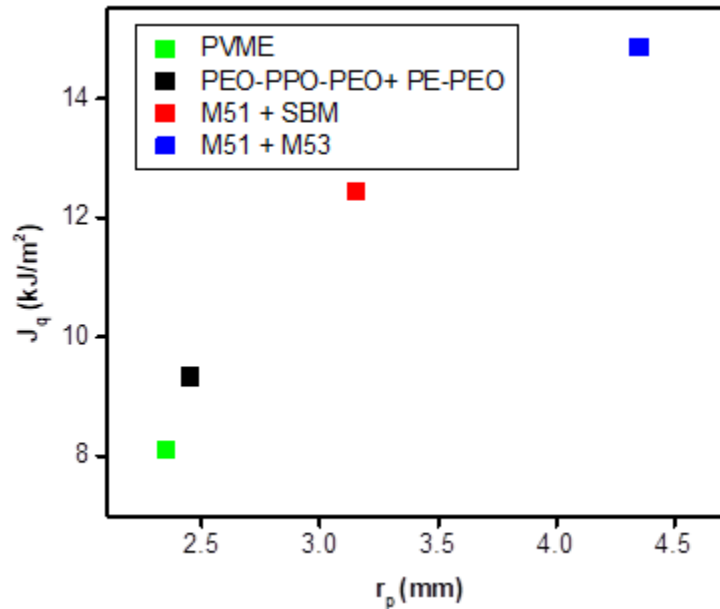


Figure 4.11: Fracture energy release rate vs size of the process zone

In compact tension samples, the deformation patterns and mechanisms can be erased due to ligaments and fibril formation as the crack propagates unstably, especially in ductile systems. So, it is necessary to arrest the crack and get a critically developed process zone. For this, we used the double notch four-point bend test which has been shown to be effective in probing the micromechanics of deformation occurring in the process zone.⁸⁹ The double-notch four-point-bend technique (DN-4PB) is used to study the fracture mechanisms of multiphase polymers. This technique is found to be effective for an unambiguous determination of the fracture mechanisms and the sequence of toughening events of polymer composite when fracture occurs. In this technique, two nearly identical cracks are cut into the same edge of a rectangular beam. This beam is loaded in a four-point bending geometry with the cracks positioned on the tensile side. The portion of the beam between the two inner loading points is subjected to a constant bending moment.

Thus, the two cracks experience nearly identical stresses. As load is applied, plastic zones form in front of the crack tips. Since the two cracks cannot be identical, one crack will propagate unstably, leaving behind the other crack with a nearly critically developed process zone at its tip. Since this crack is arrested, the events in the crack tip process zone are not obliterated by the last process, which in ductile plastics often involves tearing of the plastic ligaments spanning the crack faces. SEM samples made by petrographic polishing were used to image inside and outside the process zone of the composition containing 15 wt% M51+M53 in DGEBA resin cured with D-230. This helped visualize the mechanisms of damage formation like cavitation or shear banding and other plastic deformation mechanisms in the process zone, giving greater clarity to the mechanisms of toughening due to the non-spherical morphologies.

The SEM image taken inside the process zone (Figure 4.12) shows that in the non-spherical, high surface area particles cavitation had occurred at different places in the same particle. This leads to the dissipation of energy over a larger area and thus increase in the fracture toughness of these systems.

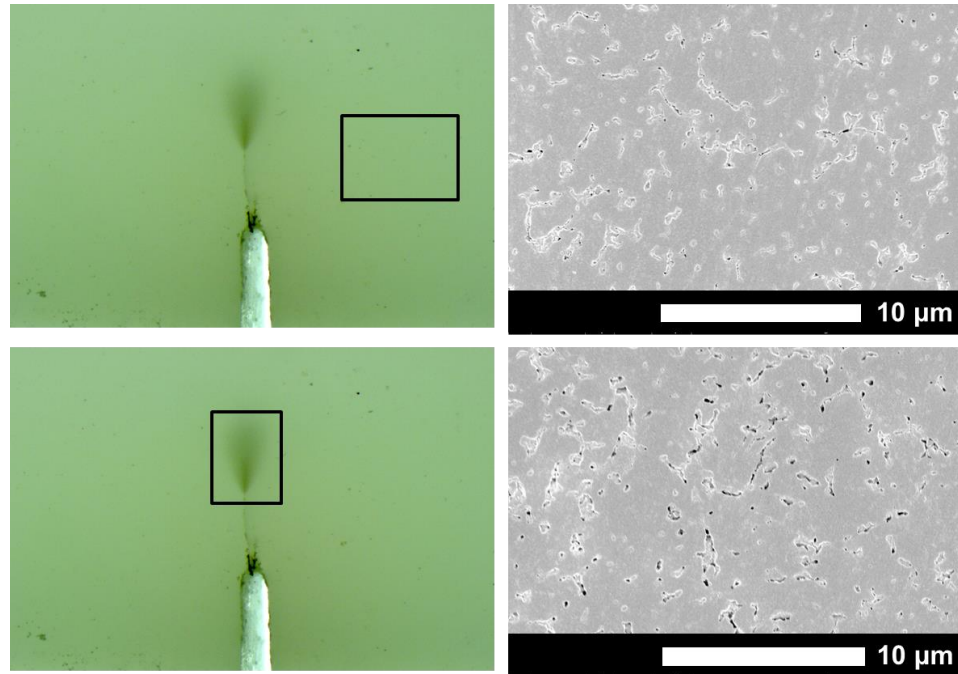


Figure 4.12: SEM images of the non-spherical domains 1) outside 2) inside the process zone

To quantitatively correlate the effect of morphology on the fracture toughness, optical profilometry was conducted on the process zones of samples with both the spherical and non-spherical morphologies. The root-mean square roughness calculated from optical profilometry can be related to the mechanisms of deformation inside the process zone, such as plastic fibrillation and change in volume due to domain cavitation. The non-spherical impact modifiers have higher process zone roughness. This increased volume of material involved in the failure process is possibly due to higher inelastic fibrillation deformation and/or domain cavitation. Cavitation and fibrillation are energy dissipating mechanisms activated by material in front of the crack tip. Non-spherical systems, owing to their shape and consequent higher stress concentration at their interface are more efficient/effective in plastic deformation of the matrix. The non-spherical particles also lead to more inter and intra particle interactions because the cavitation can occur at different surfaces within the same particle where the stress concentration is higher.

Figure 4.13 shows the difference between the roughness of the process zone of the spherical and non-spherical modifiers and how it scales with the fracture toughness of these systems.

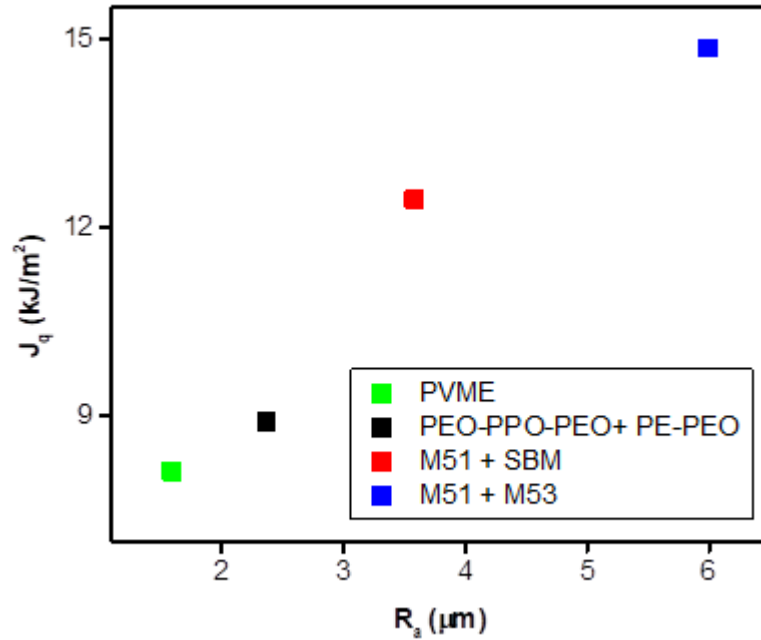


Figure 4.13: Fracture energy release rate vs roughness of the process zone

4.3.2 Metric for relating the fracture toughness to the particle shape:

In a spherical particle, the particle size can be defined as the radius of the sphere of a rubber particle which can be related to the interparticle distance and concentration in these impact modified systems. When stress is applied to an impact modified material, the surface of the particle experiences significantly higher stress as compared to the far field stress. Stress concentration at the interface is dictated by the shape of the phase separated domains, as given by equation 4.1. In the event of fracture, crack tip region experiences a triaxial state of stress. Under such triaxial state of stress, phase separated domains cavitate.

The critical mean stress required for the cavitation of the spherical particles depends on the size of the domain as shown in the following equation:

$$\sigma_m = K_m \left(\frac{6\gamma}{R_c K_R} \right)^{3/4} \quad (4.9)$$

Here, σ_m is function of stress at the surface of the particle and depends on applied far-field stress. The cavitation stress is inversely proportional to the size of the particle.

$$\sigma_m \sim \left(\frac{1}{R_c} \right)^{3/4} \quad (4.10)$$

The state of stress at the crack tip is given by equation 4.5 and the stress intensity factor can be expressed in terms of limit of the stress responsible for mode of failure at the crack tip.

$$K_I = \sqrt{2\pi r} \sigma \quad (4.11)$$

Thus, based on equation 4.5 to 4.10, fracture toughness of a sample varies inversely with the size of the phase separated domains. Also, we can see that the fracture toughness is proportional to the applied stress.

$$K_I \sim \left(\frac{1}{R_c} \right)^{3/4} \quad (4.12)$$

$$J_q \sim \left(\frac{1}{R_c} \right)^{3/2} \quad (4.13)$$

In spherical impact modification, it has been established that the particle size dictates the cavitation stress of the soft particle and the concentration and interparticle distance governs the yielding in the matrix. In non-spherical systems, we need to take into account factors of particle size, shape, aspect ratio, orientation of the domains and therefore need a parameter to quantify which parameters σ are needed to completely describe the system.

Quantitative stereology has been used as a technique to evaluate and gather statistical information on the 3D morphology of spherical impact modified systems based

on its 2D image. In order to describe these complex hybrid morphologies and evaluate the dependence of fracture toughness on the shape of the material we proposed simple metric of shape factor. In a 3-D morphology, the particle can be described as highly non-spherical if its surface area is large compared to its volume. Converting the same to a 2-D morphology, the area of the particle should be greater compared to its perimeter for it to be considered highly non-spherical. So we calculated the effective radius of the particle from the perimeter and area assuming it to be a circle. The shape factor was then defined as the ratio of radius calculated from the perimeter, R_p of the sample to the radius obtained from the surface area, R_a of the phase separated domain. This ratio should be proportional to a_c/r . Hence, in the case of spherical particles, ratio is 1, but when the particles shape is non-spherical in nature this ratio would be higher than 1. For particles in 2D, higher the shape factor indicates higher the ratio of perimeter to the area thus, more the non-spherical nature of the particle. Thus, the shape factor can be used as a metric for comparative evaluation of different morphologies. We will evaluate the dependence of fracture toughness on the shape factor for the systems described below.

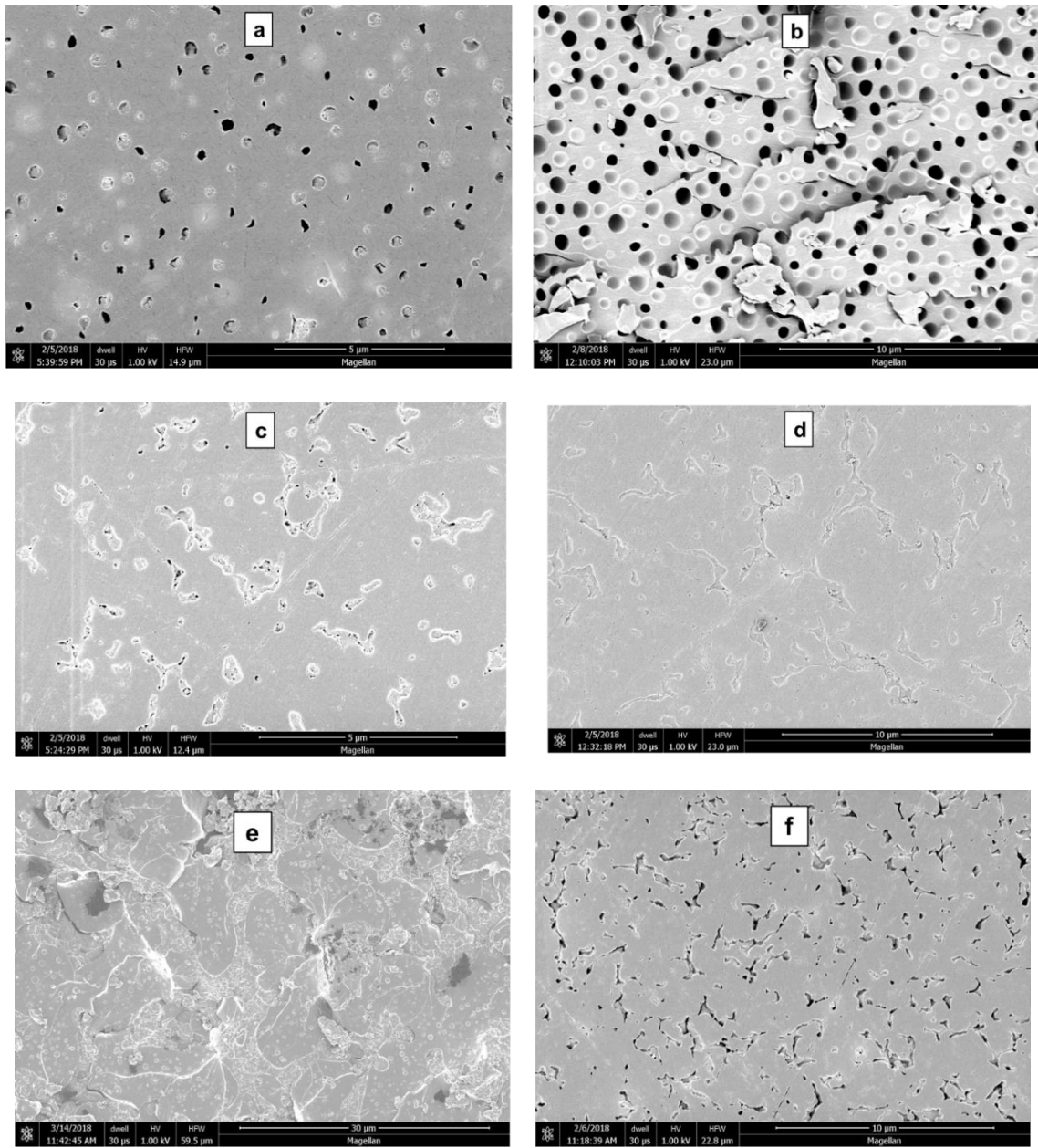


Figure 4.14 a) PEO-PPO-PEO ($M_n = 5.8k$) + PE-PEO ($M_n = 2250$) b) PVME c) M51+ SBM d) M51 + M53 e) M51 f) M53

$$\text{Shape factor} = \frac{R_p}{R_a} \quad (4.14)$$

We evaluated the six different compositions on which we performed the fractographic analysis for their shape factor. Figure 4.14 shows the SEM images of these

compositions cured with D-230. The system with the conventional spherical impact modifier had an average particle size of around 600 nm. The blend of PEO-PPO-PEO + PE-PEO demonstrated a core shell morphology with average particle size of around 0.4 μm . Both these compositions show a shape factor very close to 1 which is expected from that of a fairly spherical morphology. The block copolymer M51 shows interesting morphology with large islands of high surface area and almost co-continuous domains ranging throughout the sample along with small spherical domains which measure around 500 nm. The compositions with M53, M51 + SBM and M51 + M53 all show non-spherical morphologies with different sizes, size distributions and shape factors.

As particle shape plays a role in determining stress concentration at the interface, we anticipate a relation between J_q and shape factor. To investigate the dependence of the particle size on fracture toughness, we plotted the log-log plot of non-linear fracture energy release rate as a function of the shape factor and the slope of the line should provide the correlation between these two quantities. We used ImageJ analysis software to count the particles and calculated the radii of our particles based on the area and perimeter of the phase separated domains of the systems listed above. These were then plotted against the fracture toughness normalized by the control as seen in Figure 4.15. The normalization by the fracture toughness by the control takes into account effects due to decrease in the T_g and modulus of these systems on the fracture toughness. We see that there is a correlation between the fracture toughness and the shape factor. The spherical particles have a lower shape factor and exhibit lower fracture toughness whereas with higher surface area particles, the fracture toughness is the highest. The system impact modified with M51 is an outlier from the trendline and that can be because of the large domains acting as defects

and lowering the fracture toughness instead of enhancing it. Thus, from a preliminary evaluation of systems with morphologies of different shapes we saw that there is a dependence of shape of the particles on the particle size that can be described in terms of shape factor. According to equation 4.11, fracture toughness is proportional to σ_∞ and R_p/R_a is proportional to a_c/r . Therefore, $J_q \sim (R_p/R_a)^\alpha$ and by performing a linear fit of the data plotted in Figure 4.15, we can obtain shape factor intensity according to equation 4.4.

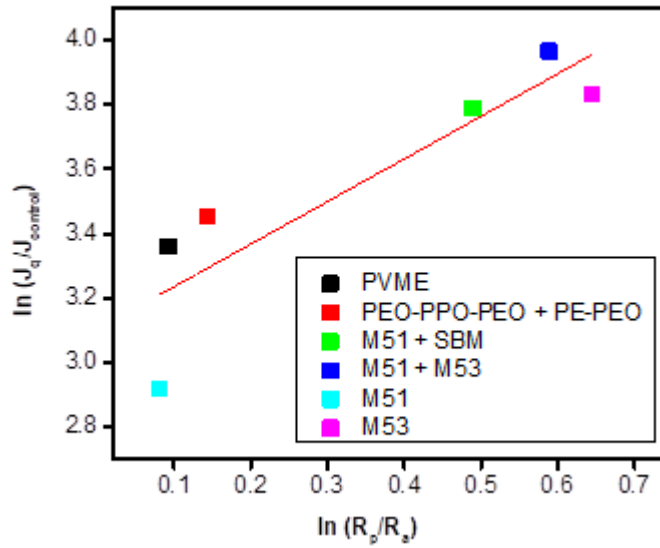


Figure 4.15: Correlation between normalized fracture toughness and shape factor of spherical vs non-spherical impact modifiers.

The shape factor intensity obtained by performing this fit is $\alpha = 1.32$. Therefore we can see from Figure 4.16, for our highest performing system with the ratio of $a_c/r = 1.21$, the cavitation stress already be reduced to around 80% of that required for a spherical particle according to the following equation which might lead to the increase in fracture toughness of the systems.

$$\frac{\sigma_\infty^{NS}}{\sigma_\infty^S} = \left(\frac{a_c}{r}\right)^{-\left(\frac{3}{4}\right)\alpha}$$

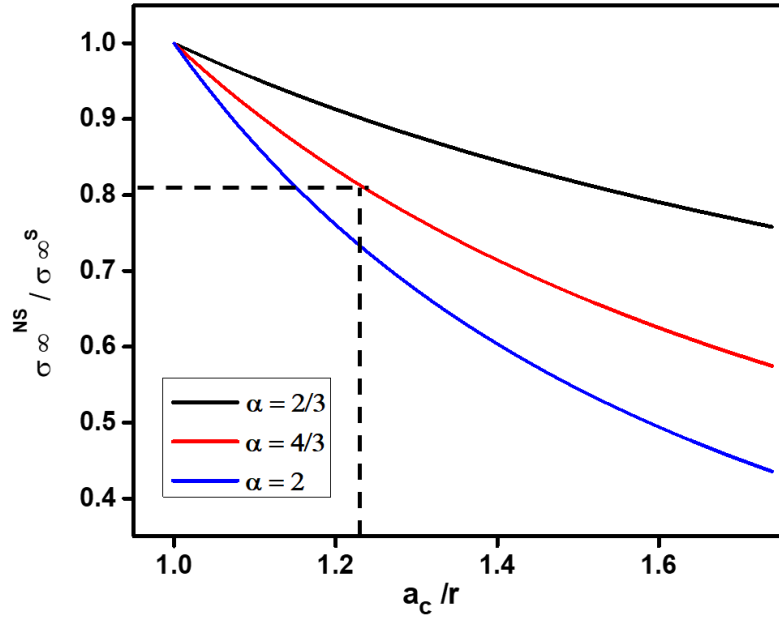


Figure 4.16: Reduction in stress required for cavitation

Further analysis is needed to parametrize the effect of size, shape, orientation and distribution of the impact modifier domains and completely describe the fracture mechanisms of these systems. Further work needs to be done on these systems to comprehensively study the damage mechanisms of this system.

4.4 Conclusions

Different strategies were investigated for achieving non-spherical phase separated morphologies in the epoxy networks. Acrylate based block copolymers are very promising candidates for blending into epoxy systems in order to achieve non-spherical morphologies. These block copolymers phase separate into individual morphologies like lamellae, cylinders, micelles and could be blended with other block copolymers to frustrate the local curvature of the phase separated morphology to get unusual morphology. Impact modification with non-spherical morphologies leads to an increase in fracture toughness without significant adverse effect on physical properties of the matrix. In our research, with

selected block copolymer blend compositions, toughness was increased 3 times compared to the. Fractographic analysis was done on these systems to understand and compare them to conventional methods of impact modification using spherical impact modification. A simple metric of shape factor was introduced to correlate the fracture toughness to the morphology of the non-spherical systems. Future work involves understanding the mechanisms of formation of these non-spherical morphologies and quantitatively correlating the shape of the domains to the fracture toughness of these systems using different metrics of evaluation and different analytical techniques.

4.5 Future work

In this chapter we were able to demonstrate that non-spherical impact modification led to improvements in fracture toughness as compared to conventional spherical impact modifiers. However, different issues that still need to be addressed when formulating these systems with block copolymer blends are:

4.5.1 Shape metric descriptors

We could see from the equations for cavitation stress and the data in this chapter that particle size and concentration alone were not sufficient to describe the increase in fracture toughness of these systems. Thus, more complex metrics would be required which take into account information related to particle shape and size. Also, as 3-D configuration of these particles is very important, more complex methods of quantitative stereology using non-spherical polydispersed particles should be considered (e.g. Dehoff vs Saltikov methods). These metrics are needed so that impact modification of these systems can be evaluated in each system based on both shape and size of the particle.

4.5.2 Screening of different systems for further demonstrating proof of concept

As non-spherical impact modification is based on a micromechanical rationale, it can be translated to various other polymeric systems including thermoplastics. Compared to conventional spherical impact modification, non-spherical impact modification can lead to improvement in the toughness of the systems which showed limited enhancement. Hence, model systems of block copolymer blends can be used to evaluate the impact modification performance of different thermoset as well as thermoplastic systems. This technology can be used in systems for 3-d printing for example as well as for thermoplastics by employing thermal induced phase separation instead of reaction induced phase separation.

4.5.3 Modeling and simulation studies

Finite Element Modeling (FEM) can be done on blends of block copolymers to identify the ideal hierarchical structures and the distribution required for optimum fracture toughness. The optimum energy dissipation can be studied by evaluating the cavitation efficiency of the non-spherical particles, the interparticle interactions and yield percolation in the matrix due to these particles. This modeling can then help in choosing the block copolymers with the required chemical structures, overall and individual molecular weights. This also will dictate the physical parameters like concentrations, curing temperatures and times required to obtain these structures.

BIBLIOGRAPHY

1. Argon, A. S. & Cohen, R. E. Toughenability of polymers. *Polymer* **44**, 6013-6032 (2003)
2. Eyring, H. Viscosity, Plasticity, and Diffusion as Examples of Absolute Reaction Rates. *J. Chem. Phys.* **4**, 283 (1936).
3. Crawford, E. D. & Lesser, A. J. Brittle to ductile: Fracture toughness mapping on controlled epoxy networks. *Polym. Eng. Sci.* **39**, 385–392 (1999).
4. Bagheri, R., Marouf, B. T. & Pearson, R. A. Rubber-Toughened Epoxies: A Critical Review. *Polym. Rev.* **49**, 201–225 (2009).
5. Lesser, A. J. & Crawford, E. The role of network architecture on the glass transition temperature of epoxy resins. *J. Appl. Polym. Sci.* **66**, 387–395 (1997).
6. Beck Tan, N. C. *et al.* Network structure of bimodal epoxies—a small angle X-ray scattering study. *Polymer (Guildf)*. **40**, 4603–4614 (1999).
7. Yang, Z. H., Detwiler, A. T. & Lesser, A. J. Prestressed double network thermoset: Preparation and characterization. *J. Mater. Sci.* **47**, 4251–4261 (2012).
8. Detwiler, A. T. & Lesser, A. J. Characterization of double network epoxies with tunable compositions. *J. Mater. Sci.* **47**, 3493–3503 (2012).
9. Ganguly, R., Gorman, I., Desbois, P. & Lesser, A. J. Structure-property relationships in asymmetric double-network glasses. *Polymer (Guildf)*. **116**, 27–34 (2017).
10. Sultan, J. N. & McGarry, F. J. Effect of rubber particle size on deformation mechanisms in glassy epoxy. *Polym. Eng. Sci.* **13**, 29–34 (1973).
11. Kim, H. S. & Ma, P. Correlation between stress-whitening and fracture toughness in rubber-modified epoxies. *J. Appl. Polym. Sci.* **61**, 659–662 (1996).
12. Dean, J. M., Lipic, P. M., Grubbs, R. B., Cook, R. F. & Bates, F. S. Micellar structure and mechanical properties of block copolymer-modified epoxies. *J. Polym. Sci. Part B Polym. Phys.* **39**, 2996–3010 (2001).
13. Liu, J. *et al.* Toughening of epoxies with block copolymer micelles of wormlike morphology. *Macromolecules* **43**, 7238–7243 (2010).
14. Lipic, P. M., Bates, F. S. & Hillmyer, M. A. Nanonstructured thermosets from self-assembled amphiphilic block copolymer/epoxy resin mixtures. *J. Am. Chem. Soc.* **120**, 8963–8970 (1998).
15. Chen, Y. *et al.* Thermal and mechanical properties of epoxy resin toughened with epoxidized soybean oil. *J. Therm. Anal. Calorim.* **113**, 939–945 (2012).
16. Bascom, W. D., Ting, R. Y., Moulton, R. J., Riew, C. K. & Siebert, A. R. The fracture of an epoxy polymer containing elastomeric modifiers. *J. Mater. Sci.* **16**, 2657–2664 (1981).

17. Barcia, F. L., Abrahão, M. A. & Soares, B. G. Modification of epoxy resin by isocyanate-terminated polybutadiene. *J. Appl. Polym. Sci.* **83**, 838–849 (2002).
18. Grishchuk, S., Sorochynska, L., Vorster, O. C. & Karger-Kocsis, J. Structure, thermal, and mechanical properties of DDM-hardened epoxy/benzoxazine hybrids: Effects of epoxy resin functionality and ETBN toughening. *J. Appl. Polym. Sci.* **127**, 5082–5093 (2013).
19. Unnikrishnan, K. P. & Thachil, E. T. Toughening of epoxy resins. *Des. Monomers Polym.* **9**, 129–152 (2006).
20. Chikhi, N., Fellahi, S. & Bakar, M. Modification of epoxy resin using reactive liquid (ATBN) rubber. *Eur. Polym. J.* **38**, 251–264 (2002).
21. Xu, S.-A., Song, X.-X. & Xu, S.-A. Introduction to Rubber toughened Epoxy Polymers. doi:10.1007/978-3-319-18158-5_1-1
22. Dompas, D. & Groeninckx, G. Toughening behaviour of rubber-modified thermoplastic polymers involving very small rubber particles: 1. A criterion for internal rubber cavitation. *Polymer (Guildf)*. **35**, 4743–4749 (1994).
23. Pearson, R. A. & Yee, A. F. Toughening mechanisms in thermoplastic-modified epoxies: 1. Modification using poly(phenylene oxide). *Polymer (Guildf)*. **34**, 3658–3670 (1993).
24. Shin, S. & Jang, J. Toughness improvement of high-performance epoxy resin using aminated polyetherimide. *J. Appl. Polym. Sci.* **65**, 2237–2246 (1997).
25. Venderbosch, R. W., Nelissen, J. G. L., Meijer, H. E. H. & Lemstra, P. J. Polymer blends based on epoxy resin and polyphenylene ether as a matrix material for high-performance composites. *Makromol. Chemie. Macromol. Symp.* **75**, 73–84 (1993).
26. Blanco, M. *et al.* Thermoplastic-modified epoxy resins cured with different functionalities amine mixtures: Morphology, thermal behavior, and mechanical properties. *J. Appl. Polym. Sci.* **114**, 1753–1760 (2009).
27. Moloney, A. C., Kausch, H. H., Kaiser, T. & Beer, H. R. Parameters determining the strength and toughness of particulate filled epoxide resins. *J. Mater. Sci.* **22**, 381–393 (1987).
28. Fu, S.-Y., Feng, X.-Q., Lauke, B. & Mai, Y.-W. Effects of particle size, particle/matrix interface adhesion and particle loading on mechanical properties of particulate–polymer composites. *Compos. Part B Eng.* **39**, 933–961 (2008).
29. Kinloch, A. J. & Young, R. J. *Fracture Behaviour of Polymers*. Springer Netherlands, (1995)
30. Marouf, B. T., Mai, Y.-W., Bagheri, R. & Pearson, R. a. Toughening of Epoxy Nanocomposites: Nano and Hybrid Effects. *Polym. Rev.* **3724**, 00–00 (2016).

31. Chen, J., Kinloch, A. J., Sprenger, S. & Taylor, A. C. The mechanical properties and toughening mechanisms of an epoxy polymer modified with polysiloxane-based core-shell particles. *Polym. (United Kingdom)* **54**, 4276–4289 (2013).
32. Liang, Y. L. & Pearson, R. A. The toughening mechanism in hybrid epoxy-silica-rubber nanocomposites (HESRNs). *Polymer (Guildf)*. **51**, 4880–4890 (2010).
33. Hsieh, T. H. *et al.* The toughness of epoxy polymers and fibre composites modified with rubber microparticles and silica nanoparticles. *J. Mater. Sci.* **45**, 1193–1210 (2010).
34. Kanninen, M. F. & Popelar, C. H. *Advanced Fracture Mechanics*. (Oxford University Press, 1985).
35. Guild, F. J., Kinloch, A. J. & Taylor, A. C. Particle cavitation in rubber toughened epoxies: The role of particle size. *J. Mater. Sci.* **45**, 3882–3894 (2010).
36. Bucknall, C. B., Karpodinis, A. & Zhang, X. C. A model for particle cavitation in rubber-toughened plastics. *J. Mater. Sci.* **29**, 3377–3383 (1994).
37. Bagheri, R. & Pearson, R. A. Role of particle cavitation in rubber-toughened epoxies: II. Inter-particle distance. *Polymer (Guildf)*. **41**, 269–276 (2000).
38. He, J., Raghavan, D., Hoffman, D. & Hunston, D. The Influence of Elastomer Concentration on Toughness in Dispersions Containing Preformed Acrylic Elastomeric Particles in an Epoxy Matrix.
39. Day, R., Lovell, P. & Wazzan, A. Thermal and mechanical characterization of epoxy resins toughened using preformed particles. *Polym. Int.* **50**, 849–857 (2001).
40. Bagheri, R. & Pearson, R. A. Role of particle cavitation in rubber-toughened epoxies: I. Microvoid toughening. *Polymer (Guildf)*. **37**, 4529–4538 (1996).
41. Bascom, W. D., Cottington, R. L., Jones, R. L. & Peyser, P. The fracture of epoxy- and elastomer-modified epoxy polymers in bulk and as adhesives. *J. Appl. Polym. Sci.* **19**, 2545–2562 (1975).
42. Fröhlich, J., Kautz, H., Thomann, R., Frey, H. & Mülhaupt, R. Reactive core/shell type hyperbranched blockcopolyethers as new liquid rubbers for epoxy toughening. *Polymer (Guildf)*. **45**, 2155–2164 (2004).
43. Lee, C. Y.-C. & Jones, W. B. Fracture toughness (KQ) testing with a mini-compact tension (CT) specimen. *Polym. Eng. Sci.* **22**, 1190–1198 (1982).
44. Hinkley, J. A. Small compact tension specimens for polymer toughness screening. *J. Appl. Polym. Sci.* **32**, 5653–5655 (1986).
45. Yamanaka, K., Takagi, Y. & Inoue, T. Reaction-induced phase separation in rubber-modified epoxy resins. *Polymer (Guildf)*. **30**, 1839–1844 (1989).
46. Matějka, L. Amine Cured Epoxide Networks: Formation, Structure, and Properties †. *Macromolecules* **33**, 3611–3619 (2000).

47. Vallo, C. I., Frontini, P. M. & Williams, R. J. J. The glass transition temperature of nonstoichiometric epoxy–amine networks. *J. Polym. Sci. Part B Polym. Phys.* **29**, 1503–1511 (1991).
48. Bellenger, V. *et al.* Glass transition temperature predictions for non-stoichiometric epoxide-amine networks. *Polymer (Guildf)*. **30**, 2013–2018 (1989).
49. Umboh, M. K., Adachi, T., Nemoto, T., Higuchi, M. & Major, Z. Non-stoichiometric curing effect on fracture toughness of nanosilica particulate-reinforced epoxy composites. *J. Mater. Sci.* **49**, 7454–7461 (2014).
50. Gude, M. R., Prolongo, S. G. & Ureña, A. Effect of the epoxy/amine stoichiometry on the properties of carbon nanotube/epoxy composites. *J. Therm. Anal. Calorim.* **108**, 717–723 (2011).
51. Calzia, K. J. Molecular aspects of yield and fracture in glassy thermosets and their nano-composites. *Doctoral Dissertations* (2006).
52. Detwiler, A. T. & Lesser, A. J. Aspects of network formation in glassy thermosets. *J. Appl. Polym. Sci.* **117**, 1021–1034 (2010).
53. Haward, R. N. The application of a Gauss-Eyring model to predict the behavior of thermoplastics in tensile experiments. *J. Polym. Sci. Part B Polym. Phys.* **33**, 1481–1494 (1995).
54. van Melick, H. G. H., Govaert, L. E. & Meijer, H. E. H. On the origin of strain hardening in glassy polymers. *Polymer (Guildf)*. **44**, 2493–2502 (2003).
55. Tervoort, T. A. & Govaert, L. E. Strain-hardening behavior of polycarbonate in the glassy state. *J. Rheol. (N. Y. N. Y)*. **44**, 1263 (2000).
56. Lesser, A. J. & Calzia, K. J. Molecular parameters governing the yield response of epoxy-based glassy networks. *J. Polym. Sci. Part B Polym. Phys.* **42**, 2050–2056 (2004).
57. Calzia, K. J. & Lesser, A. J. Correlating yield response with molecular architecture in polymer glasses. *J. Mater. Sci.* **42**, 5229–5238 (2007).
58. Calzia, K. J., Forcum, A. & Lesser, A. J. Comparing reinforcement strategies for epoxy networks using reactive and non-reactive fortifiers. *J. Appl. Polym. Sci.* **102**, 4606–4615 (2006).
59. Fox, T. G. & Loshaek, S. Influence of molecular weight and degree of crosslinking on the specific volume and glass temperature of polymers. *J. Polym. Sci.* **15**, 371–390 (1955).
60. Ward, I. M. & Hadley, D. W. *An introduction to the mechanical properties of solid polymers*. J. Wiley & Sons (1993).
61. G.'Sell, C. & McKenna, G. B. Influence of physical ageing on the yield response of model DGEBA/poly(propylene oxide) epoxy glasses. *Polymer (Guildf)*. **33**, 2103–2113 (1992).

62. Cook, W., Mehrabi, M. & Edward, G. Ageing and yielding in model epoxy thermosets. *Polymer (Guildf)*. **40**, 1209–1218 (1999).
63. Oyanguren, P. A., Vallo, C. I., Frontini, P. M. & Williams, R. J. J. Rejuvenation of epoxy glasses subjected to uniaxial compression. *Polymer (Guildf)*. **35**, 5279–5282 (1994).
64. Bellenger, V., Dhaoui, W., Verdu, J., Boye, J. & Lacabanne, C. Internal antiplasticization in diglycidyl ether of bisphenol A diamino diphenyl methane non-stoichiometric epoxy networks. *Polym. Eng. Sci.* **30**, 321–325 (1990).
65. Palmese, G. R. & McCullough, R. L. Effect of epoxy–amine stoichiometry on cured resin material properties. *J. Appl. Polym. Sci.* **46**, 1863–1873 (1992).
66. McKenna, G. B. Mechanical rejuvenation in polymer glasses: fact or fallacy? *J. Phys. Condens. Matter* **15**, S737–S763 (2003).
67. Boyce, M. C. & Arruda, E. M. Constitutive Models of Rubber Elasticity: A Review. *Rubber Chem. Technol.* **73**, 504–523 (2000).
68. Hoy, R. S. & Robbins, M. O. Strain hardening of polymer glasses: Effect of entanglement density, temperature, and rate. *J. Polym. Sci. Part B Polym. Phys.* **44**, 3487–3500 (2006).
69. Tervoort, T. A. & Govaert, L. E. Strain-hardening behavior of polycarbonate in the glassy state. *J. Rheol. (N. Y. N. Y.)*. **44**, 1263–1277 (2000).
70. Treloar, L. R. . *The Physics of Rubber Elasticity*. (Oxford University Press, USA, 1975).
71. Haward, R. N. & Thackray, G. The Use of a Mathematical Model to Describe Isothermal Stress-Strain Curves in Glassy Thermoplastics. *Proc. R. Soc. A Math. Phys. Eng. Sci.* **302**, 453–472 (1968).
72. Cook, W. D., Scott, T. F., Quay-Thevenon, S. & Forsythe, J. S. Dynamic Mechanical Thermal Analysis of Thermally Stable and Thermally Reactive Network Polymers. *J Appl Polym Sci* **93**, 1348–1359 (2004).
73. Nakka, J. S., Jansen, K. M. B. & Ernst, L. J. Effect of chain flexibility in the network structure on the viscoelasticity of epoxy thermosets. *Journal of Polymer Research* **18**, 1879–1888 (2011).
74. Sprenger, S. Fiber-reinforced composites based on epoxy resins modified with elastomers and surface-modified silica nanoparticles. *J. Mater. Sci.* **49**, 2391–2402 (2014).
75. Williams J.G. Fracture Mechanics of Polymers. *Polym. Eng. Sci.* **17**, 144–149 (1977).
76. Vukovic, I., Brinke, G. ten & Loos, K. Block copolymer template-directed synthesis of well-ordered metallic nanostructures. *Polymer (Guildf)*. **54**, 2591–2605 (2013).
77. Swann, J. M. G., Topham, P. D., Swann, J. M. G. & Topham, P. D. Design and

- Application of Nanoscale Actuators Using Block-Copolymers. *Polymers (Basel)*. **2**, 454–469 (2010).
78. Ritzenthaler, S. *et al.* ABC Triblock Copolymers/Epoxy-Diamine Blends. 1. Keys To Achieve Nanostructured Thermosets. doi:10.1021/ma0121868
 79. Ruiz-Pérez, L., Royston, G. J., Fairclough, J. P. A. & Ryan, A. J. Toughening by nanostructure. *Polymer (Guildf)*. **49**, 4475–4488 (2008).
 80. Zhu, J. *et al.* Disk-cylinder and disk-sphere nanoparticles via a block copolymer blend solution construction. *Nat. Commun.* **4**, 2297 (2013).
 81. Wright, D. B. *et al.* The Copolymer Blending Method: A New Approach for Targeted Assembly of Micellar Nanoparticles. *Macromolecules* **48**, 6516–6522 (2015).
 82. Matsen, M. W. Phase Behavior of Block Copolymer/Homopolymer Blends. *Macromolecules* **28**, 5765–5773 (1995).
 83. Cho, A. *et al.* Mix-and-Match Assembly of Block Copolymer Blends in Solution. *Macromolecules* **50**, 3234–3243 (2017).
 84. Cui, H., Chen, Z., Zhong, S., Wooley, K. L. & Pod, D. Block Copolymer Assembly via Kinetic Control. *Science* **317**, 647–650 (2007)
 85. Schuetz, P. *et al.* Controlling the micellar morphology of binary PEO-PCL block copolymers in water-THF through controlled blending. *Soft Matter* **7**, 749-759 (2011)
 86. Pochan, D. J. *et al.* Multicompartment and multigeometry nanoparticle assembly. *Soft Matter* **7**, 2500 (2011).
 87. Hamley, I. W. *The physics of block copolymers*. (Oxford University Press, 1998).
 88. Liu, J. Toughening of Epoxies Based on Self-Assembly of Nano-sized Amphiphilic block copolymer micelles. *Dissertation* (2009).
 89. Sue, H. J. & Yee, A. F. Study of fracture mechanisms of multiphase polymers using the double-notch four-point-bending method. *J. Mater. Sci.* **28**, 2975–2980 (1993).